Feeding a Molecular Squid. A Pliable Nanocarbon Receptor for Electron-Poor Aromatics

Supplementary Information

by Rafał Frydrych, Tadeusz Lis, Wojciech Bury, Joanna Cybińska, and Marcin Stępień*

Table of Contents

Experimental

General. Tetrahydrofuran, toluene, 1,4-dioxane and N,N-Dimethylformamide were freeze-pump-thawed prior to use. All other solvents and reagents were used as received. Compounds **S1, S2, S3, S4** and **2a** were prepared according to modified literature procedures.[1–5] ^{1}H NMR spectra were recorded on high-field spectrometers (^{1}H frequency 500.13 or 600.13 MHz), equipped with broadband inverse or conventional gradient probeheads. Spectra were referenced to the residual solvent signals (chloroform-*d*, 7.26 ppm, dichloromethane-d_2, 5.32 ppm, acetone-d_6, 2.05). Two-dimensional NMR spectra were recorded with 2048 data points in the t_2 domain and up to 2048 points in the t_1 domain, with a 1.5 s recovery delay. All 2D spectra were recorded with gradient selection, with the exception of ROESY. ^{13}C NMR spectra were recorded with ^{1}H broadband decoupling and referenced to solvent signals ($^{13}CDCl_3$, 77.0 ppm). High resolution mass spectra were recorded using ESI ionization in the positive mode on Bruker Apex ultra FT-ICR. Absorption spectrometry was performed using Agilent Cary 60 UV-Vis spectrophotometer. Recycling gel permeation chromatography (GPC) was carried out using an JAI LaboACE LC-7080 chromatograph equipped with a RID (RI-700 LA) and UV-Vis (UV-VIS4ch 800LA) detectors and a preparative GPC columns JAIGEL-2HR and JAIGEL-2.5HR (size 20.0 mm ID × 600 mm each) in series, using chloroform as an eluent with a flow rate of 10 mL/min at 30°C.

^{1}H NMR spectroscopic titration studies.[6,7] The receptor solutions of **1** (1.81 or 0.906 mM, acetone-d_6 or CD_2Cl_2, 300 K) were titrated in an NMR tube sealed with a plastic stopper, by adding known quantities of a stock solution of either $[DQ^{2+}][PF_6^-]_2$, $[PQ^{2+}][PF_6^-]_2$, $[MA^+][PF_6^-]$ or AQ in the same solvent. These solutions contained compound **1** to ensure a constant concentration of the guest throughout the titration. After each addition the NMR tube was quickly shaken to ensure good mixing of the solutions and after temperature stabilization the spectra were recorded. [AQ] was purchased from Sigma–Aldrich. $[DQ^{2+}][PF_6^-]_2$, $[PQ^{2+}][PF_6^-]_2$, $[MA^+][PF_6^-]$ were prepared according to modified literature procedures.[8–10] The fitting, performed with the Bindfit software,[11] takes into account all data sets at the same time, thus improving the quality of the non-linear curve fitting. The data for $[DQ^{2+}][PF_6^-]_2$, $[PQ^{2+}][PF_6^-]_2$ and $[MA^+][PF_6^-]$ were fitted to the 1:1 and 2:1 (**1**:G) binding model, **1** being the receptor and G the guest molecule. The data obtained for AQ were fitted to the 1:1 binding model only.

Gas and Vapor Sorption Analyses. All gas and vapor sorption isotherms were measured on a Micromeritics ASAP 2020M surface area and porosimetry system. Prior to the measurements, the sample of **1** was recrystallized from the benzene/methanol solvent mixture. The precipitate was filtered off and degassed at 50 °C for 24 h. N_2 sorption measurements were performed at 77 K using a liquid N_2 bath. For the CO_2 measurement carried out at 195 K, an isopropanol/dry ice cooling bath was used. For all other measurements (CO_2, cyclohexane, MeOH, water) carried out in the 273–293 K temperature range, chilled water/ethylene glycol bath was used for temperature control. All gases used were of 99.999% purity. Helium was used for the free-space determination. The isosteric heats of adsorption (Q_{st}) were calculated by fitting the CO_2 adsorption isotherms using the single-site Langmuir–Freundlich model (1) and Q_{st} was calculated using the Clausius–Clapeyron equation

$$q = \frac{q_{sat} K p^n}{1 + K p^n} \quad (1)$$

where q is the gravimetric uptake of CO_2 (mmol/g) at pressure p. q_{sat}, K and n are the saturation loading and the Langmuir-Freundlich constants, respectively.

Excitation and emission spectra were obtained using a FLS980 spectrofluorimeter (Edinburgh Instruments Ltd.) equipped with a 450 W Xenon lamp excitation source and a red-sensitive

photomultiplier (Hamamatsu R-928P) operating within 200–870 nm. The former spectra were corrected for the incident light intensity and the latter for the wavelength-dependence of the emission channel sensitivity. Quantum yields were measured using a cooled extended-red Hamamatsu photomultiplier operating in a range of 200 – 1050 nm. Quantum yield measurements were performed by using an Edinburgh Instruments integrating sphere equipped with a small elliptical mirror and a baffle plate for beam steering and shielding against directly detected light. For the measurement, the integrating sphere replaces the standard sample holder inside the sample chamber. Calculations of quantum yields were made using the software provided by Edinburgh Instruments. The luminescence decay traces were registered by means of F-G05PM featuring a Hamamatsu H5773-04 detector. As an excitation source picosecond pulsed light emitting diode 360 nm was used.

Computational methods. Tight-binding density functional theory calculations were performed using xTB v. 6.1 with the GFN2 parameterization, and the GBSA solvation model as necassary.[12–14] CREST[12] metadynamics searches were performed using default parameters. Density functional theory (DFT) calculations were performed using Gaussian 16.[15] DFT geometry optimizations were carried out in unconstrained C_1 symmetry, typically using the entire CREST ensemble and selecting the conformer with lowest DFT Gibbs free energy. DFT geometries were refined to meet standard convergence criteria, and the existence of a local minimum was verified by a normal mode frequency calculation. Geometry optimizations, frequency calculations were performed using the hybrid functional B3LYP[16–18] and the 6-31G(d,p) basis set and Grimme's GD3BJ dispersion correction.[19] The CAM modification was employed as discussed in the manuscript.

X-ray crystallography. X-ray quality crystals were grown as follows: **5**·C_6H_{14}·H_2O by slow diffusion of *n*-hexane into ethyl acetate, **1**·3C_6H_6 by slow diffusion of methanol into benzene, **1**·3.2CH_2Cl_2 by slow diffusion of methanol into dichloromethane, [**1**⊃AQ]·2.5CH_4O by slow diffusion of methanol into a dichloromethane solution of **1** and 4 equiv of AQ. Crystals of [**1**⊃DQ^{2+}][PF_6^-]$_2$·C_3H_6O and [**1**⊃PQ^{2+}][PF_6^-]$_2$·C_3H_6O were obtained from crystals of **1**·3C_6H_6, which were placed in an acetone–methanol solution of [DQ^{2+}][PF_6^-]$_2$ or [PQ^{2+}][PF_6^-]$_2$, respectively. These samples were kept in the presence of methanol vapors until the crystal-to-crystal transformation was complete. Diffraction measurements were performed on a κ-geometry Ruby PX diffractometer (ω scans) with graphite-monochromatized Mo Kα or Cu Kα radiation. The data were collected at 100 K, corrected for Lorenz and polarization effects. Data collection, cell refinement, data reduction and analysis were carried out with the Xcalibur PX software, CRYSALIS CCD and CRYSALIS RED, respectively (Oxford Diffraction Ltd., Abignon, England, 2009). An analytical absorption correction was applied with the use of CRYSALIS RED. All structures were solved by direct methods with the SHELXS-97 program and refined using SHELXL-97 with anisotropic thermal parameters for non-H atoms. In the final refinement cycles, all H atoms were treated as riding atoms in geometrically optimized positions. CCDC 2016786 (**1**·3C_6H_6), 2016787 (**5**·C_6H_{14}·H_2O), 2016788 (**1**·3.2CH_2Cl_2), 2016789 ([**1**⊃PQ^{2+}][PF_6^-]$_2$·C_3H_6O), 2016790 ([**1**⊃AQ]·2.5CH_4O), and 2016791 ([**1**⊃DQ^{2+}][PF_6^-]$_2$·C_3H_6O) contain the supplementary crystallographic data for this paper. These data are provided free of charge by The Cambridge Crystallographic Data Centre via www.ccdc.cam.ac.uk/data_request/cif.

Synthesis

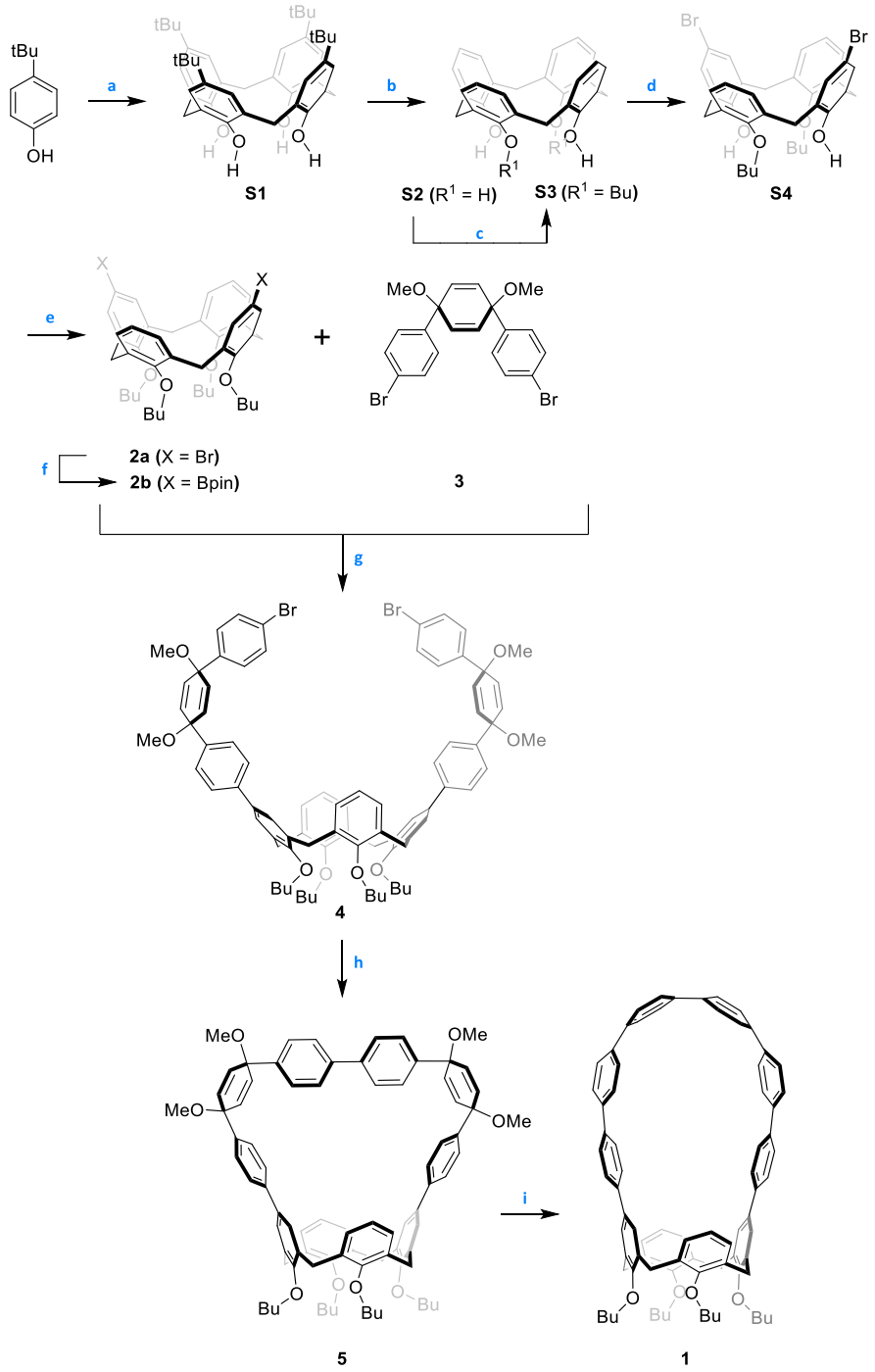

Scheme S1. Synthesis of compound **1**: (**a**) 37% solution of formaldehyde in water, NaOH, Ph_2O, reflux; (**b**) $AlCl_3$, toluene; (**c**) BuBr, K_2CO_3, reflux; (**d**) Br_2, $CHCl_3$, 0°C; (**e**) BuBr, NaH, reflux, 0 °C to RT; (**f**) $Pd(dppf)Cl_2$, $[B(pin)]_2$, CH_3COOK, dioxane, 110 °C, 12 h; (**g**) $Pd(OAc)_2$, dppf, Ag_2O, K_2CO_3, toluene, water, 80 °C, 24 h; (**h**) $Ni(cod)_2$, bpy, THF, DMF, 80 °C, 16 h; (**i**) H_2SnCl_4, THF, RT, overnight.

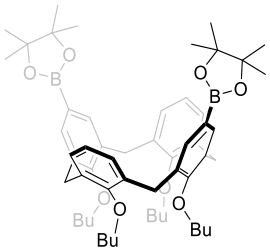

2,2'-(1^2,3^2,5^2,7^2-Tetrabutoxy-1,3,5,7(1,3)-tetrabenzenacyclooctaphane-1^5,5^5-diyl)bis(4,4,5,5-tetramethyl-1,3,2-dioxaborolane) (2b). Inside the glove box, compound **2a** (0.700 g, 0.868 mmol, 1.0 equiv), bis(pinacolato)diboron (0.529 g, 2.08 mmol, 2.4 equiv), Pd(dppf)Cl_2 (34.43 mg, 0.43 mmol, 0.05 equiv) and potassium acetate (0.204 g, 2.08 mmol, 2.4 equiv) were dissolved in 1,4-dioxane (14 mL) in a pressure tube equipped with a stir bar. The tube was sealed with a cap, transferred out of the glove box and stirred at 110°C for 12 h. The reaction mixture was cooled to room temperature, brine was added, followed by extraction with dichloromethane. Combined organic layers were dried over sodium sulfate and evaporated under reduced pressure. The product was purified by column chromatography (silica, dichloromethane/hexane, 3:1) (0.651 g, 83%). **^{1}H NMR** (500 MHz, chloroform-*d* , 300 K): δ 7.60 (4H, s), 6.19 (2H, t, ^3J = 7.6 Hz), 6.10 (4H, d, ^3J = 7.6 Hz), 4.42 (4H, d, ^2J = 13.3 Hz), 4.12 (4H, t, ^3J = 8.3 Hz), 3.69 (4H, t, ^3J = 6.5 Hz), 3.20 (4H, d, ^2J = 13.4 Hz), 1.90 (4H, quint, ^3J = 8.1 Hz), 1.84 (4H, quint, ^3J = 7.1 Hz) 1.61 (4H, sextet, ^3J = 7.5 Hz), 1.39 (24H, s) 1.26 (4H, sextet, ^3J = 7.5 Hz), 1.00 (6H, t, ^3J = 7.4 Hz), 0.96 (6H, t, ^3J = 7.4 Hz). **^{13}C NMR** (125 MHz, chloroform-*d* , 300 K): δ 161.2, 155.1, 136.7,135.7, 133.0, 127.5, 122.0, 83.5, 74.9, 74.7, 32.6, 32.0, 30.8, 25.0, 19.6, 19.0, 14.1, 13.9. **HRMS** (ESI–TOF): *m*/*z*: [M + Na]$^+$ Calcd for $C_{56}H_{78}B_2O_8Na^+$: 923.5793; Found 923.5731.

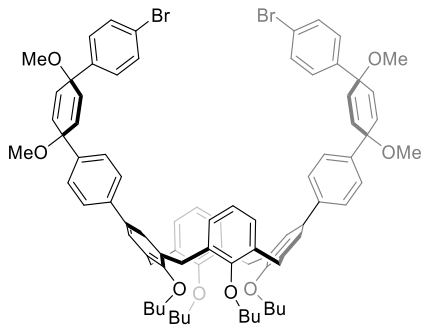

1^5,5^5-bis(4''-bromo-1',4'-dimethoxy-1',4'-dihydro-[1,1':4',1''-terphenyl]-4-yl)-1^2,3^2,5^2,7^2-tetrabutoxy-1,3,5,7(1,3)-tetrabenzenacyclooctaphane (4). Inside the glove box, Pd$(OAc)_2$ (14.95 mg, 0.066 mmol, 0.12 equiv), dppf (41.54 mg, 0.075 mmol, 0.135 equiv) and anhydrous toluene (4 mL) were added to a 5 mL vial equipped with a stir bar. The mixture was stirred in the glove box at room temperature for 30 min. Then it was added to a pressure tube containing a solution of compound **2b** (0.500 g, 0.55 mmol, 1.0 equiv), **3** (1.999 g, 4.44 mmol, 8.0 equiv), K_2CO_3 (0.153 g, 1.11 mmol, 2.0 equiv), and Ag_2O (0.579 g, 1.33 mmol, 4.5 equiv) in 36 mL of anhydrous toluene. The pressure tube was sealed with a septum cap and transferred out of the glove box. Degassed water (4 mL) was added through the septum via a syringe, and the septum cap was replaced with the pressure bushing under a blanket of argon. The reaction mixture was stirred at 80 °C in an oil bath for 24 h, cooled down to room temperature, and filtered through celite. The solvent was removed under reduced pressure. Excess of the substrate **3** was removed from the mixture by column chromatography (basic alumina

grade III, dichloromethane/hexane/ethyl acetate, 1:2:0.01). The crude product was dissolved in dichloromethane, loaded on alumina by slow evaporation, and purified by column chromatography (basic alumina grade III, 15% ethyl acetate in hexane) to get compound **4** (0.451 g, 59%). **^{1}H NMR** (600 MHz, chloroform-*d* , 300 K): δ 7.55 (4H, d, ^3J = 8.3 Hz), 7.46 (4H, d, ^3J = 8.5 Hz), 7.41 (4H, d, ^3J = 8.3 Hz), 7.31 (4H, d, ^3J = 8.5 Hz), 7.27 (4H, s), 6.26 (6H, m), 6.19 (4H, d, ^3J = 10.2 Hz), 6.07 (4H, d, ^3J = 10.2 Hz), 4.50 (4H, d, ^2J = 13.2 Hz), 4.09 (4H, t, ^3J = 8.1 Hz), 3.77 (4H, t, ^3J = 6.7 Hz), 3.45 (6H, s), 3.44 (6H, s), 3.22 (4H, d, ^2J = 13.3 Hz), 1.97 (4H, quint, ^3J = 7.9 Hz), 1.89 (4H, quint, ^3J = 7.2 Hz), 1.60 (4H, sextet, ^3J = 7.5 Hz), 1.35 (4H, sextet, ^3J = 7.5 Hz), 1.04 (6H, t, ^3J = 7.3 Hz), 1.00 (6H, t, ^3J = 7.3 Hz). **^{13}C NMR** (151 MHz, chloroform-*d* , 300 K): δ 157.6, 155.5, 142.7, 141.4, 140.6, 137.0, 134.0, 133.9, 133.3, 132.8, 131.5, 127.9, 127.7, 127.3, 126.9, 126.2, 122.2, 121.6, 75.0, 75.0, 74.7, 74.6, 52.0, 32.5, 32.2, 31.2, 29.7, 19.6, 19.2, 14.2, 14.0. **HRMS** (ESI–TOF): *m*/*z*: [M + Na]$^+$ Calcd for $C_{84}H_{90}O_8Br_2Na^+$: 1407.4895; Found 1407.4952.

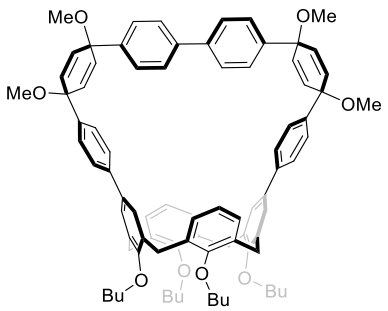

Compound (5). Inside the glove box, Ni(cod)$_2$ (88.53 mg, 0.32 mmol, 2.5 equiv), 2,2'-bipyridyl (50.27 mg, 0.32 mmol, 2.5 equiv), and anhydrous THF (21.0 mL) were sequentially added to a pressure tube equipped with a stir bar. After 5 min of stirring, a DMF solution of compound **4** (178.63 mg, 0.13 mmol, 1.0 equiv, 26.5 mL) was added dropwise to above mixture during 2 h. The tube was sealed with cap, transferred out of the glove box and stirred at 80 °C for 16 h in an oil bath. The reaction mixture was cooled down to room temperature and evaporated under reduced pressure. Brine was added and the mixture was extracted with dichloromethane. The organic layer was dried over anhydrous sodium sulfate and evaporated under reduced pressure. The crude product was dissolved in dichloromethane, loaded on alumina by slow evaporation and purified by column chromatography (basic alumina grade III, 15% ethyl acetate in hexane) to get compound **5** (0.116 g, 74%) as a colorless solid. **^{1}H NMR** (600 MHz, chloroform-*d*, 300 K): δ 7.51 (4H, d, ^3J = 8.4 Hz), 7.42 (8H, m), 7.28 (4H, d, ^3J = 8.6 Hz), 7.22 (4H, s), 7.03 (4H, d, ^3J = 7.6 Hz), 6.65 (2H, t, ^3J = 7.6 Hz), 6.29 (4H, d, ^3J = 10.2 Hz), 6.03 (4H, d, ^3J = 10.2 Hz), 4.57 (4H, d, ^2J = 12.0 Hz), 3.98 (4H, t, ^3J = 7.9 Hz), 3.91 (4H, t, ^3J = 7.8 Hz), 3.47 (6H, s), 3.44 (6H, s), 3.32 (4H, d, ^2J = 12.1 Hz), 2.18 (4H, quint, ^3J = 5.2 Hz), 2.03 (4H, quint, ^3J = 7.8 Hz), 1.52 (4H, sextet, ^3J = 7.6 Hz), 1.47 (4H, sextet, ^3J = 7.6 Hz), 1.09 (6H, t, ^3J = 7.4 Hz), 1.05 (6H, t, ^3J = 7.4 Hz). **^{13}C NMR** (151 MHz, chloroform-*d* , 300 K): δ 155.8, 155.7, 142.3, 141.6, 141.5, 139.3, 135.9, 135.8, 134.7, 133.9, 132.8, 128.2, 127.7, 127.6, 126.8, 126.2, 126.0, 123.3, 75.7, 75.5, 75.0, 74.4, 52.0, 51.9, 32.5, 32.3, 30.5, 19.3, 19.3, 14.3, 14.2. **HRMS** (ESI–TOF): *m*/*z*: [M + H]$^+$ Calcd for $C_{84}H_{90}O_8H^+$: 1227.6708; Found 1227.6723. *m*/*z*: [M + Na]$^+$ Calcd for $C_{84}H_{90}O_8Na^+$: 1249.6528; Found 1249.6543.

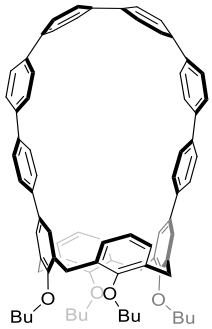

Compound (1). Under a nitrogen atmosphere, concentrated hydrochloric acid (207 µL, 3.05 mmol, 16 equiv) was added to a sunspension of $SnCl_2{\cdot}2H_2O$ (354.71 mg, 1.52 mmol, 8 equiv) in 9 mL THF and stirred for 15 min. Subsequently, the resulting mixture was added dropwise to a solution containing compound **5** (234 mg, 0.19 mmol, 1 equiv) in 14 mL of THF, which turned immedately from colorless to yellow and was stirred at RT overnight. To the resulting mixture, a 10% aqueous NaOH solution was added, and extracted with dichloromethane. The combined organic layers were washed with brine, dried over sodium sulfate, filtered and concentrated under reduce pressure. The crude residue was passed through a short column (silica, dichloromethane/ethyl acetate, 1:0.01). The pure compound **5** was obtained after purification by GPC (**Figure S1**, 180 mg, 86%). **^{1}H NMR** (600 MHz, chloroform-*d*, 300 K): δ 7.59 (4H, d, ^3J = 9.0 Hz), 7.54 (4H, d, ^3J = 9.0 Hz), 7.51(4H, d, ^3J = 8.6 Hz), 7.39 (4H, d, ^3J = 8.6 Hz), 7.36 (4H, d, ^3J = 8.5 Hz), 7.29 (4H, d, ^3J = 8.5 Hz), 7.15 (4H, s), 7.09 (4H, d, ^3J = 7.7 Hz), 6.74 (2H, t, ^3J = 7.6 Hz), 4.55 (4H, d, ^2J = 12.2 Hz), 4.06 (4H, t, ^3J = 8.2 Hz), 3.83 (4H, t, ^3J = 7.6 Hz), 3.30 (4H, d, ^2J = 12.2 Hz), 2.22 (4H, quint, ^3J = 8.0 Hz), 1.94 (4H, quint, ^3J = 7.6 Hz), 1.47 (8H, septet, ^3J = 7.5 Hz), 1.09 (6H, t, ^3J = 7.4 Hz), 1.02 (6H, t, ^3J = 7.4 Hz). **^{13}C NMR** (151 MHz, chloroform-*d* , 300 K): δ 156.6, 155.7, 138.7, 138.4, 138.3, 138.0, 137.9, 136.9, 135.7, 134.1, 133.6, 128.7, 127.9, 127.4, 127.4, 127.3, 127.1, 126.5, 126.4, 123.1, 76.2, 74.7, 32.4, 32.2, 31.0, 19.4, 19.3, 14.3, 14.1. **HRMS** (ESI–TOF): *m*/*z*: $[M + Na]^+$ Calcd for $C_{80}H_{78}O_4Na^+$: 1125.5792; Found 1125.5733. **UV-vis** (dichloromethane, 298 K) *λ* [nm] (*ε* in M^{-1} cm^{-1}): 327 (78500), 377 (18200).

Additional Schemes

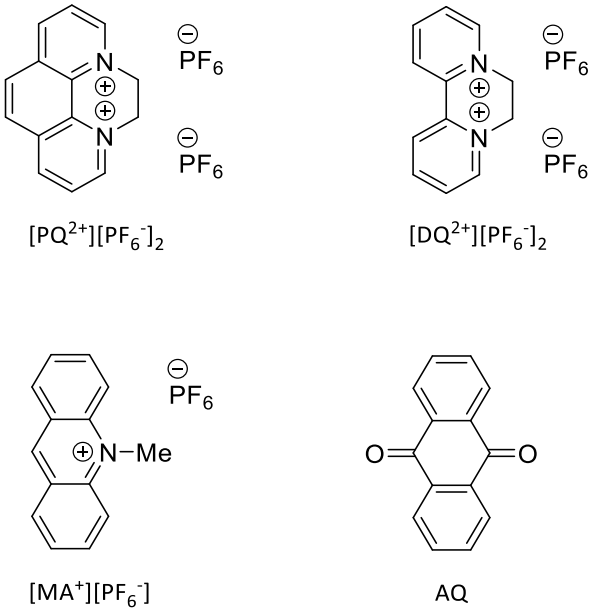

Scheme S2. Structures of the guests molecules.

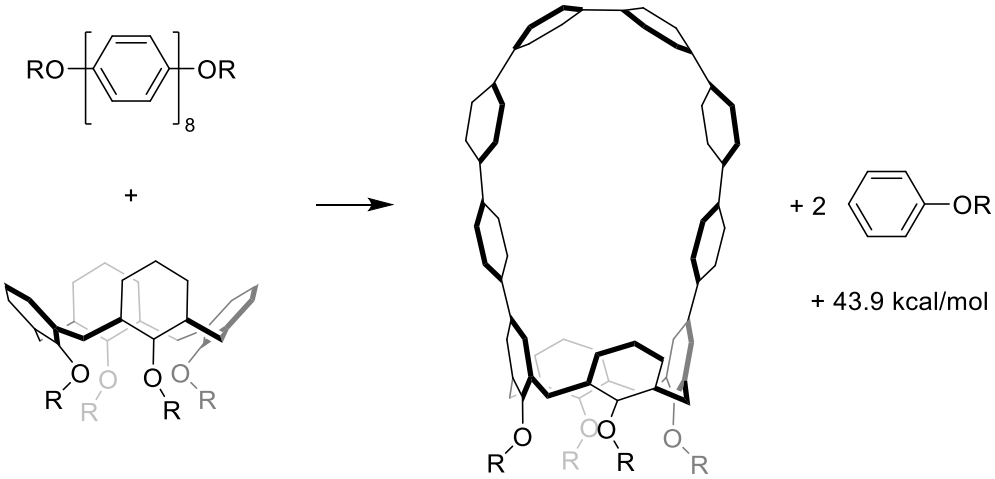

Scheme S3. Homodesmotic strain calculation for **1**. Δ*H* is given at the B3LYP-GD3BJ/6-31G(d,p) level of theory.

^{13}C NMR:

1. 14.31
2. 19.38 or 19.28
3. 32.22
4. 74.75
5. 156.64
6. 135.74
7. 128.71
8. 123.13
9. 14.09
10. 19.38 or 19.28
11. 32.41
12. 76.21
13. 31.02
14. 155.74
15. 134.13
16. 126.37
17. 138.74
18. 138.36 or 138.33
19. 127.10
20. 126.47
21. 133.57
22. 138.02
23. 127.36
24. 127.30
25. 138.36 or 138.33
26. 136..89
27. 127.93
28. 127.43
29. 137.90

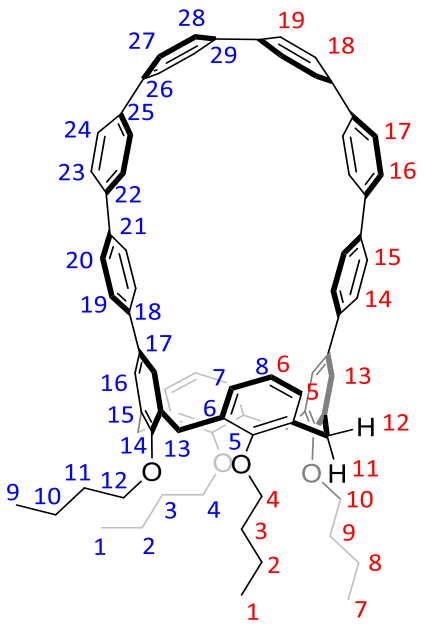

^{1}H NMR:

1. 1.09
2. 1.47
3. 2.22
4. 4.06
5. 7.09
6. 6.74
7. 1.02
8. 1.47
9. 1.94
10. 3.83
11. 4.55
12. 3.30
13. 7.15
14. 7.29
15. 7.36
16. 7.39
17. 7.51
18. 7.54
19. 7.59

Scheme S4. ^{1}H and ^{13}C NMR chemical shifts of **1**. The assignment was based on data obtained from COSY, NOESY (**Figure S2**), HSQC and HMBC (**Figure S3**, **Figure S4**) experiments.

Additional Figures

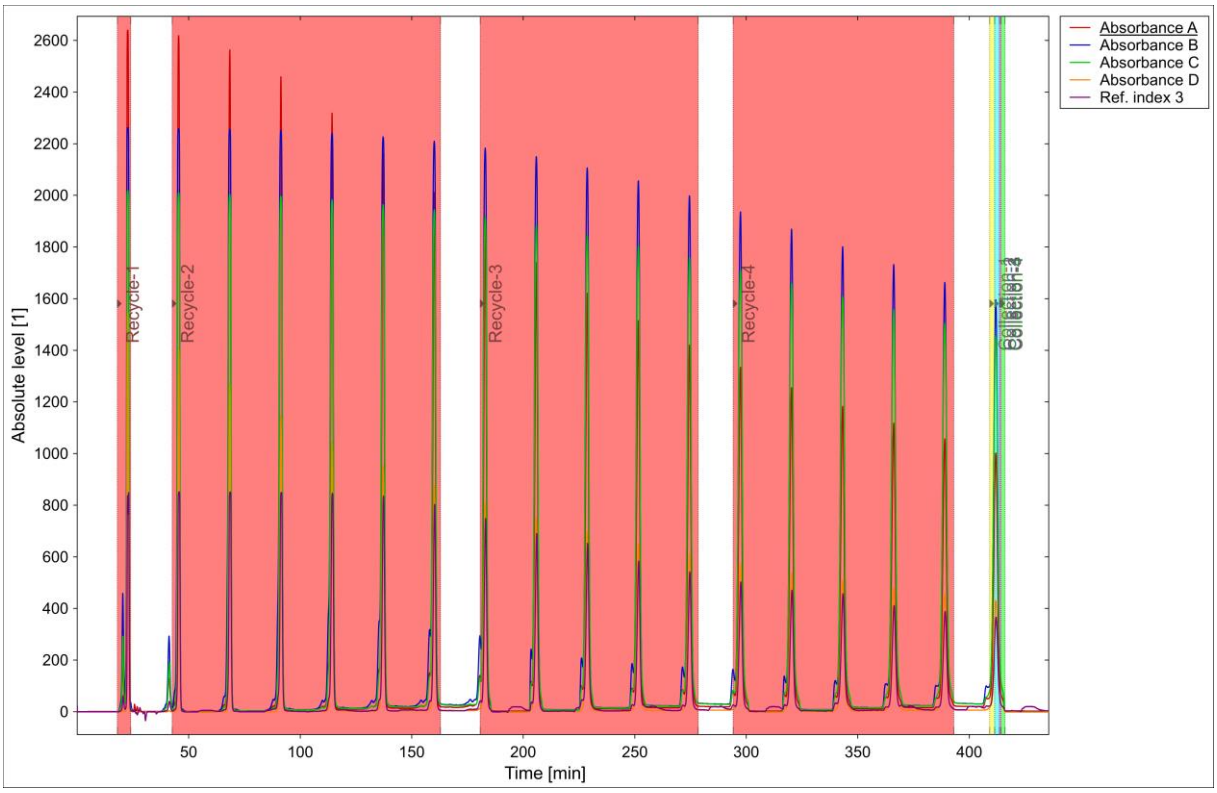

Figure S1. GPC chromatogram for compound **1** purification. Wavelenghts: A = 254 nm, B = 310 nm, C = 350 nm, D = 415 nm.

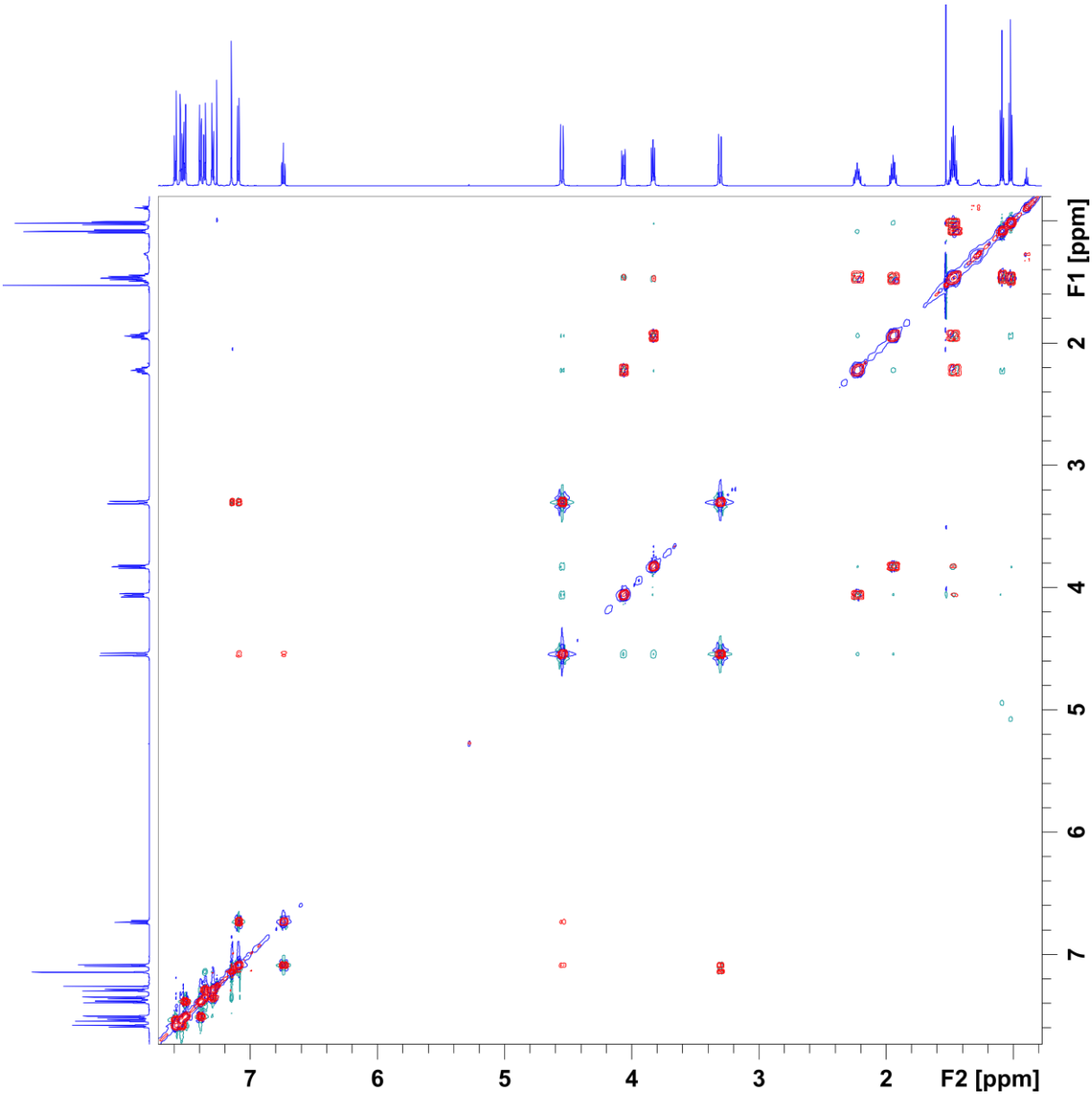

Figure S2. Overlaid NOESY (blue/green) and COSY (red) spectra of **1** (600 MHz, chloroform-*d*, 300 K).

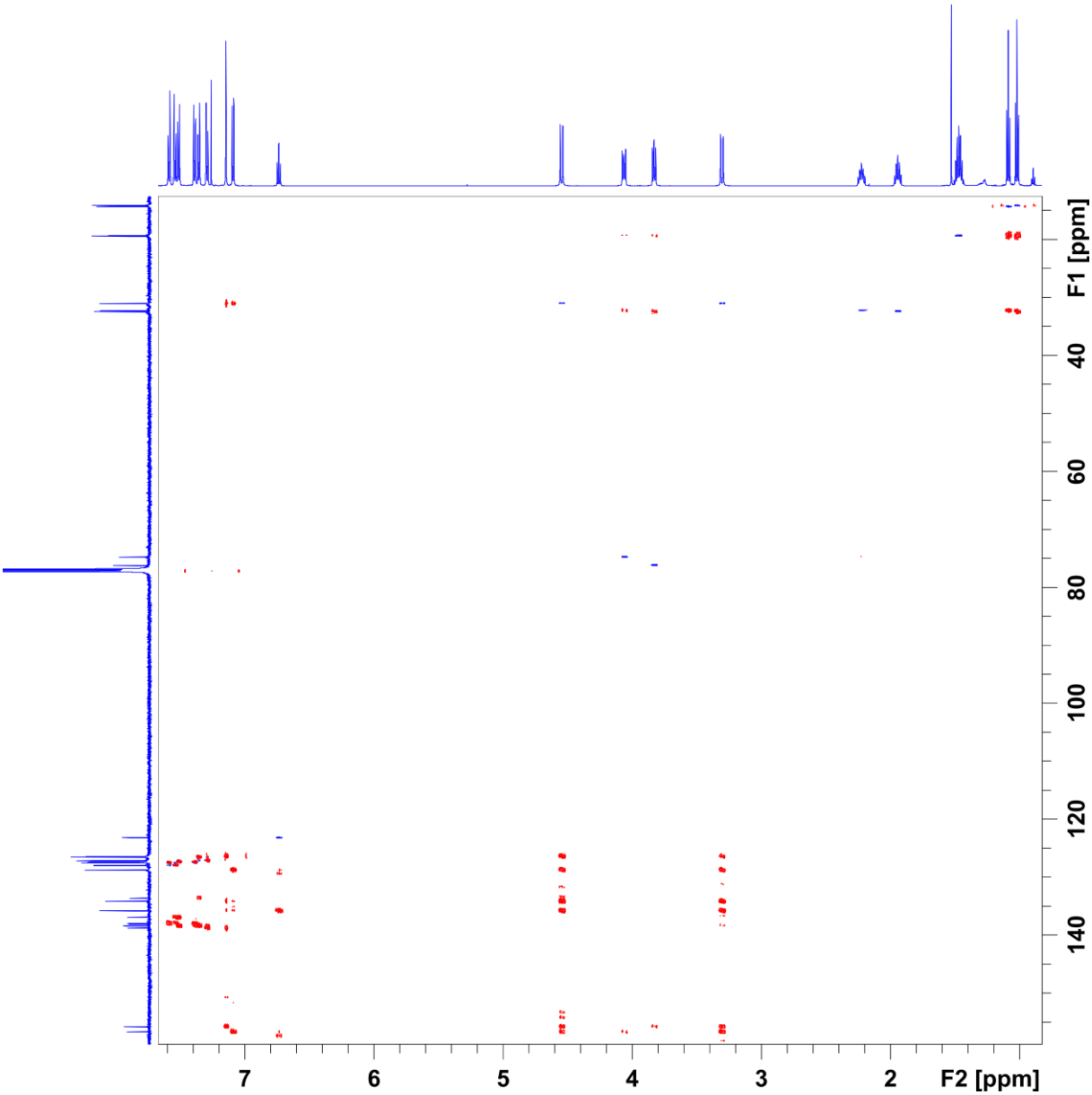

Figure S3. Overlaid HSQC (blue) and HMBC (red) spectra of **1** (600 MHz, chloroform-*d*, 300 K).

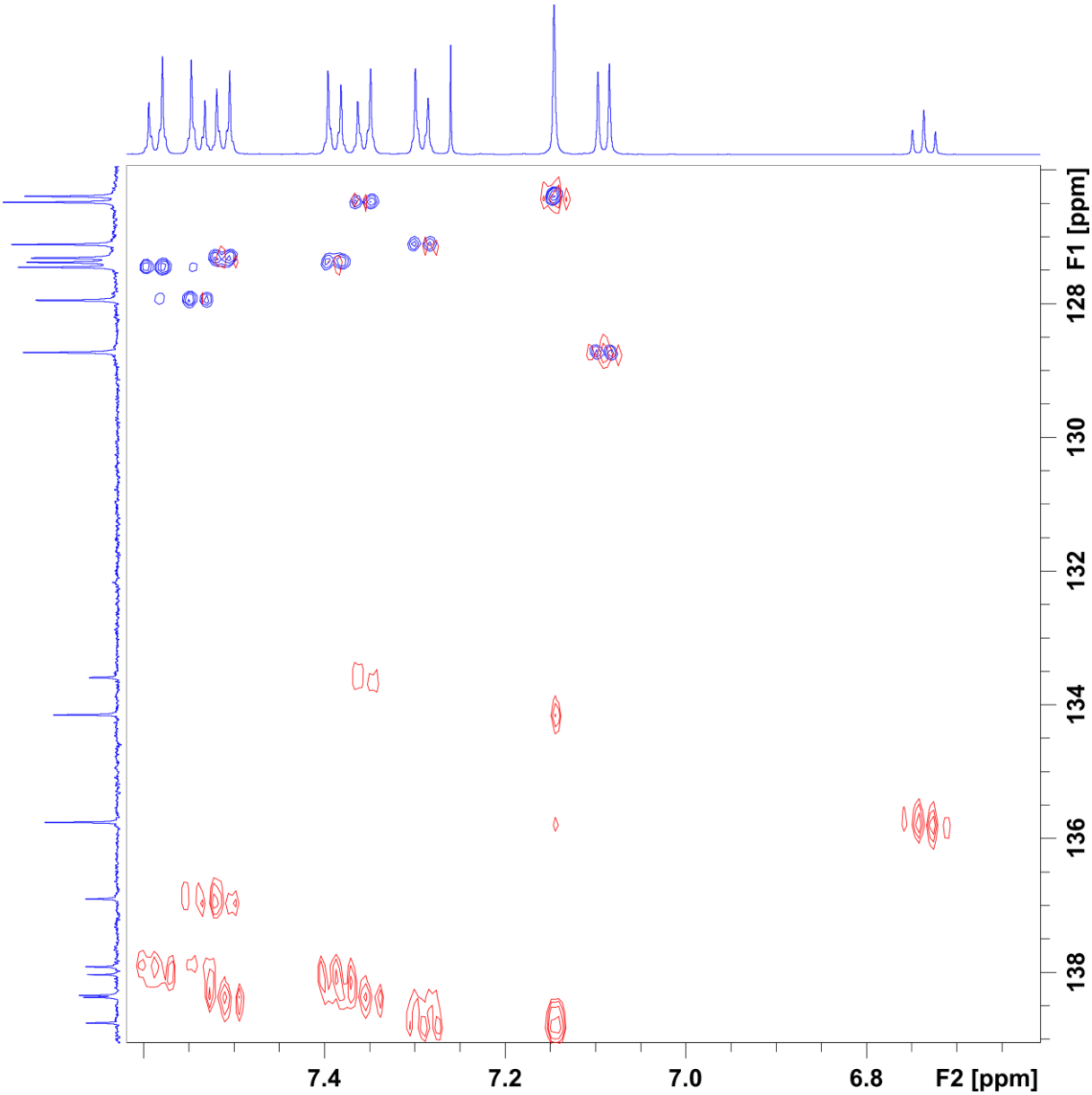

Figure S4. Partial HSQC (blue) and HMBC (red) spectra of **1** (600 MHz, chloroform-*d*, 300 K).

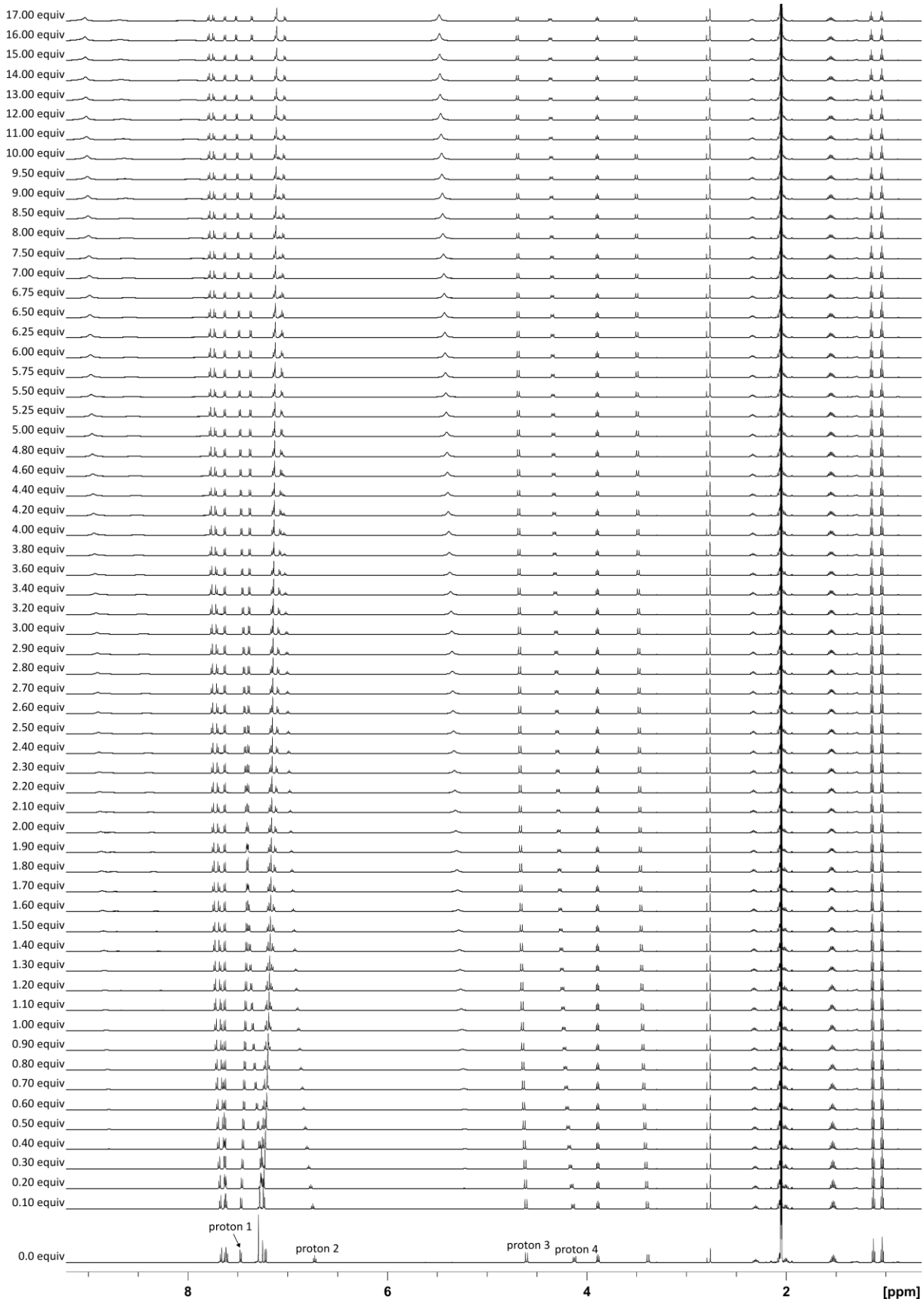

Figure S5. ^{1}H NMR titration spectra (600 MHz, acetone-d_6, 300 K) obtained upon addition of 0–17 equiv. of a 10.87 mM solution of $[DQ^{2+}][PF_6^{-}]_2$, prepared with a 1.81 mM solution of **1**, to a 1.81 mM solution of **1**.

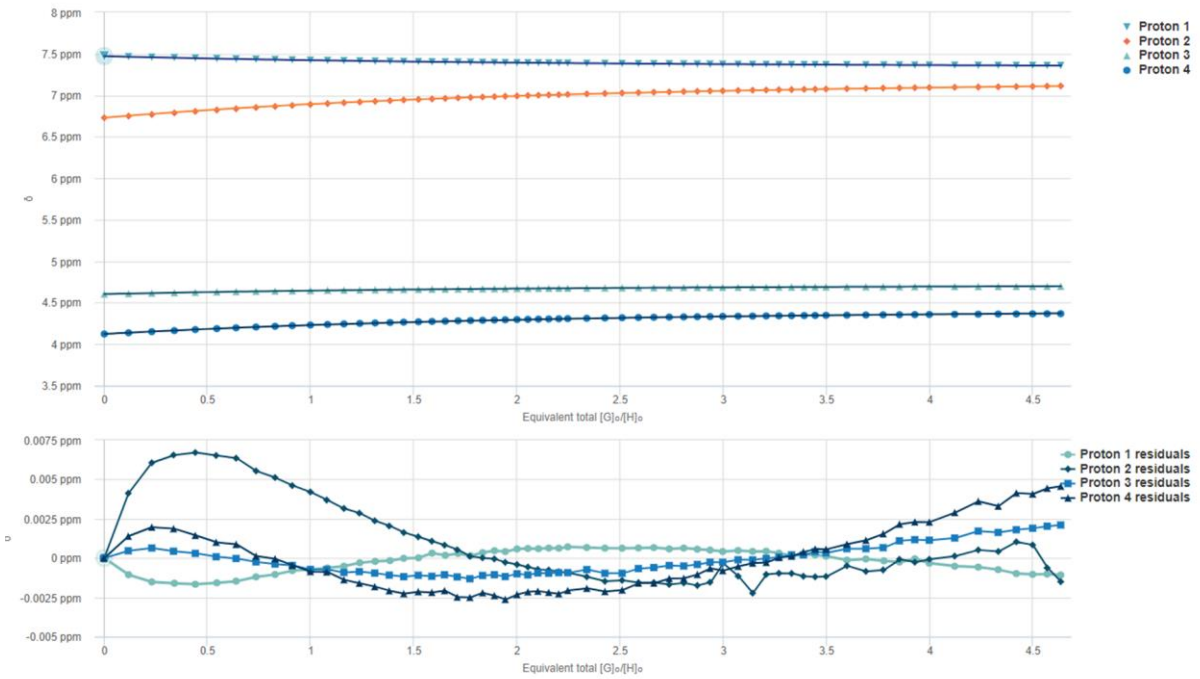

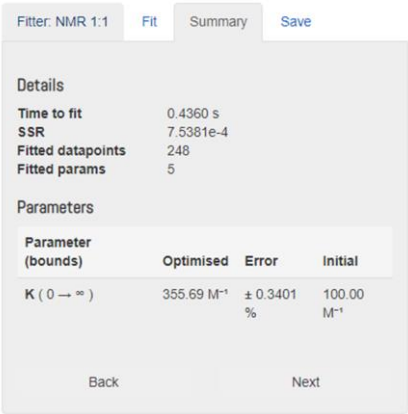

Fitter: NMR 1:1 | Fit | Summary | Save

Details

Time to fit	0.4360 s
SSR	7.5381e-4
Fitted datapoints	248
Fitted params	5

Parameters

Parameter (bounds)	Optimised	Error	Initial
K (0 → ∞)	355.69 M^{-1}	± 0.3401 %	100.00 M^{-1}

Back | Next

Figure S6. Nonlinear least-squares analysis of the ^{1}H NMR binding data (**Figure S5**) corresponding to the formation of [**1**⊃DQ^{2+}][PF_6^-]$_2$ complex. The data were fitted to a 1:1 (host:guest) binding model to give K_{11} = 3.56(1)·10^2 M^{-1}. The residual distribution is shown below the binding isotherm. All solid lines were obtained from non-linear curve-fitting with the Nelder–Mead method to a 1:1 binding model using the http://supramolecular.org/ web applet.

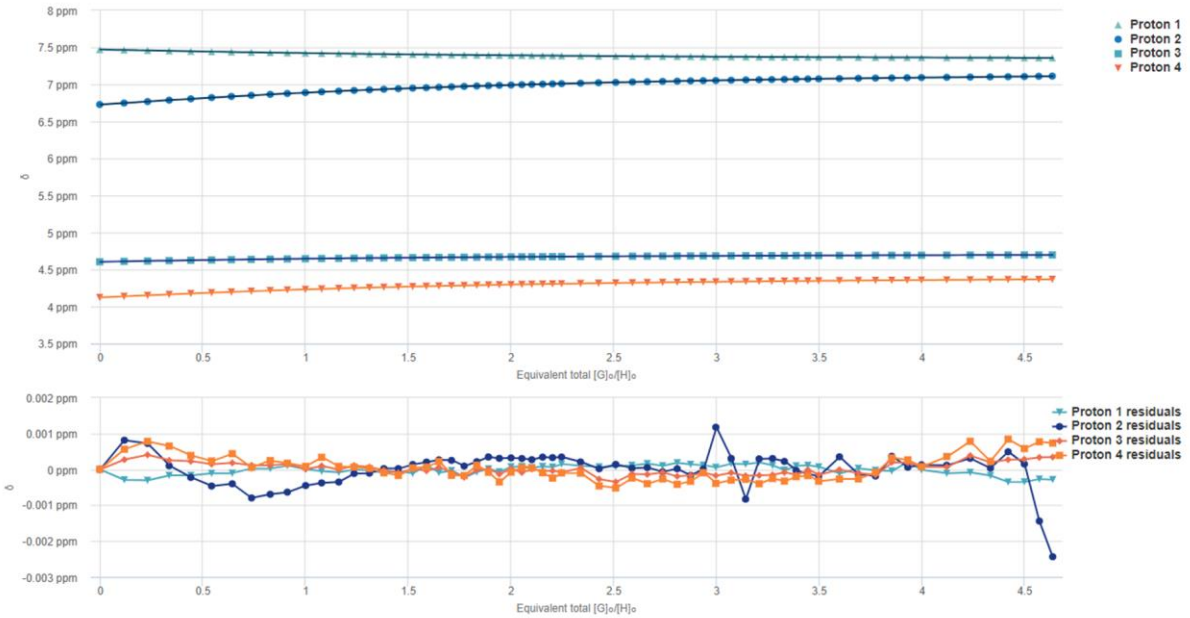

Fitter: NMR 2:1 | Fit | Summary | Save

Details

Time to fit	3.1979 s
SSR	2.6513e-5
Fitted datapoints	248
Fitted params	10

Parameters

Parameter (bounds)	Optimised	Error	Initial
K_{11} (0 → ∞)	603.37 M^{-1}	± 0.3700 %	100.00 M^{-1}
K_{21} (0 → ∞)	33.63 M^{-1}	± 1.0099 %	10.00 M^{-1}

Back | Next

Figure S7. Nonlinear least-square analysis of the ^{1}H NMR binding data (**Figure S5**) corresponding to the formation of [**1**⊃DQ^{2+}][PF_6^-]$_2$ and [**1**$_2$⊃DQ^{2+}][PF_6^-]$_2$ complexes. The data were fitted to a 2:1 (host:guest) binding model to give K_{11} = 6.03(2)·10^2 M^{-1} and K_{21} = 3.36(3)·10^1 M^{-1}. The residual distribution is shown below the binding isotherm. All solid lines were obtained from non-linear curve-fitting with the Nelder-Mead method to a 2:1 binding model using the http://supramolecular.org/ web applet.

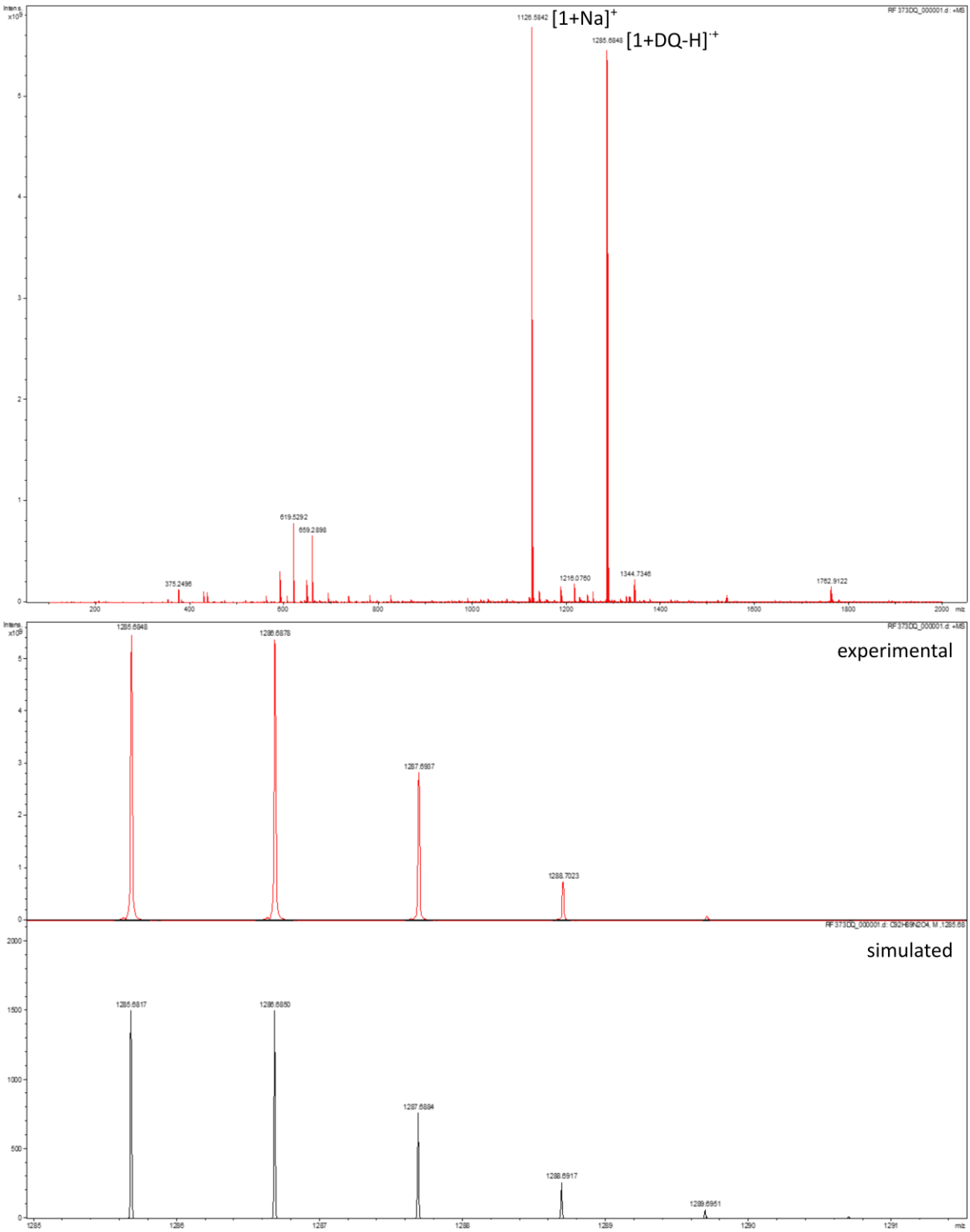

Figure S8. ESI-TOF mass spectrum of an equimolar mixture of **1** and $[DQ^{2+}][PF_6^-]_2$ in acetone. $[\mathbf{1}+DQ-H]^{\cdot+}$ = $C_{92}H_{89}N_2O_4$.

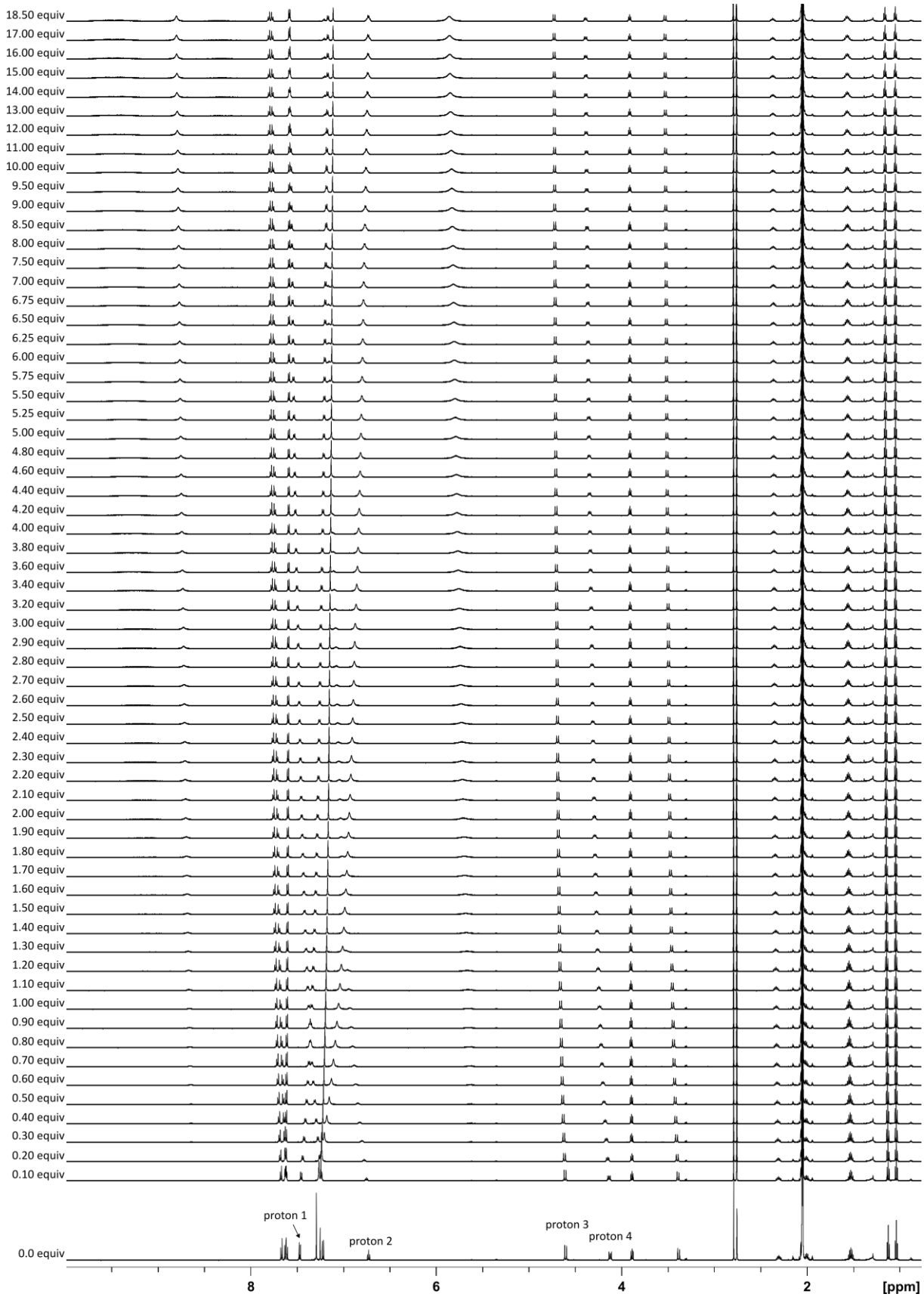

Figure S9. ^{1}H NMR titration spectra (600 MHz, acetone-d_6, 300 K) obtained upon addition of 0–18.5 equiv of a 5.437 mM solution of $[PQ^{2+}][PF_6^{-}]_2$, prepared with a 0.906 mM solution of **1**, to a 0.906 mM solution of **1**.

Figure S10. Nonlinear least-square analysis of the ^{1}H NMR binding data (**Figure S9**) corresponding to the formation of [**1**⊃PQ^{2+}][PF_6^-]$_2$ complex. The data were fitted to a 1:1 (host:guest) binding model to give K_{11} = 7.19(3)·10^2 M^{-1}. The residual distribution is shown below the binding isotherm. All solid lines were obtained from non-linear curve-fitting with the Nelder–Mead method to a 1:1 binding model using the http://supramolecular.org/ web applet.

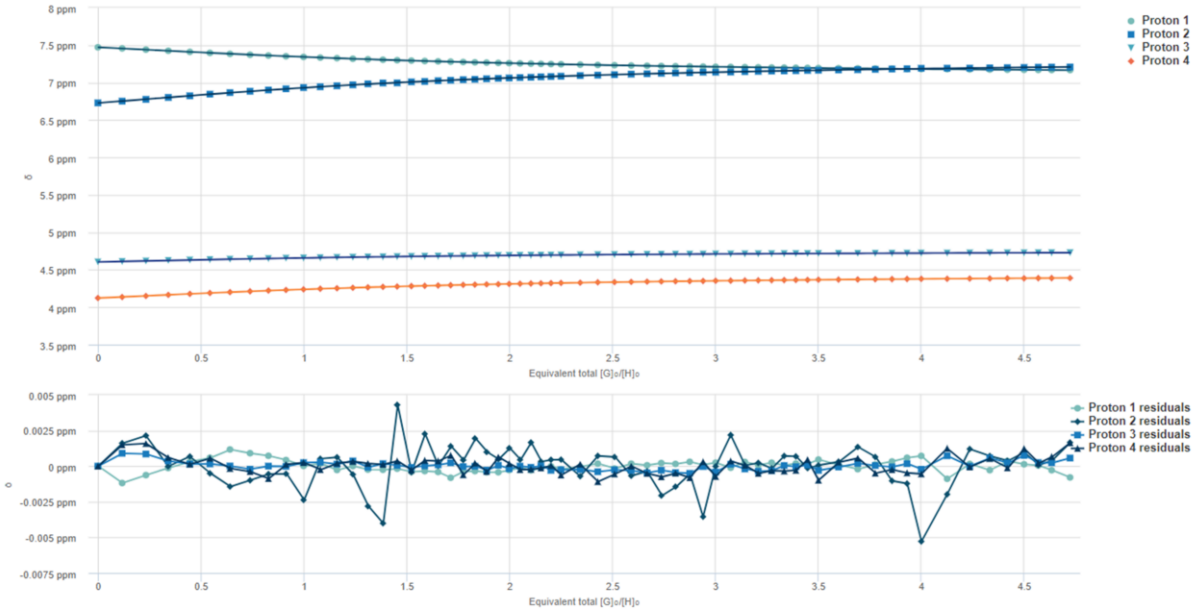

Details

Time to fit	3.6179 s
SSR	1.8773e-4
Fitted datapoints	252
Fitted params	10

Parameters

Parameter (bounds)	Optimised	Error	Initial
K_{11} (0 → ∞)	1429.51 M^{-1}	± 0.9369 %	1000.00 M^{-1}
K_{21} (0 → ∞)	178.59 M^{-1}	± 1.9911 %	100.00 M^{-1}

Back Next

Figure S11. Nonlinear least-square analysis of the ^{1}H NMR binding data (**Figure S9**) corresponding to the formation of [**1**⊃PQ^{2+}][PF_6^-]$_2$ and [**1**$_2$⊃PQ^{2+}][PF_6^-]$_2$ complexes. The data were fitted to a 2:1 (host:guest) binding model to give K_{11} = 1.43(1)·10^3 M^{-1} and K_{21} = 1.78(4)·10^2 M^{-1}. The residual distribution is shown below the binding isotherm. All solid lines were obtained from non-linear curve-fitting with the Nelder–Mead method to a 2:1 binding model using the http://supramolecular.org/ web applet.

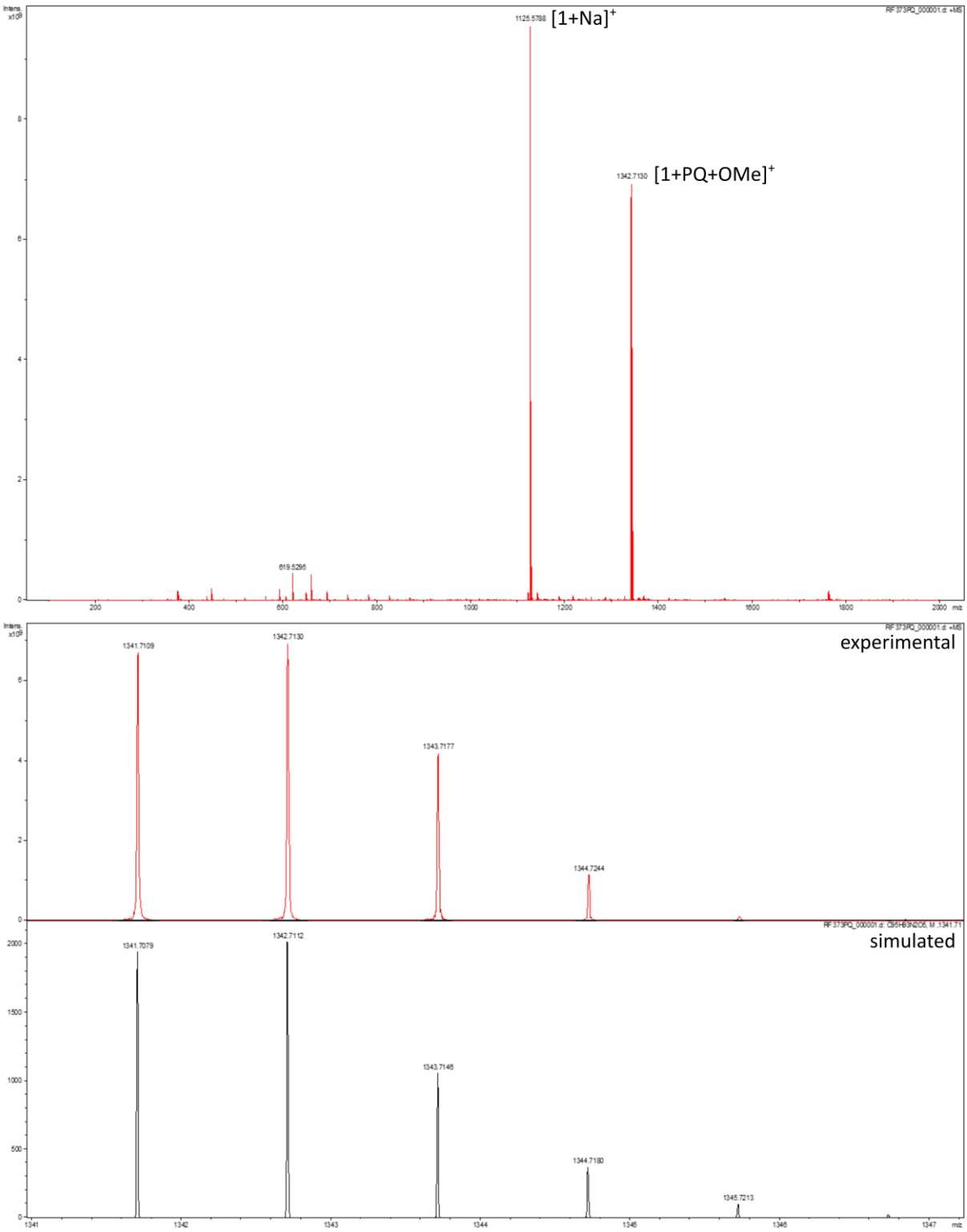

Figure S12. ESI-TOF mass spectrum of an equimolar mixture of **1** and $[PQ^{2+}][PF_6^-]_2$ in acetone. [**1**+PQ+OMe]$^+$ = $C_{95}H_{93}N_2O_5$.

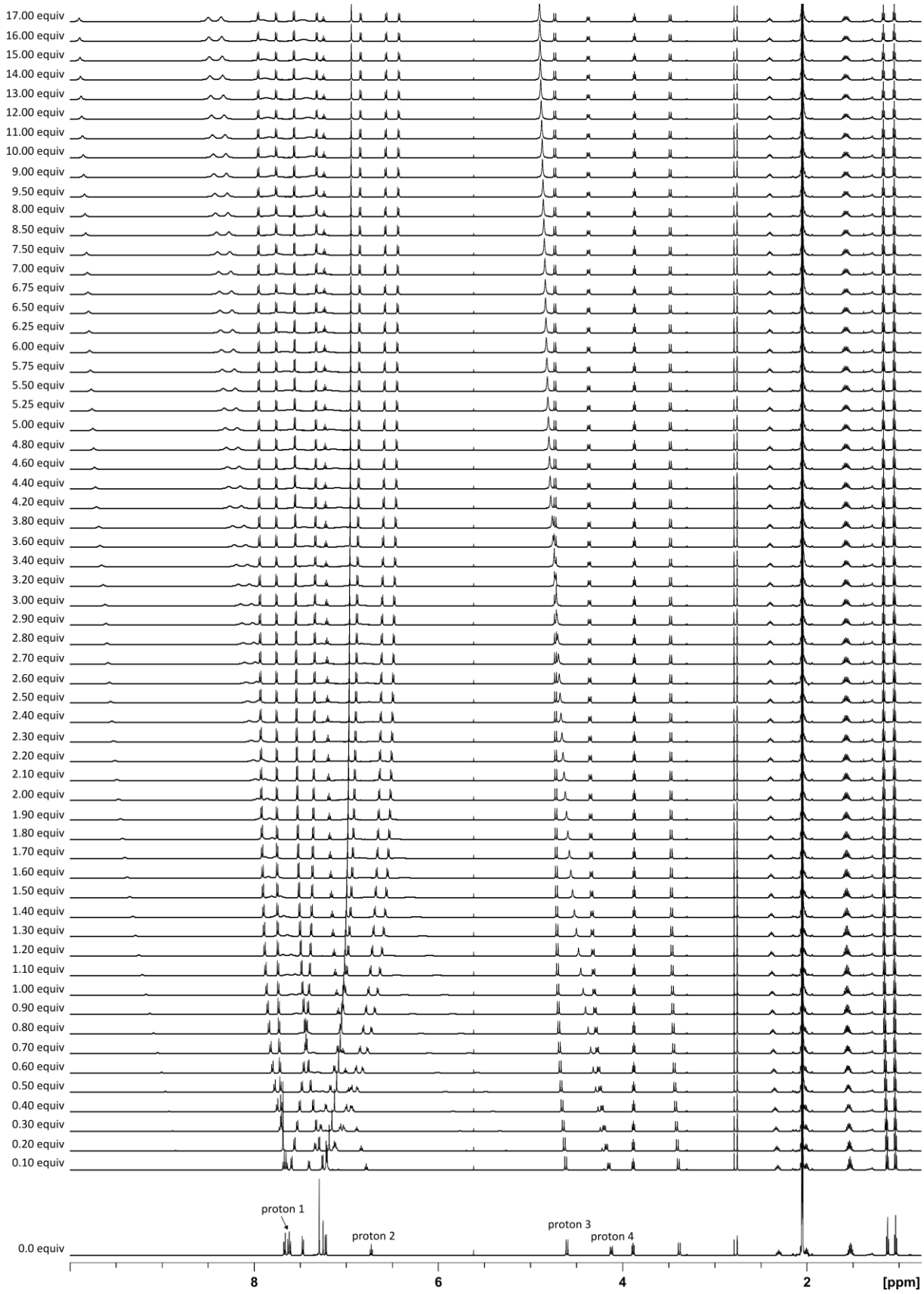

Figure S13. ^{1}H NMR titration spectra (600 MHz, acetone-d_6, 300 K) obtained upon addition of 0–17 equiv. of a 10.87 mM solution of [MA^{+}][PF$_6^{-}$], prepared with a 1.81 mM solution of **1**, to a 1.81 mM solution of **1**.

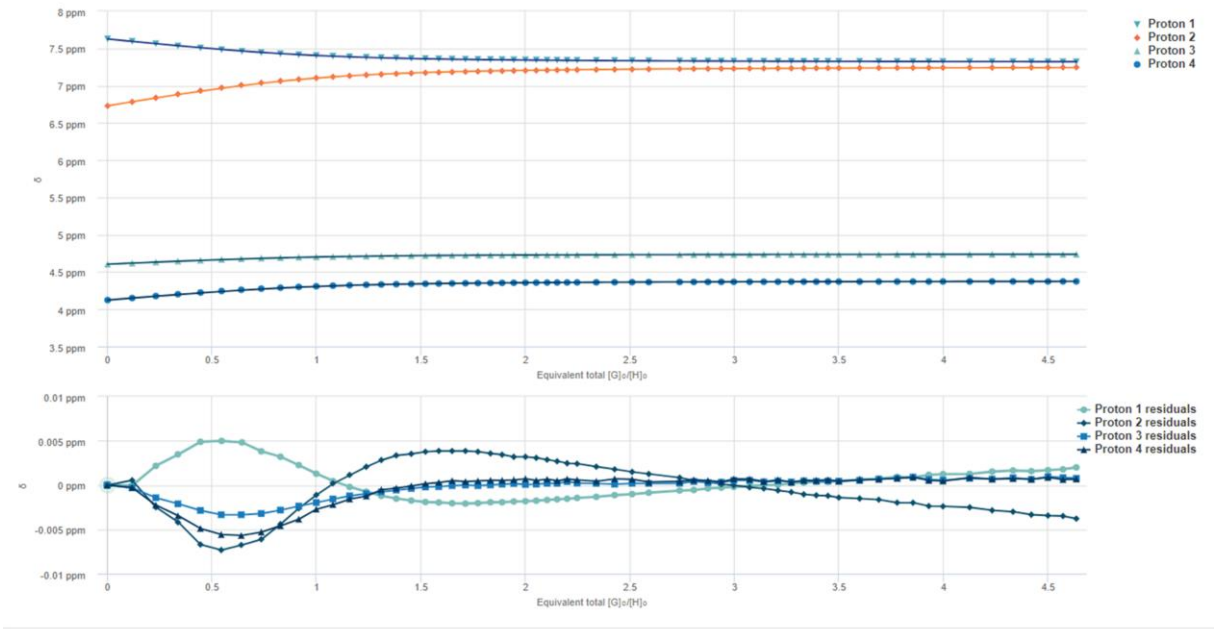

Details

Time to fit	0.3042 s
SSR	1.0275e-3
Fitted datapoints	244
Fitted params	5

Parameters

Parameter (bounds)	Optimised	Error	Initial
K (0 → ∞)	4372.81 M⁻¹	± 1.0202 %	1000.00 M⁻¹

Back Next

Figure S14. Nonlinear least-square analysis of the ^{1}H NMR binding data (**Figure S13**) corresponding to the formation of [**1**⊃MA^+][PF_6^-] complex. The data were fitted to a 1:1 (host:guest) binding model to give K_{11} = 4.37(4)·10^3 M^{-1}. The residual distribution is shown below the binding isotherm. All solid lines were obtained from non-linear curve-fitting with the Nelder–Mead method to a 1:1 binding model using the http://supramolecular.org/ web applet.

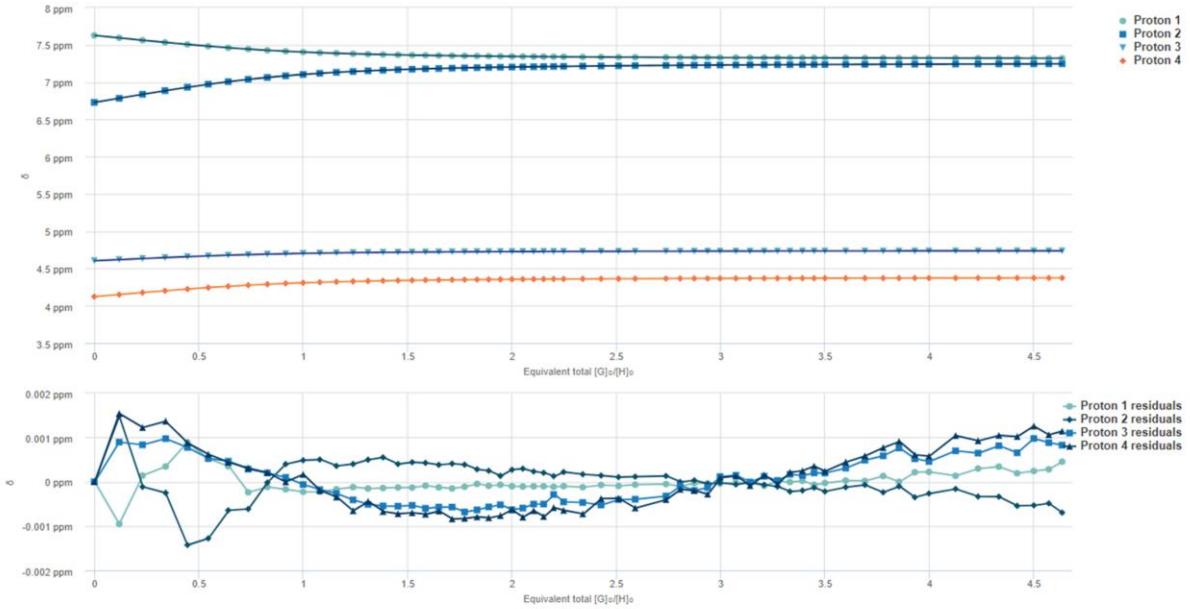

Details

Time to fit	3.7762 s
SSR	6.0726e-5
Fitted datapoints	244
Fitted params	10

Parameters

Parameter (bounds)	Optimised	Error	Initial
K_{11} (0 → ∞)	5918.73 M^{-1}	± 1.2136 %	1000.00 M^{-1}
K_{21} (0 → ∞)	434.57 M^{-1}	± 3.3114 %	100.00 M^{-1}

Back Next

Figure S15. Nonlinear least-square analysis of the ^{1}H NMR binding data (**Figure S13**) corresponding to the formation of [**1**⊃MA^+][PF_6^-] and [$\mathbf{1}_2$⊃MA^+][PF_6^-] complexes. The data were fitted to a 2:1 (host:guest) binding model to give K_{11} = 5.92(7)·10^3 M^{-1} and K_{21} = 4.3(1)·10^2 M^{-1}. The residual distribution is shown below the binding isotherm. All solid lines were obtained from non-linear curve-fitting with the Nelder-Mead method to a 2:1 binding model using the http://supramolecular.org/ web applet.

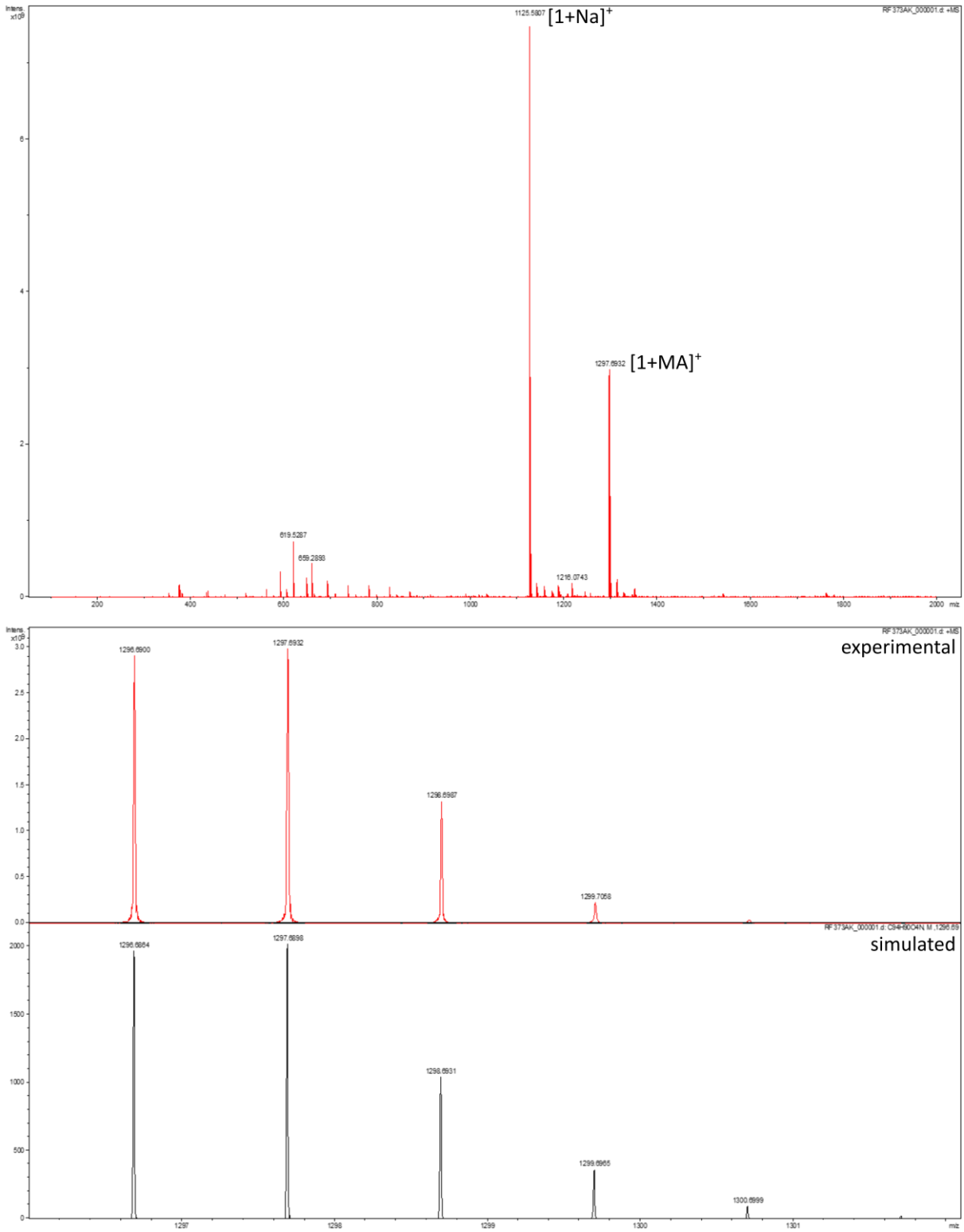

Figure S16. ESI-TOF mass spectrum of an equimolar mixture of **1** and $[MA^+][PF_6]$ in acetone. $[\mathbf{1}+MA]^+$ = $C_{94}H_{90}NO_4$.

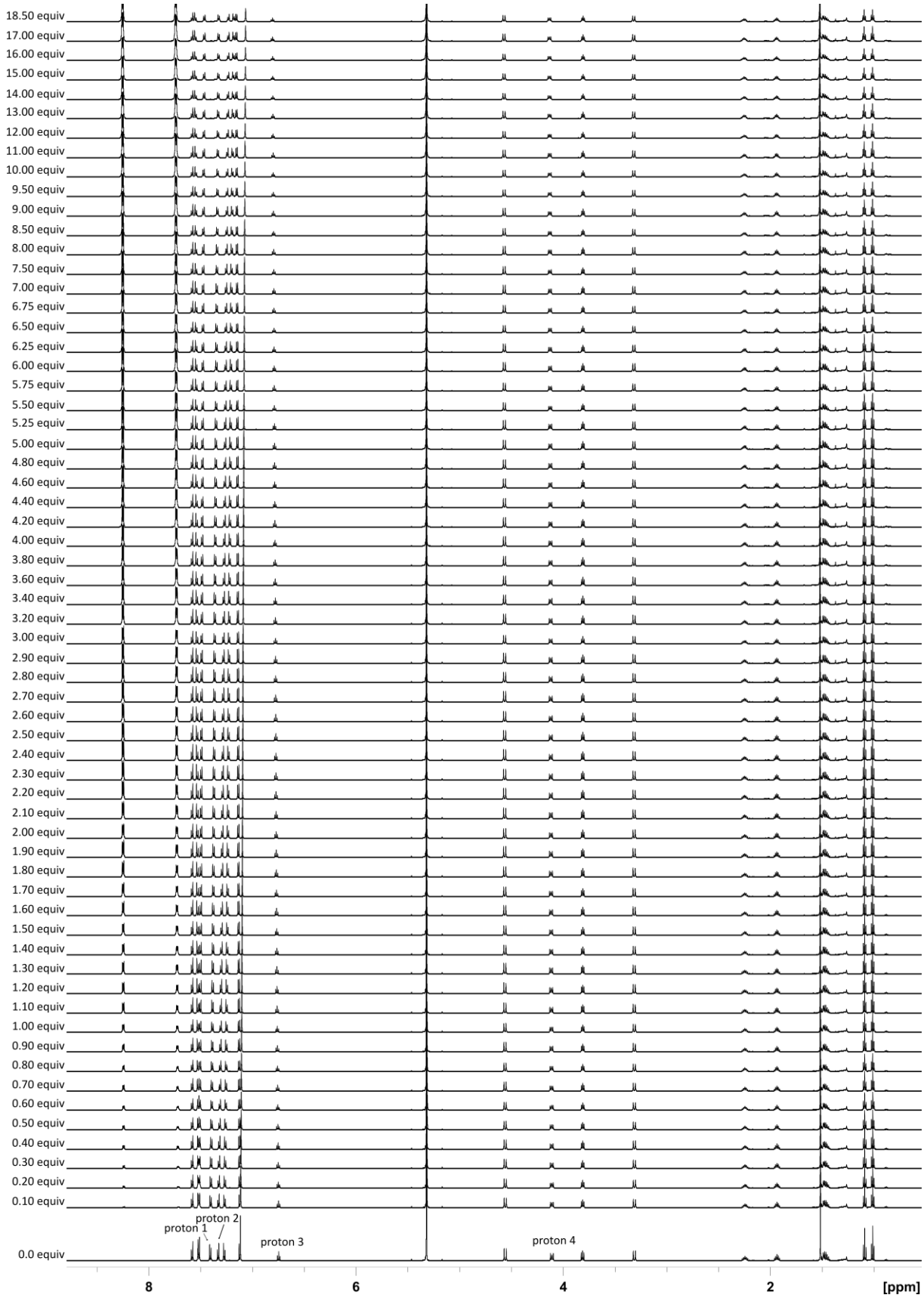

Figure S17. ^{1}H NMR titration spectra (600 MHz, dichoromethane-d_2, 300 K) obtained upon addition of 0-18.5 equiv. of a 10.87 mM solution of AQ, prepared with a 1.81 mM solution of **1**, to a 1.81 mM solution of **1**.

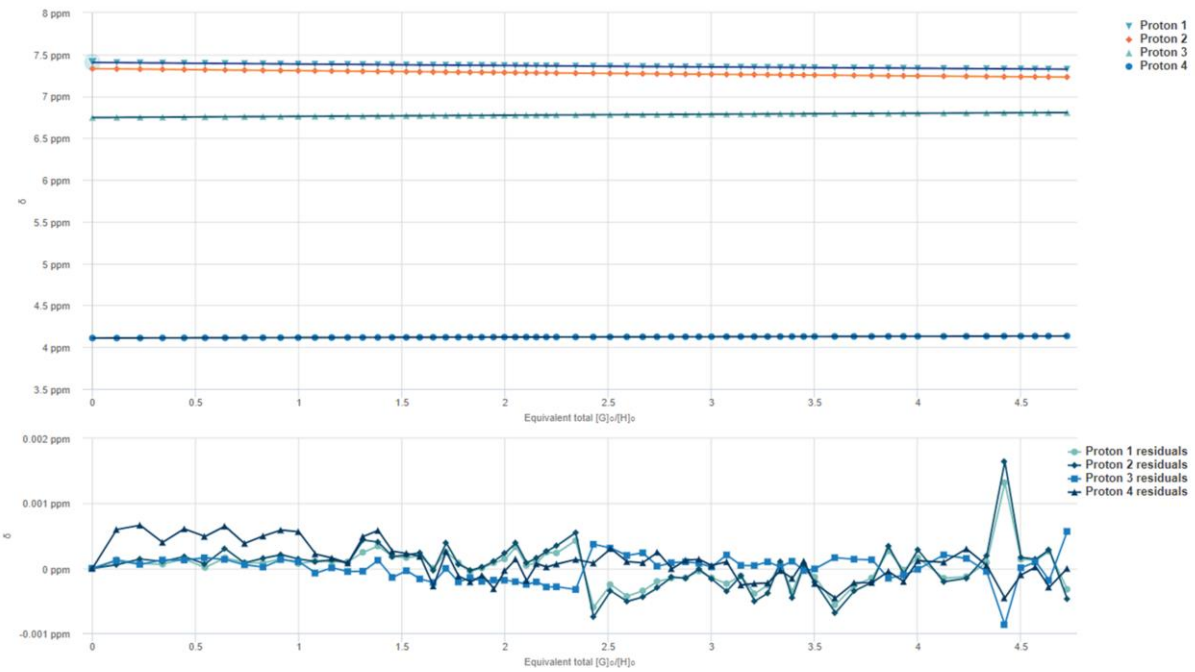

Details

Time to fit	0.4419 s
SSR	2.0602e-5
Fitted datapoints	252
Fitted params	5

Parameters

Parameter (bounds)	Optimised	Error	Initial
K (0 → ∞)	19.68 M⁻¹	± 0.0951 %	100.00 M⁻¹

Back Next

Figure S18. Nonlinear least-square analysis of the ^{1}H NMR binding data (**Figure S17**) corresponding to the formation of **1**⊃AQ complex. The data were fitted to a 1:1 (host:guest) binding model to give K_{11} = 1.968(2)·10^{1} M^{-1}. The residual distribution is shown below the binding isotherm. All solid lines were obtained from non-linear curve-fitting with the Nelder-Mead method to a 1:1 binding model using the http://supramolecular.org/ web applet.

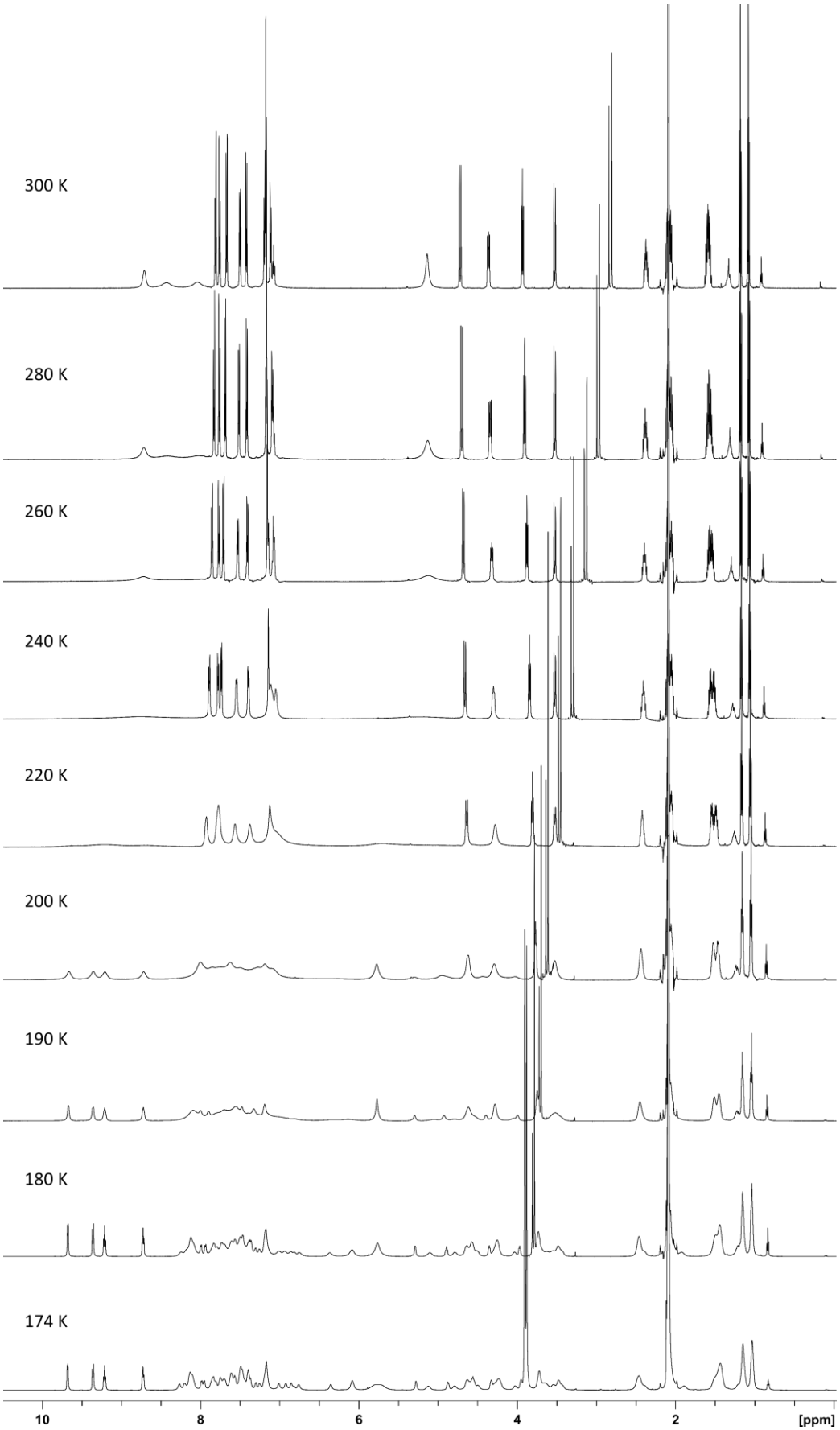

Figure S19. Variable temperature ^{1}H NMR spectra (600 MHz, acetone-d_6) of **1** with 1.5 equiv of $[DQ^{2+}][PF_6^-]_2$.

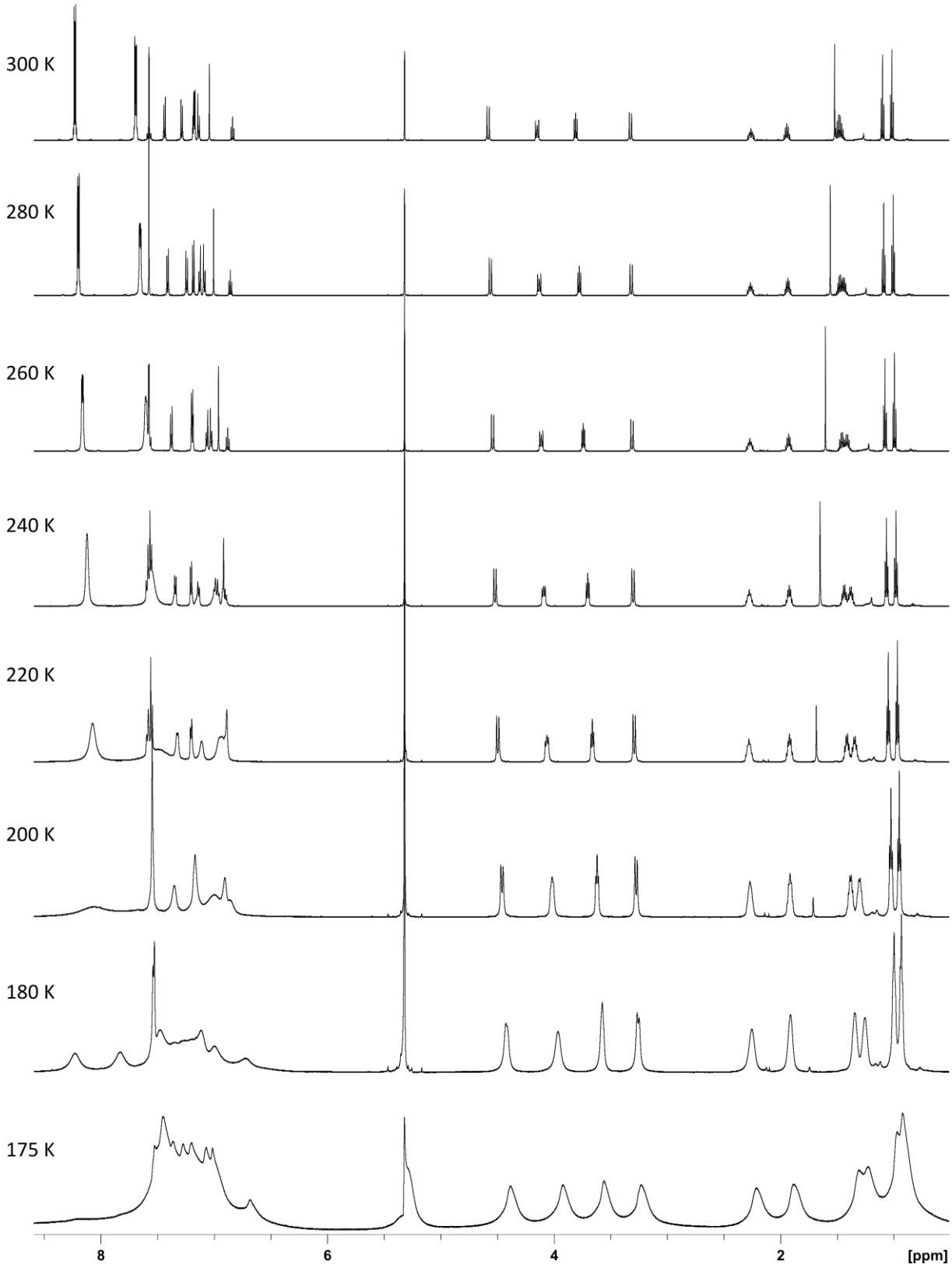

Figure S20. Variable temperature ^{1}H NMR spectra (600 MHz, dichloromethane-d_2) of **1** with 4.0 equiv of [AQ].

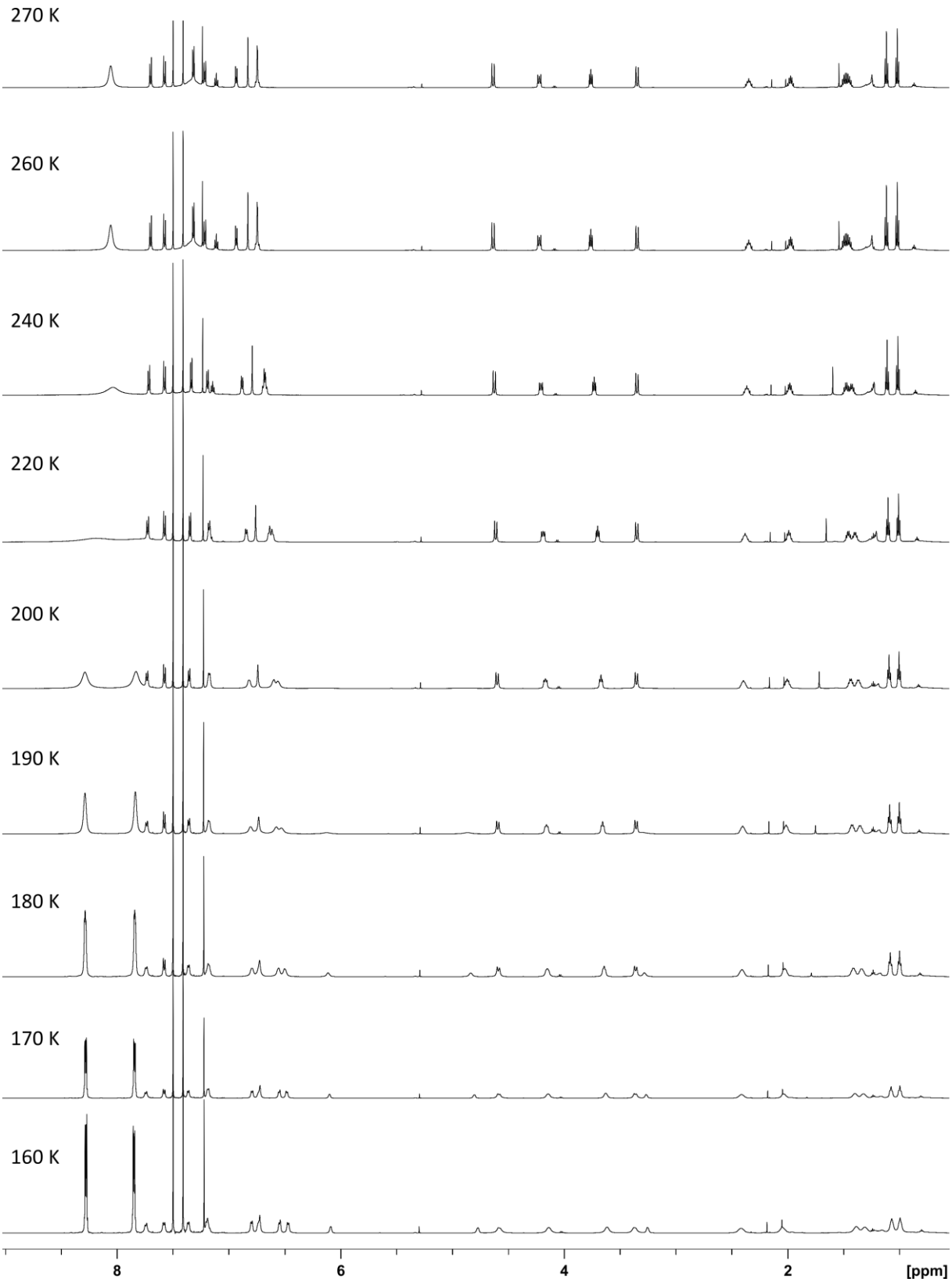

Figure S21. Variable temperature ^{1}H NMR spectra (600 MHz, DCFM-*d*) of **1** with 4.0 equiv of [AQ].

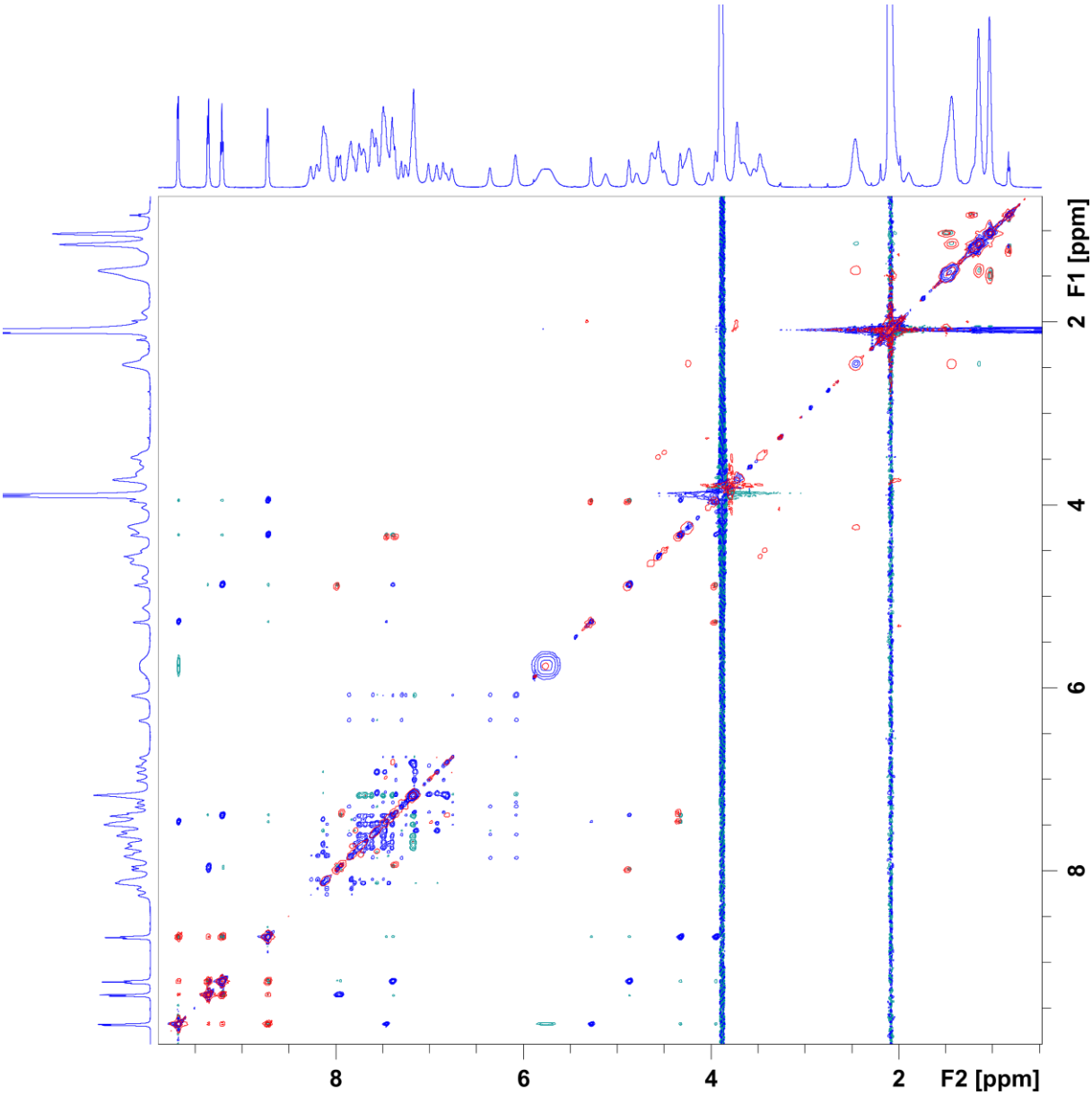

Figure S22. Overlaid ROESY (blue/green for positive/negative contours) and COSY (red) spectra of **1** with 1.5 equiv of $[DQ^{2+}][PF_6^-]_2$ (600 MHz, acetone-d_6, 174 K).

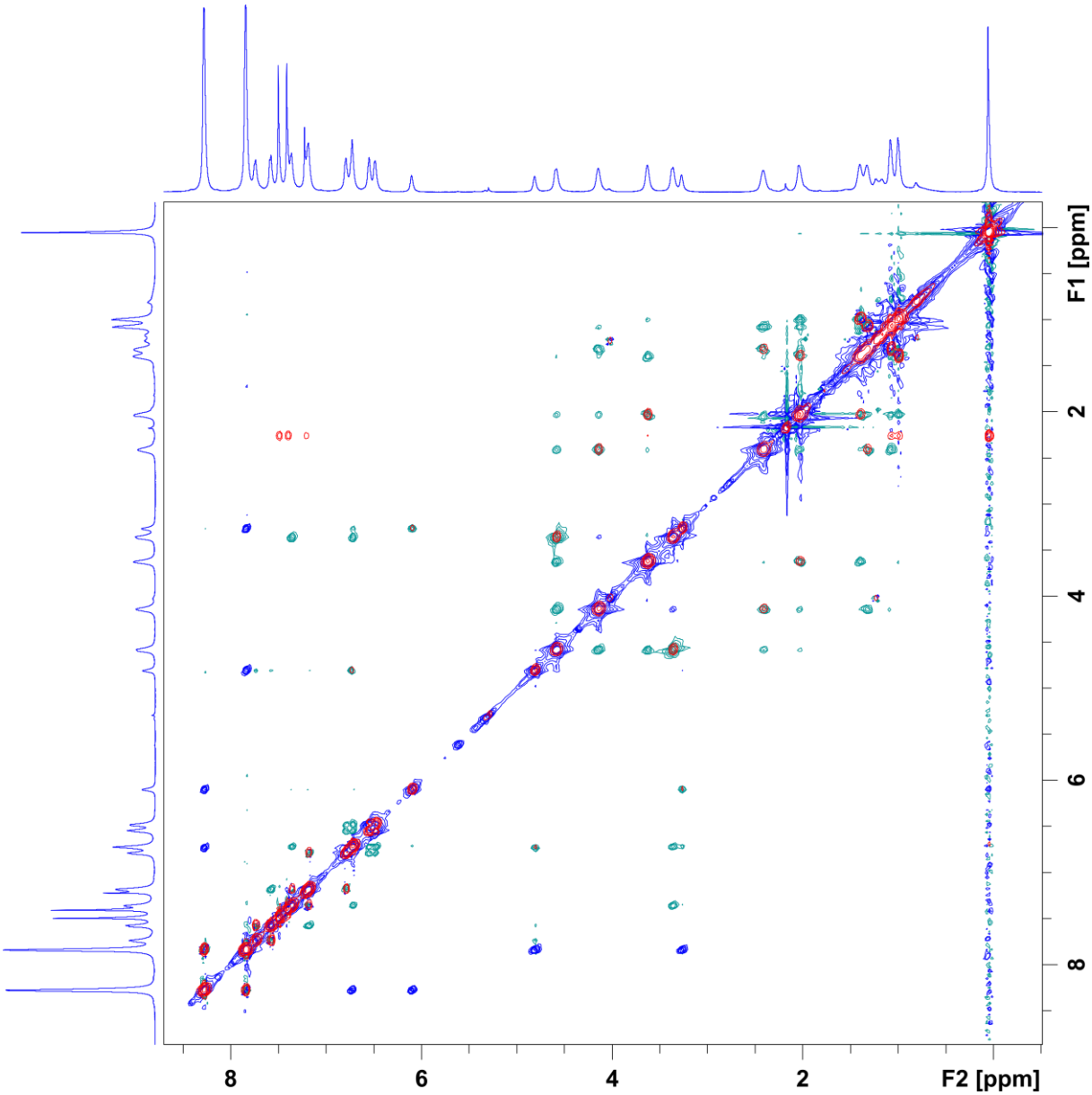

Figure S23. Overlaid ROESY (blue/green for positive/negative contours) and COSY (red) spectra of **1** with 4.0 equiv of AQ (600 MHz, DCFM-*d*, 170 K).

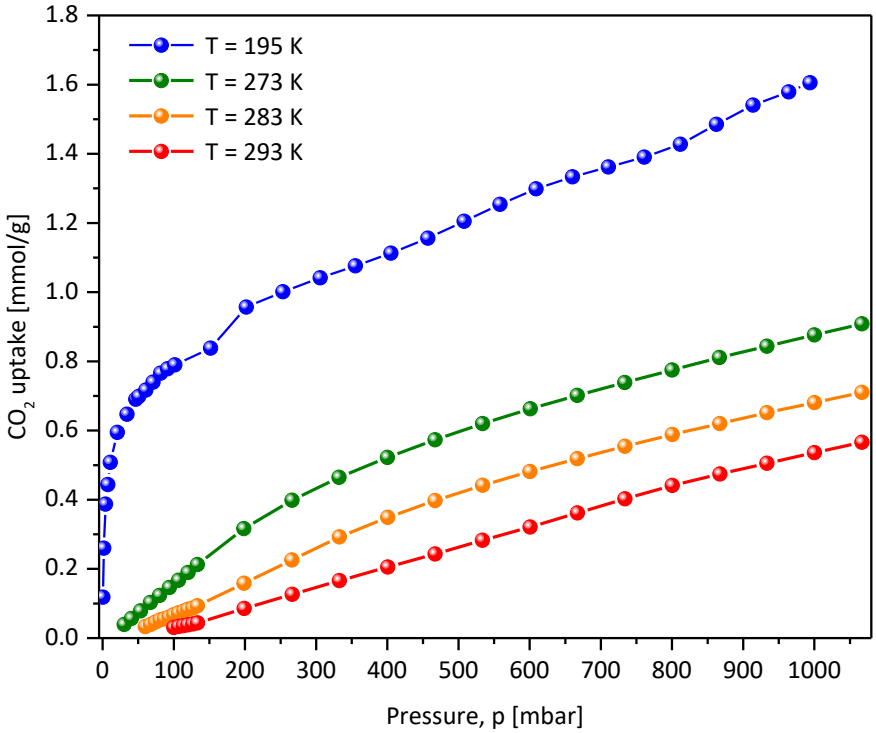

Figure S24. Experimental CO_2 adsorption isotherms for **1** at 195, 273, 283 and 293 K.

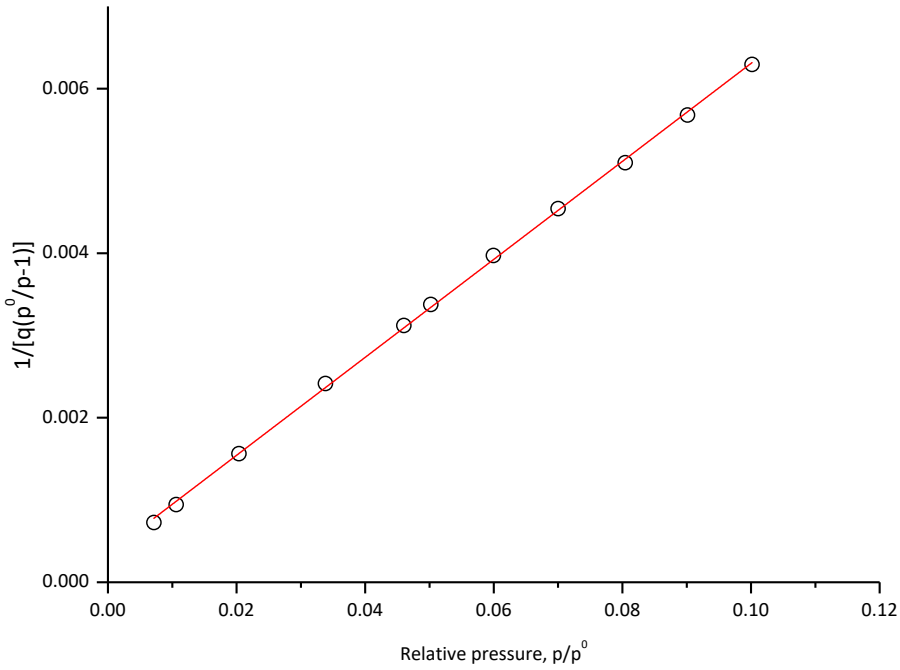

Figure S25. The BET plot derived from CO_2 isotherm at 195 K for **1**.

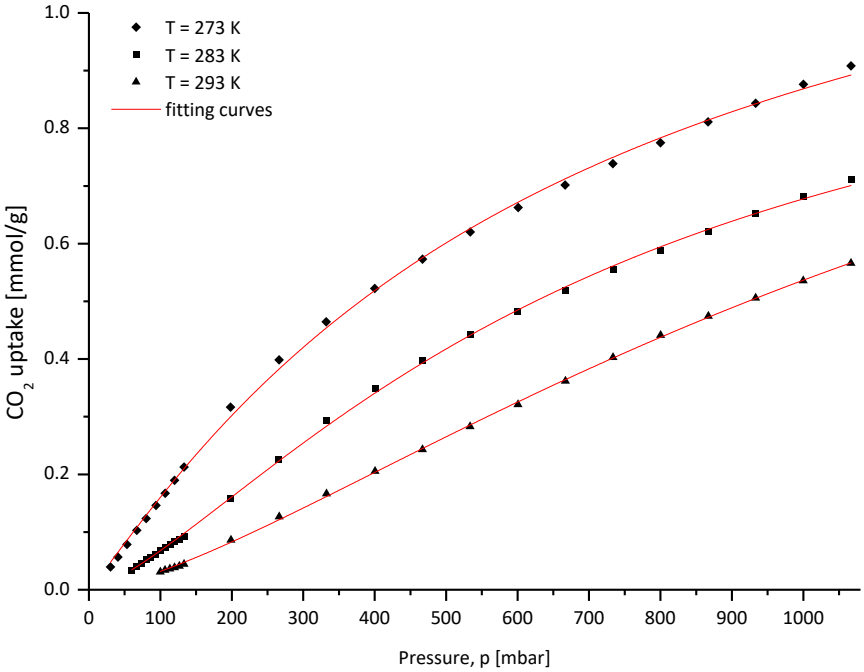

Figure S26. CO_2 isotherms for **1** at 273, 283 and 293 K fitted with Langmuir-Freundlich model curves.

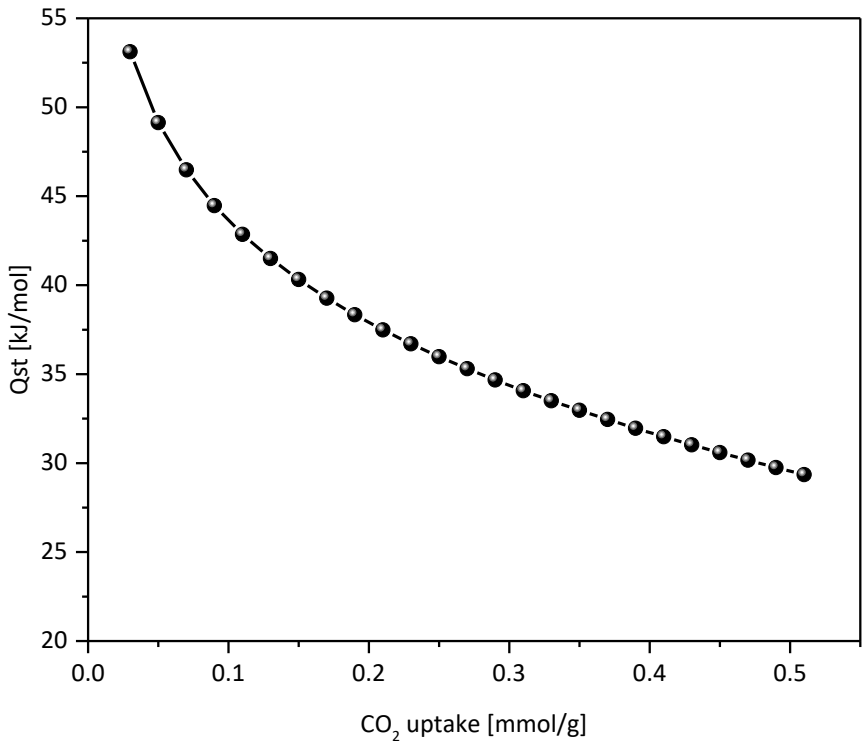

Figure S27. The CO_2 isosteric heat of adsorption plot for **1**.

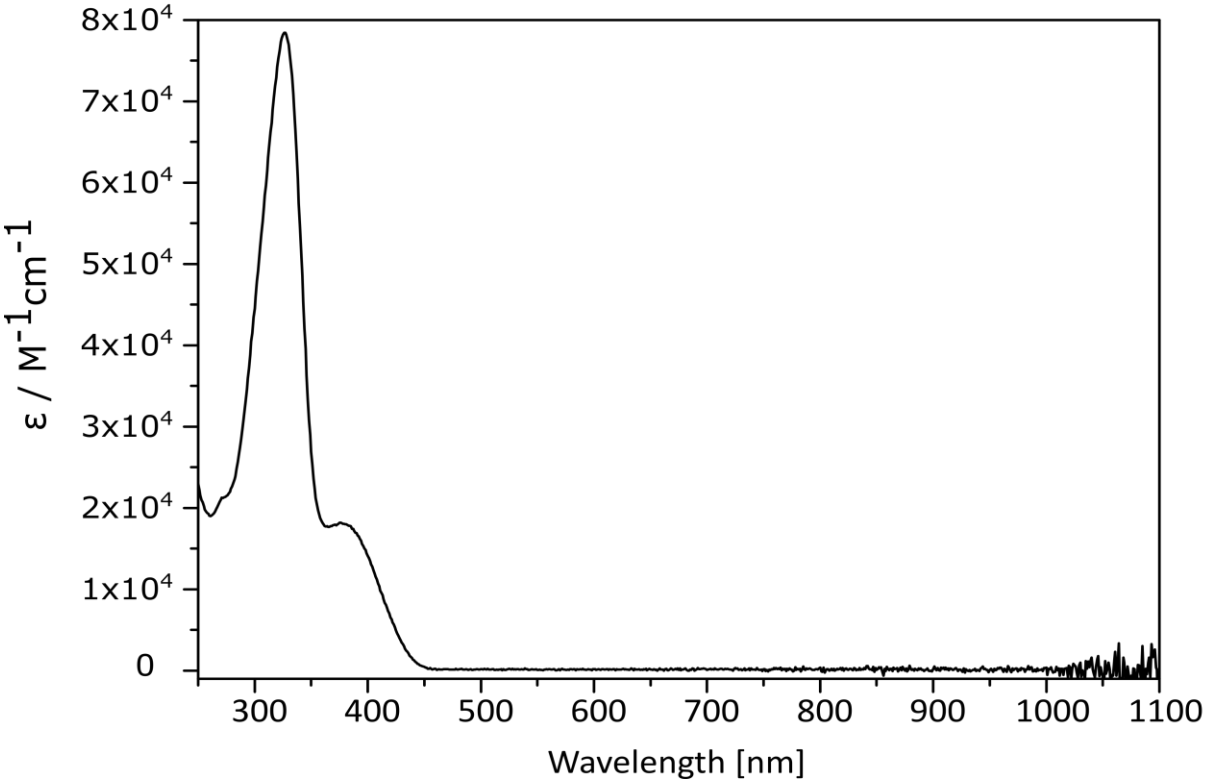

Figure S28. Absorption spectrum of **1** in dichloromethane (1 cm path length).

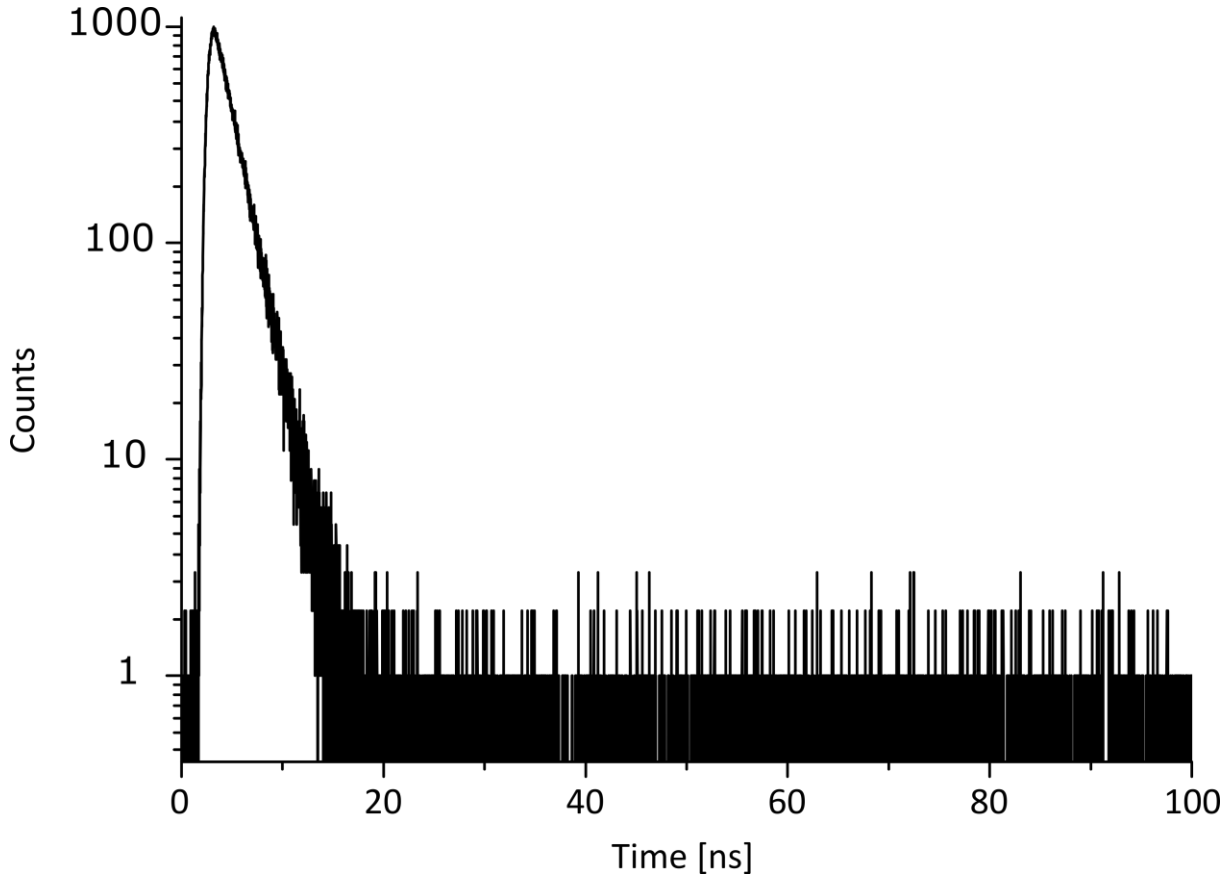

Figure S29. Fluorescence decay traces of **1** in dichloromethane (λ_{em} = 490 nm).

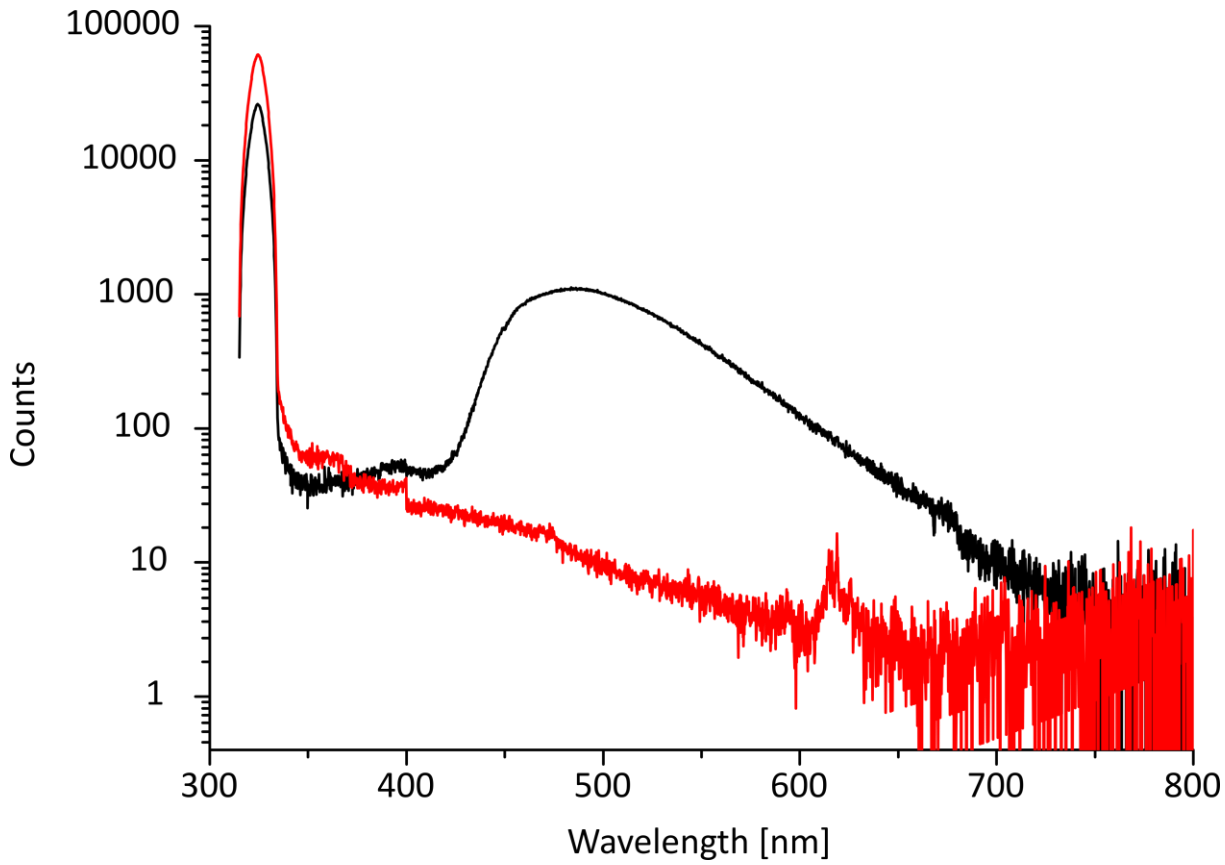

Figure S30. Spectra used for determination of the fluorescence quantum yield for compound **1** (black), solvent (red). Excitation range: 315.00 to 335.20 nm; luminescence range: 375.00 to 800.00 nm. QY = 33.45%.

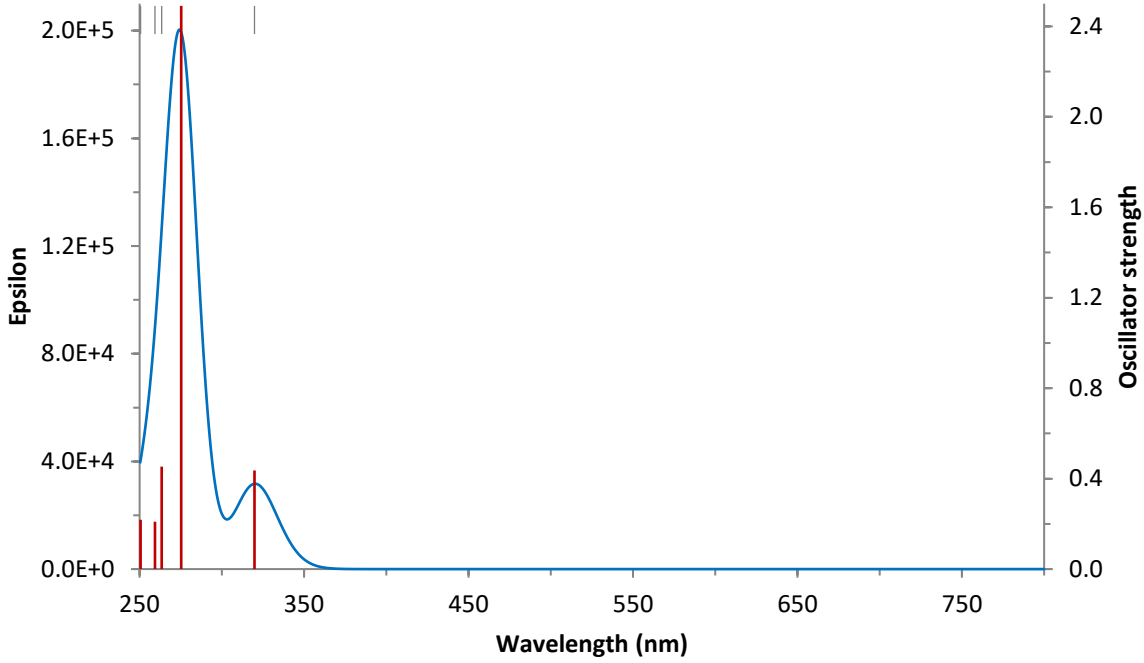

Figure S31. Simulated electronic absorption spectrum of **1** (TDA/PCM(acetone)/CAM-B3LYP-GD3BJ/6-31G(d,p)).

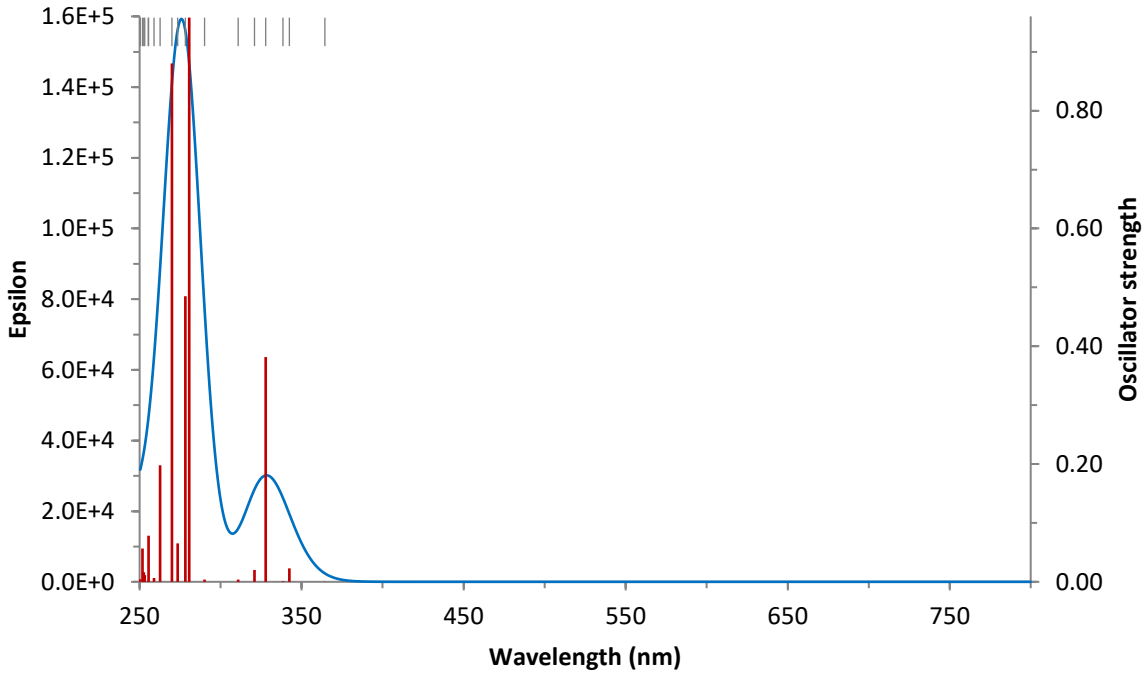

Figure S32. Simulated electronic absorption spectrum of [**1**⊃AQ] (TDA/PCM(acetone)/CAM-B3LYP-GD3BJ/6-31G(d,p)).

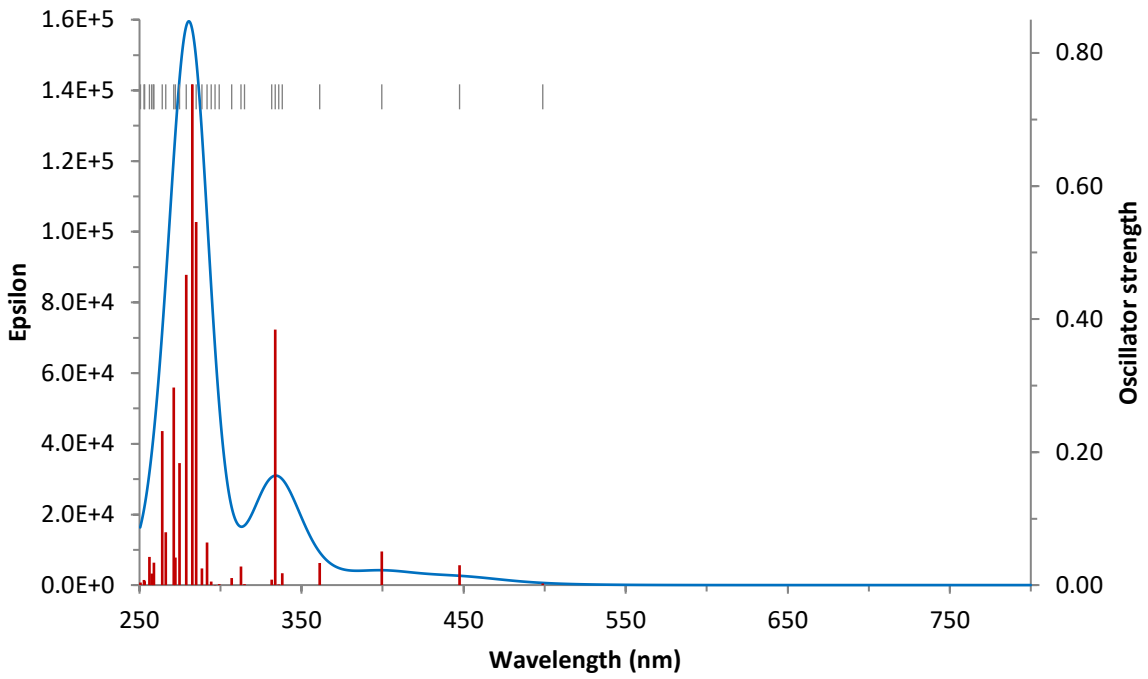

Figure S33. Simulated electronic absorption spectrum of [**1**⊃MA^+] (TDA/PCM(acetone)/CAM-B3LYP-GD3BJ/6-31G(d,p)).

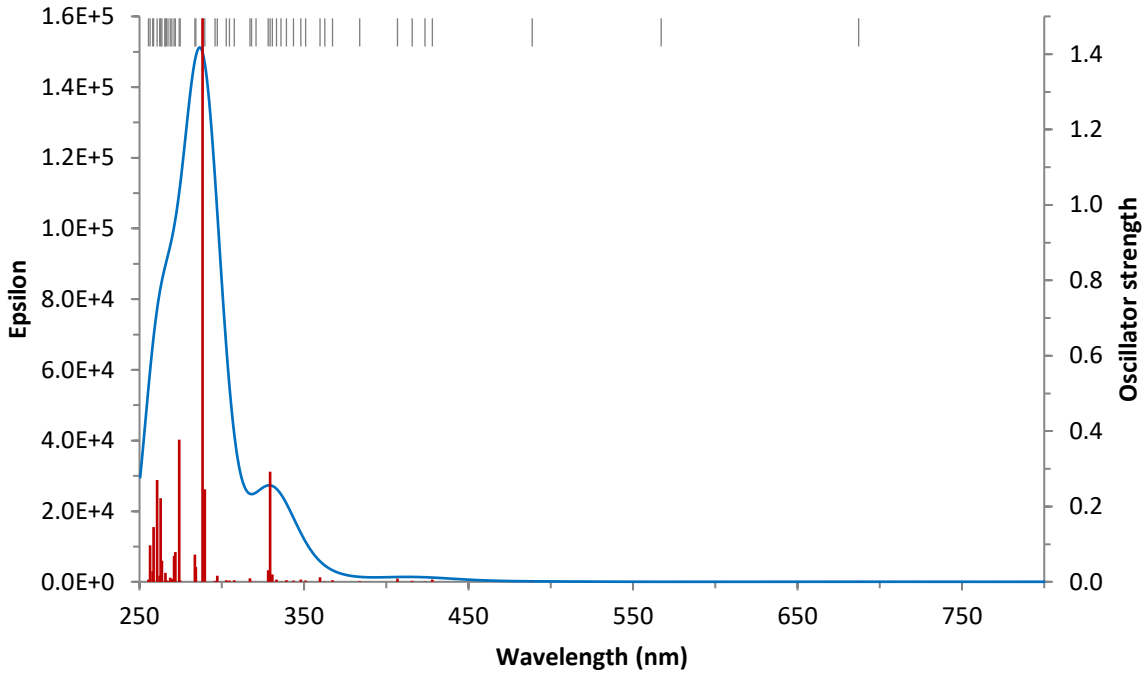

Figure S34. Simulated electronic absorption spectrum of [**1**⊃DQ^{2+}] (TDA/PCM(acetone)/CAM-B3LYP-GD3BJ/6-31G(d,p)).

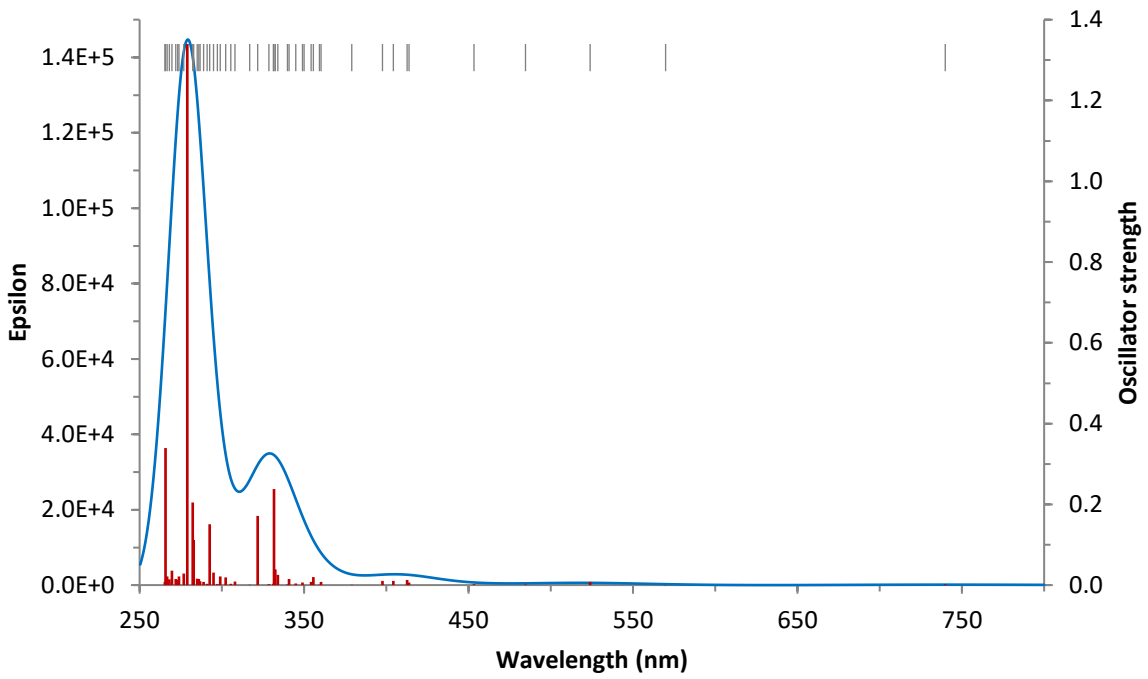

Figure S35. Simulated electronic absorption spectrum of [**1**⊃PQ^{2+}] (TDA/PCM(acetone)/CAM-B3LYP-GD3BJ/6-31G(d,p)).

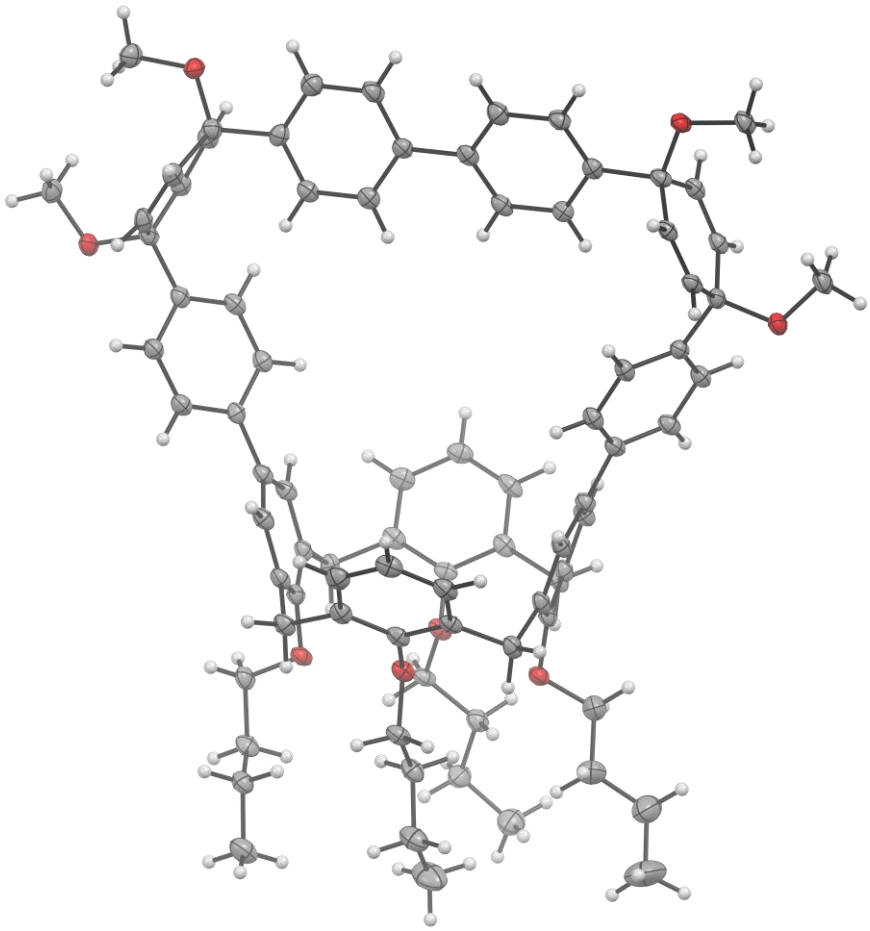

Figure S36. Crystal structure of **5**·C_6H_{14}·H_2O. Solvent molecules are removed for clarity.

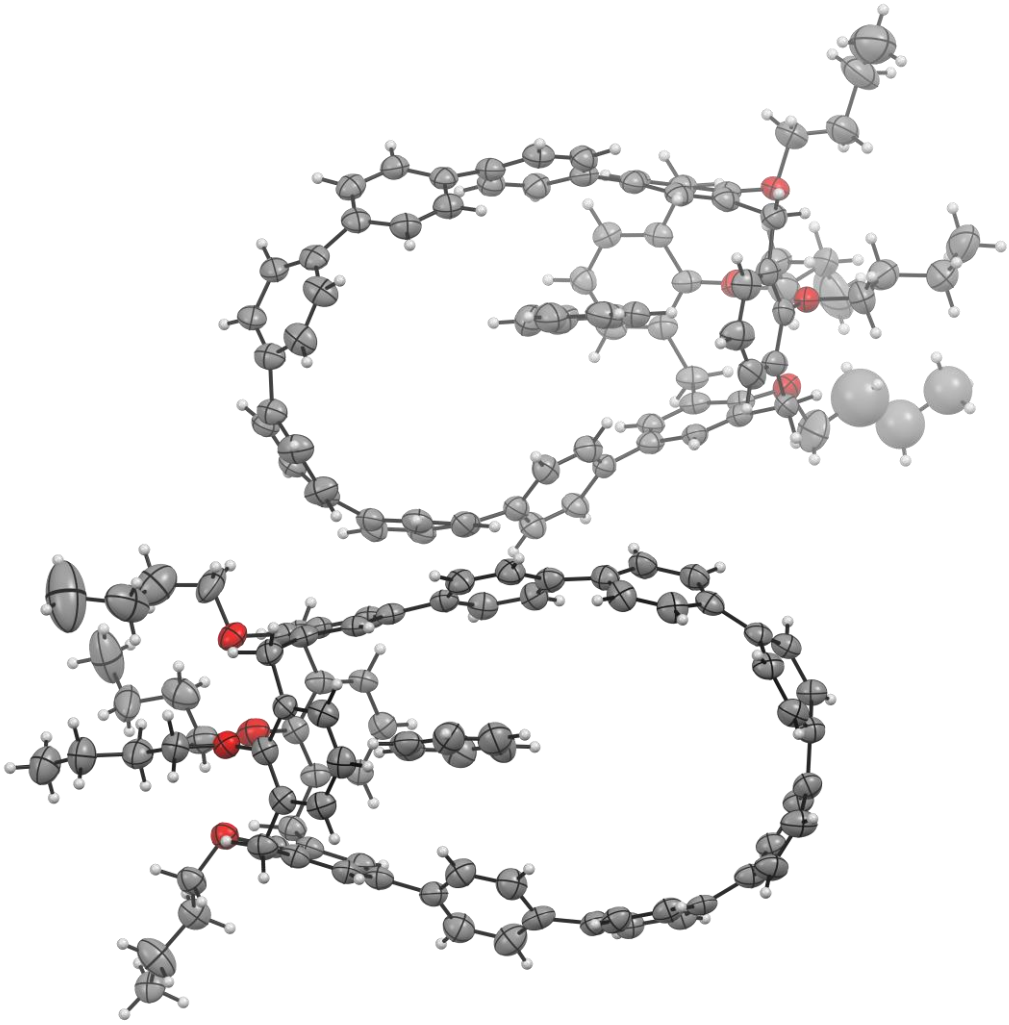

Figure S37. Crystal structure of **1**·3C_6H_6. Solvent molecules and disorder positions are removed for clarity.

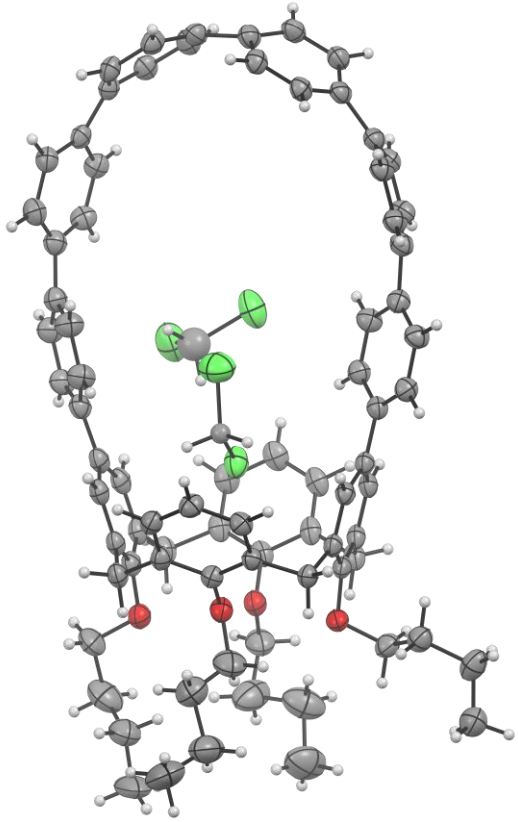

Figure S38. Crystal structure of **1**·3.2CH_2Cl_2. Solvent molecules and disorder positions are removed for clarity.

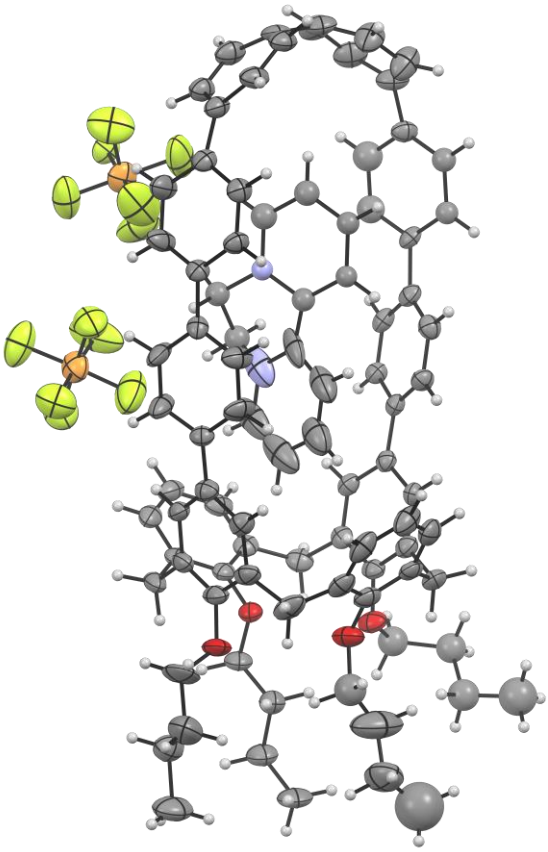

Figure S39. Crystal structure of [**1**⊃DQ^{2+}][PF_6^-]$_2$·C_3H_6O. Solvent molecules and disorder positions are removed for clarity.

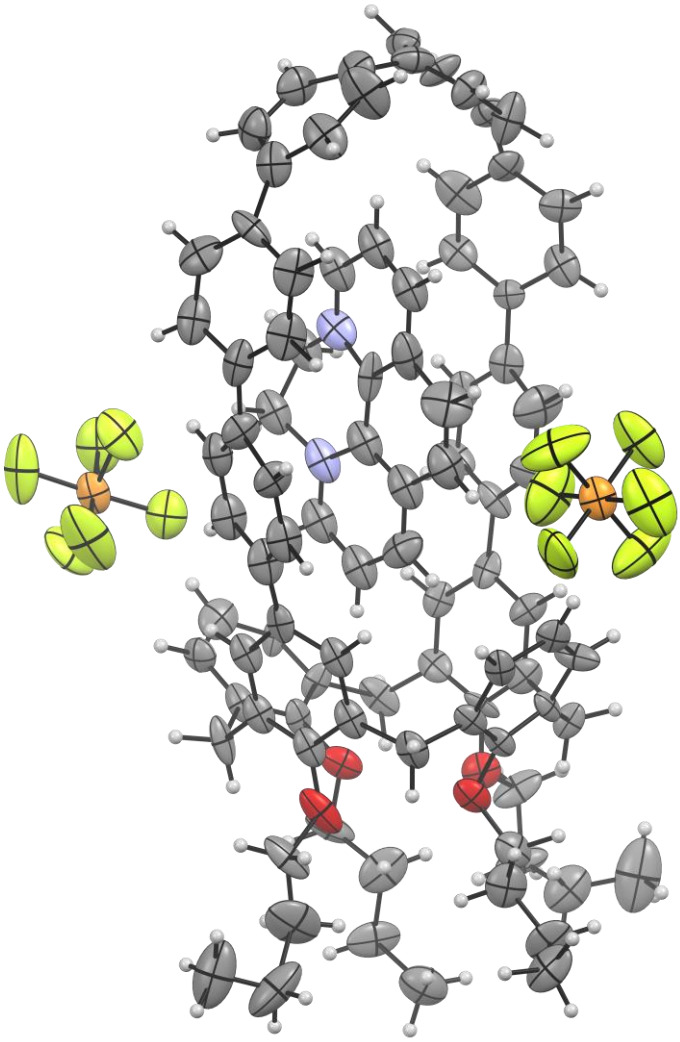

Figure S40. Crystal structure of [**1**⊃PQ^{2+}][PF_6^-]$_2$·C_3H_6O. Solvent molecules and disorder positions are removed for clarity.

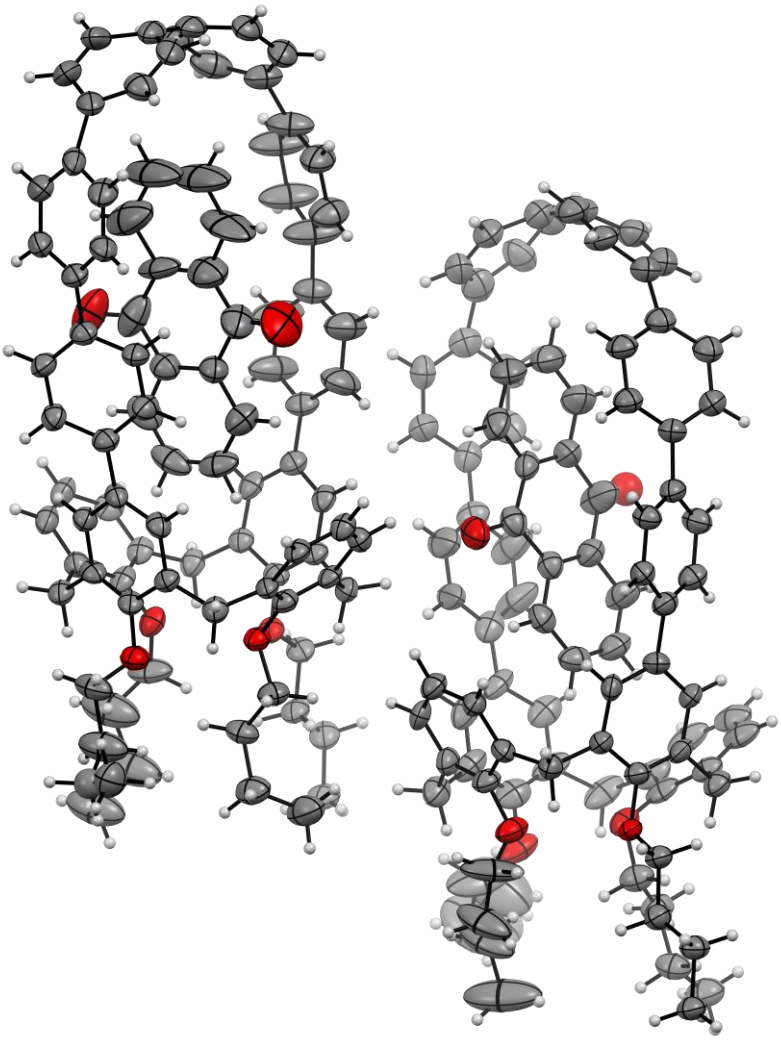

Figure S41. Crystal structure of [**1**⊃AQ]·2.5CH_4O. Solvent molecules and disorder positions are removed for clarity.

Additional Tables

Table S1. Association constants for host–guest complexes of **1**[a].

Guest	Model	K_{11}		K_{21}		SSR
		optimized	error	optimized	error	
DQ[b]	2:1[d]	$6.0337 \cdot 10^{2}$	$2.23 \cdot 10^{0}$	$3.3631 \cdot 10^{1}$	$3.40 \cdot 10^{-1}$	$2.65 \cdot 10^{-5}$
DQ[b]	1:1[e]	$3.5569 \cdot 10^{2}$	$1.21 \cdot 10^{0}$			$7.54 \cdot 10^{-4}$
PQ[b]	2:1[f]	$1.4295 \cdot 10^{3}$	$1.34 \cdot 10^{1}$	$1.7859 \cdot 10^{2}$	$3.56 \cdot 10^{0}$	$1.88 \cdot 10^{-4}$
PQ[b]	1:1[g]	$7.1878 \cdot 10^{2}$	$2.72 \cdot 10^{0}$			$1.72 \cdot 10^{-3}$
MA[b]	2:1[h]	$5.9187 \cdot 10^{3}$	$7.18 \cdot 10^{1}$	$4.3457 \cdot 10^{2}$	$1.439 \cdot 10^{1}$	$6.07 \cdot 10^{-5}$
MA[b]	1:1[i]	$4.3728 \cdot 10^{3}$	$4.46 \cdot 10^{1}$			$1.03 \cdot 10^{-3}$
AQ[c]	1:1[j]	$1.9679 \cdot 10^{1}$	$1.9 \cdot 10^{-2}$			$2.06 \cdot 10^{-5}$

[a] based on ^{1}H NMR titration data (300 K). [b] in acetone-d_6, [c] in CD_2Cl_2. [d] **Figure S7**. [e] **Figure S6**. [f] **Figure S11**. [g] **Figure S10**. [h] **Figure S15**. [i] **Figure S14**. [j] **Figure S18** .

Table S2. The BET fitting parameters derived from the CO_2 isotherm for **1**.

Parameter	Value
Slope	0.0596 ± 0.0004 g/cm³ STP
Y-intercept	0.000350 ± 0.000025 g/cm³ STP
Correlation coefficient	0.9998
BET surface area	63.7 ± 0.4 m²/g
C	171

.

Table S3. Single-site Langmuir-Freudlich parameters for adsorption of CO_2 in **1**. These parameters were determined by fitting adsorption isotherms for temperatures ranging from 273 to 293 K.

	T = 273 K	T = 283 K	T = 293 K
q_{sat}	1.438 ± 0.059	1.103 ± 0.025	1.33 ± 0.06
K	$8.43 \cdot 10^{-4} \pm 9.4 \cdot 10^{-5}$	$1.09 \cdot 10^{-4} \pm 1.0 \cdot 10^{-5}$	$3.16 \cdot 10^{-5} \pm 3.1 \cdot 10^{-6}$
n	1.09 ± 0.03	1.39 ± 0.02	1.44 ± 0.02

.

Table S4. Computational data.

File name[a]	Formula	Level of theory	SCF E[b]	ZPV[c]	lowest freq.[d]	*H*[e]	*G*[f]	HOMO[g]	LUMO[g]	HLG[g]
			a.u.	a.u.	cm^{-1}	a.u.	a.u.	eV	eV	eV
1_AQ_CAMacetone	$C_{86}H_{70}O_6$	CAM-B3LYP/6-31G(d,p)	-3768.966020	1.346138	12.49	-3767.544062	-3767.731012	-6.37	-1.06	5.31
1_CAMacetone	$C_{72}H_{62}O_4$	CAM-B3LYP/6-31G(d,p)	-3080.440368	1.160906	17.68	-3079.216311	-3079.375733	-6.39	-0.30	6.10
1_CO2_vac	$C_{73}H_{62}O_6$	B3LYP/6-31G(d,p)	-3270.940247	1.159592	17.94	-3269.712415	-3269.883869	-5.03	-1.45	3.58
1_MA+_CAMacetone	$C_{86}H_{74}NO_4$	CAM-B3LYP/6-31G(d,p)	-3675.527695	1.390744	11.93	-3674.061356	-3674.246670	-6.97	-2.86	4.11
1_PQ2+_CAMacetone	$C_{86}H_{74}N_2O_4$	CAM-B3LYP/6-31G(d,p)	-3730.063892	1.400629	12.78	-3728.588312	-3728.771517	-7.59	-4.34	3.25
1_DQ2+_CAMacetone	$C_{84}H_{74}N_2O_4$	CAM-B3LYP/6-31G(d,p)	-3653.866914	1.388212	19.12	-3652.404640	-3652.584363	-7.69	-4.30	3.39
1_round_vac	$C_{72}H_{62}O_4$	B3LYP/6-31G(d,p)	-3082.335748	1.147045	17.07	-3081.124552	-3081.286777	-5.10	-1.50	3.60
1_flat_vac	$C_{72}H_{62}O_4$	B3LYP/6-31G(d,p)	-3082.337646	1.147246	17.28	-3081.126386	-3081.287748	-5.05	-1.44	3.61
1_MA+_acetone	$C_{86}H_{74}NO_4$	B3LYP/6-31G(d,p)	-3677.814276	1.374917	7.86	-3676.362825	-3676.550194	-5.71	-3.84	1.87

[a] Structure code (see the zip file for Cartesian coordinates). [b] SCF electronic energy. [c] Zero-point vibrational energy. [d] Lowest vibrational frequency. [e] Enthalpy, [f] Gibbs free energy. [g] Frontier orbital energies and the HOMO–LUMO gap.

Table S5. Electronic transitions calculated for [**1**⊃MA^+] using the TDA/PCM(acetone)/CAM-B3LYP-GD3BJ/6-31G(d,p) level of theory.

No.	Energy (cm^{-1})	λ (nm)	f[a]	Major excitations[b]
1	20049	498.8	0.002	HOMO»LUMO (94%)
2	22344	447.5	0.030	H–1»LUMO (97%)
3	25033	399.5	0.051	H–2»LUMO (92%)
4	27678	361.3	0.033	H–7»LUMO (44%) H–4»LUMO (28%)
5	29577	338.1	0.018	H–6»LUMO (10%) H–5»LUMO (68%) H–4»LUMO (14%)
6	29774	335.9	0.001	H–3»LUMO (90%)
7	29963	333.7	0.384	HOMO»L+1 (80%)
8	30153	331.6	0.008	H–7»LUMO (23%) H–4»LUMO (54%)
9	31776	314.7	0.002	H–6»LUMO (76%) H–5»LUMO (11%)
10	31978	312.7	0.028	H–15»LUMO (28%) H–10»LUMO (23%)
11	32585	306.9	0.011	H–14»LUMO (59%)
12	33420	299.2	0.002	H–15»LUMO (12%) H–9»LUMO (12%) H–8»LUMO (53%)
13	33708	296.7	0.000	H–16»LUMO (19%) H–15»LUMO (30%) H–9»LUMO (12%)
14	33975	294.3	0.006	H–12»LUMO (11%) H–11»LUMO (23%) H–9»LUMO (30%)
15	34289	291.6	0.064	H–13»LUMO (31%) H–10»LUMO (25%)
16	34650	288.6	0.025	H–10»LUMO (16%) H–9»LUMO (33%) H–8»LUMO (25%)
17	35081	285.1	0.546	H–13»LUMO (43%) HOMO»L+3 (10%)
18	35379	282.7	0.753	H–12»LUMO (14%) HOMO»L+3 (11%)
19	35855	278.9	0.466	H–12»LUMO (27%)
20	36407	274.7	0.183	HOMO»L+2 (72%) HOMO»L+3 (10%)
21	36749	272.1	0.041	H–17»LUMO (12%) H–14»LUMO (11%) H–12»LUMO (10%) H–11»LUMO (41%)
22	36868	271.2	0.297	H–11»L+1 (11%) HOMO»L+7 (28%) HOMO»L+8 (14%)
23	37565	266.2	0.080	H–25»LUMO (40%) H–21»LUMO (10%) H–19»LUMO (15%) H–12»LUMO (12%)
24	37877	264.0	0.232	H–2»L+1 (19%) H–1»L+2 (10%) H–1»L+3 (22%) HOMO»L+4 (18%)
25	38625	258.9	0.034	H–25»LUMO (16%) H–20»LUMO (12%) H–19»LUMO (33%)
26	38678	258.5	0.007	H–17»LUMO (34%) H–16»LUMO (43%)
27	38829	257.5	0.017	H–1»L+2 (58%)
28	39041	256.1	0.043	HOMO»L+11 (16%)
29	39505	253.1	0.006	
30	39558	252.8	0.008	H–2»L+2 (10%) HOMO»L+3 (11%)
31	39888	250.7	0.004	H–1»L+1 (23%) HOMO»L+3 (26%)
32	40401	247.5	0.004	H–1»L+2 (16%)
33	40707	245.7	0.003	H–16»L+1 (12%) HOMO»L+18 (13%)
34	40876	244.6	0.007	H–18»LUMO (15%)
35	40947	244.2	0.014	H–18»LUMO (50%)
36	41095	243.3	0.003	
37	41302	242.1	0.025	H–24»LUMO (37%) H–20»LUMO (20%) H–18»LUMO (23%)
38	41603	240.4	0.001	H–5»L+1 (13%) H–2»L+2 (12%) H–2»L+3 (14%) H–1»L+4 (11%)
39	41859	238.9	0.003	H–2»L+2 (32%) H–2»L+3 (11%) HOMO»L+5 (20%)
40	42346	236.1	0.004	H–21»LUMO (32%) H–20»LUMO (20%) H–19»LUMO (33%)
41	42423	235.7	0.012	H–2»L+2 (13%) HOMO»L+5 (35%)
42	42938	232.9	0.026	
43	43127	231.9	0.019	
44	43218	231.4	0.002	H–2»L+1 (34%) HOMO»L+4 (35%)
45	43659	229.0	0.004	H–22»LUMO (72%) H–20»LUMO (12%)
46	44070	226.9	0.014	H–2»L+1 (10%) H–1»L+3 (36%) H–1»L+5 (13%) HOMO»L+4 (18%)
47	44579	224.3	0.844	H–7»L+2 (11%) H–4»L+2 (18%)
48	44781	223.3	0.036	H–23»LUMO (71%)
49	44875	222.8	0.590	
50	45243	221.0	0.152	H–2»L+5 (13%) HOMO»L+6 (14%)

[a] Oscillator strength. [b] Contributions smaller than 10% are not included. H = HOMO, L = LUMO. Orbitals are numbered consecutively regardless of possible degeneracies.

Table S6. Electronic transitions calculated for [**1**⊃DQ^{2+}] using the TDA/PCM(acetone)/CAM-B3LYP-GD3BJ/6-31G(d,p) level of theory.

No.	Energy (cm^{-1})	λ (nm)	f[a]	Major excitations[b]
1	14556	687.0	0.000	HOMO»LUMO (94%)
2	17634	567.1	0.000	H–1»LUMO (95%)
3	20465	488.6	0.001	H–2»LUMO (88%)
4	23361	428.1	0.006	HOMO»L+1 (85%)
5	23611	423.5	0.001	H–3»LUMO (87%)
6	24050	415.8	0.003	H–4»LUMO (77%) H–1»L+1 (15%)
7	24582	406.8	0.009	H–5»LUMO (85%)
8	26047	383.9	0.002	H–6»LUMO (88%)
9	27222	367.3	0.005	H–9»LUMO (11%) H–8»LUMO (11%) H–2»L+1 (10%) H–2»L+2 (13%) H–1»L+2 (10%) HOMO»L+2 (29%)
10	27572	362.7	0.001	H–4»LUMO (11%) H–1»L+1 (72%)
11	27801	359.7	0.012	H–10»LUMO (37%) H–8»LUMO (37%)
12	28490	351.0	0.004	H–10»LUMO (33%) H–8»LUMO (13%) HOMO»L+2 (14%)
13	28723	348.2	0.007	H–9»LUMO (49%) H–8»LUMO (21%)
14	29098	343.7	0.003	H–15»LUMO (32%) H–12»LUMO (47%)
15	29477	339.3	0.005	H–15»LUMO (39%) H–7»LUMO (35%)
16	29755	336.1	0.000	H–15»LUMO (10%) H–1»L+2 (37%)
17	30001	333.3	0.006	H–15»LUMO (11%) H–12»LUMO (19%) H–7»LUMO (24%) H–1»L+2 (15%)
18	30231	330.8	0.020	H–13»LUMO (77%)
19	30359	329.4	0.292	HOMO»L+3 (63%)
20	30475	328.1	0.030	H–14»LUMO (36%) H–11»LUMO (23%)
21	31174	320.8	0.000	H–19»LUMO (49%) H–14»LUMO (16%) H–11»LUMO (15%)
22	31429	318.2	0.002	H–19»LUMO (41%) H–14»LUMO (33%) H–11»LUMO (12%)
23	31528	317.2	0.010	H–2»L+1 (68%)
24	32510	307.6	0.004	H–2»L+2 (53%) HOMO»L+2 (22%)
25	32812	304.8	0.004	H–3»L+1 (15%) H–3»L+2 (70%)
26	33021	302.8	0.005	H–18»LUMO (56%) H–4»L+1 (12%)
27	33645	297.2	0.017	H–16»LUMO (49%) H–5»L+2 (23%)
28	33787	296.0	0.003	H–16»LUMO (31%) H–5»L+2 (47%)
29	34509	289.8	0.245	H–17»LUMO (55%)
30	34680	288.4	1.495	H–17»LUMO (18%) H–1»L+3 (18%) HOMO»L+4 (14%) HOMO»L+5 (19%)
31	35190	284.2	0.039	H–6»L+1 (12%) H–6»L+2 (65%)
32	35256	283.6	0.072	H–18»LUMO (11%) H–4»L+1 (54%) H–4»L+2 (11%)
33	36390	274.8	0.004	H–3»L+1 (73%) H–3»L+2 (15%)
34	36475	274.2	0.377	H–22»LUMO (41%)
35	36784	271.9	0.079	H–20»LUMO (78%)
36	36899	271.0	0.069	H–10»L+2 (22%) H–8»L+2 (23%) H–4»L+2 (10%)
37	37077	269.7	0.008	H–10»L+2 (10%) H–4»L+2 (32%)
38	37205	268.8	0.012	H–12»L+1 (34%) H–7»L+1 (22%)
39	37400	267.4	0.003	H–5»L+1 (71%) H–5»L+2 (11%)
40	37543	266.4	0.004	H–12»L+1 (14%) HOMO»L+4 (15%) HOMO»L+5 (11%)
41	37628	265.8	0.024	H–21»LUMO (69%)
42	37682	265.4	0.000	HOMO»L+11 (12%)
43	37926	263.7	0.056	H–10»L+2 (14%) H–9»L+2 (21%) H–8»L+2 (28%)
44	38050	262.8	0.222	H–2»L+3 (17%) H–1»L+5 (12%) HOMO»L+6 (16%)
45	38118	262.3	0.016	H–12»L+1 (13%) H–7»L+1 (30%)
46	38362	260.7	0.271	H–24»LUMO (13%) H–12»L+1 (16%) H–7»L+1 (14%)
47	38680	258.5	0.145	H–24»LUMO (17%) H–14»L+1 (16%) H–11»L+1 (13%) H–6»L+1 (10%)
48	38762	258.0	0.028	H–6»L+1 (64%) H–6»L+2 (13%)
49	38989	256.5	0.097	
50	39138	255.5	0.006	H–15»L+1 (64%) H–14»L+1 (11%)

[a] Oscillator strength. [b] Contributions smaller than 10% are not included. H = HOMO, L = LUMO. Orbitals are numbered consecutively regardless of possible degeneracies.

Table S7. Electronic transitions calculated for [**1**⊃PQ^{2+}] using the TDA/PCM(acetone)/CAM-B3LYP-GD3BJ/6-31G(d,p) level of theory.

No.	Energy (cm^{-1})	λ (nm)	f[a]	Major excitations[b]
1	13516	739.8	0.002	HOMO»LUMO (94%)
2	17550	569.8	0.000	H–1»LUMO (93%)
3	19085	524.0	0.008	H–2»LUMO (50%) HOMO»L+1 (37%)
4	20635	484.6	0.002	H–2»LUMO (42%) HOMO»L+1 (45%)
5	22062	453.3	0.002	H–3»LUMO (33%) H–1»L+1 (55%)
6	24165	413.8	0.007	H–3»LUMO (29%) H–2»L+1 (37%) H–1»L+1 (17%)
7	24233	412.7	0.013	H–5»LUMO (10%) H–4»LUMO (64%) H–4»L+1 (13%)
8	24733	404.3	0.011	H–5»LUMO (68%) H–5»L+1 (13%)
9	25149	397.6	0.010	H–3»LUMO (27%) H–2»L+1 (39%) H–1»L+1 (15%)
10	26383	379.0	0.001	H–6»LUMO (79%) H–6»L+1 (15%)
11	27750	360.4	0.008	H–12»LUMO (46%) H–8»LUMO (16%) H–7»LUMO (28%)
12	27834	359.3	0.001	H–15»LUMO (47%) H–13»LUMO (12%) H–10»LUMO (20%)
13	28118	355.6	0.020	H–10»LUMO (49%) H–10»L+1 (12%)
14	28221	354.3	0.008	H–9»LUMO (15%) H–8»LUMO (30%) H–7»LUMO (27%)
15	28575	350.0	0.001	H–3»L+1 (47%)
16	28643	349.1	0.007	H–12»LUMO (10%) H–9»LUMO (29%) H–7»LUMO (19%) H–3»L+1 (14%)
17	28989	345.0	0.004	H–12»LUMO (11%) H–11»LUMO (37%) H–9»LUMO (14%)
18	29331	340.9	0.015	H–14»LUMO (55%) H–11»LUMO (13%)
19	29417	339.9	0.002	H–5»L+1 (11%) H–4»LUMO (11%) H–4»L+1 (56%)
20	29932	334.1	0.025	H–13»LUMO (15%) H–5»L+1 (36%)
21	30069	332.6	0.039	H–15»LUMO (12%) H–13»LUMO (34%) H–13»L+1 (10%) H–5»L+1 (16%)
22	30141	331.8	0.238	HOMO»L+2 (27%) HOMO»L+4 (30%)
23	30189	331.2	0.003	H–14»LUMO (13%) H–11»LUMO (16%) H–8»LUMO (30%)
24	30432	328.6	0.002	H–19»LUMO (53%) H–18»LUMO (25%)
25	31083	321.7	0.172	HOMO»L+2 (43%) HOMO»L+4 (28%)
26	31549	317.0	0.001	H–6»LUMO (16%) H–6»L+1 (73%)
27	32475	307.9	0.009	H–15»L+1 (11%) H–11»L+1 (17%)
28	32734	305.5	0.004	H–15»L+1 (22%) H–9»L+1 (18%)
29	33065	302.4	0.019	H–19»LUMO (15%) H–18»LUMO (36%) H–15»L+1 (16%)
30	33446	299.0	0.021	H–10»LUMO (14%) H–10»L+1 (58%)
31	33646	297.2	0.003	H–17»LUMO (17%) H–16»LUMO (13%) H–15»L+1 (14%) H–9»L+1 (18%)
32	33903	295.0	0.031	H–11»L+1 (16%) H–9»L+1 (14%) H–1»L+2 (14%)
33	34181	292.6	0.151	H–1»L+2 (40%)
34	34347	291.2	0.004	H–17»LUMO (25%) H–16»LUMO (49%)
35	34603	289.0	0.008	H–12»L+1 (40%) H–7»L+1 (32%)
36	34863	286.8	0.010	H–24»LUMO (59%)
37	34953	286.1	0.015	HOMO»L+3 (60%)
38	35073	285.1	0.016	H–22»LUMO (20%) H–15»L+1 (10%) H–13»L+1 (17%) H–7»L+1 (14%)
39	35356	282.8	0.112	H–13»L+1 (17%) H–12»L+1 (13%) H–7»L+1 (23%)
40	35413	282.4	0.205	H–22»LUMO (16%) H–7»L+1 (14%) HOMO»L+5 (10%)
41	35845	279.0	1.340	H–22»LUMO (17%) HOMO»L+5 (27%)
42	36121	276.8	0.028	H–14»L+1 (41%) H–8»L+1 (14%)
43	36510	273.9	0.021	H–19»L+1 (47%) H–18»L+1 (13%) H–2»L+2 (16%)
44	36602	273.2	0.013	H–19»L+1 (14%) H–18»L+1 (10%) H–8»L+1 (22%) H–2»L+2 (21%)
45	36754	272.1	0.016	H–20»LUMO (82%) H–20»L+1 (10%)
46	37090	269.6	0.036	H–14»L+1 (29%) H–11»L+1 (14%) H–8»L+1 (15%)
47	37283	268.2	0.015	H–25»LUMO (30%) H–22»LUMO (13%)
48	37499	266.7	0.021	H–21»LUMO (10%) H–19»L+1 (16%) H–18»L+1 (29%) H–3»L+2 (10%)
49	37612	265.9	0.340	H–7»L+4 (11%) HOMO»L+12 (11%)
50	37689	265.3	0.008	H–21»LUMO (61%) H–21»L+1 (10%)

[a] Oscillator strength. [b] Contributions smaller than 10% are not included. H = HOMO, L = LUMO. Orbitals are numbered consecutively regardless of possible degeneracies.

Table S8. Electronic transitions calculated for [**1**⊃AQ] using the TDA/PCM(acetone)/CAM-B3LYP-GD3BJ/6-31G(d,p) level of theory.

No.	Energy (cm^{-1})	λ (nm)	f[a]	Major excitations[b]
1	27446	364.3	0.000	H–15»LUMO (76%)
2	29206	342.4	0.023	HOMO»LUMO (82%)
3	29543	338.5	0.001	H–23»LUMO (17%) H–22»LUMO (60%) H–15»L+3 (10%)
4	30500	327.9	0.382	HOMO»L+1 (76%)
5	31161	320.9	0.020	H–1»LUMO (94%)
6	32168	310.9	0.004	H–7»LUMO (20%) H–2»LUMO (47%)
7	34476	290.1	0.004	H–8»LUMO (29%) H–7»LUMO (18%) H–4»LUMO (13%)
8	35642	280.6	0.958	H–7»LUMO (12%) H–2»LUMO (13%) H–1»L+1 (14%) HOMO»L+2 (21%)
9	35941	278.2	0.485	H–8»LUMO (22%) H–2»LUMO (23%)
10	36555	273.6	0.066	H–11»LUMO (39%)
11	37046	269.9	0.880	H–1»L+1 (16%) HOMO»L+5 (21%)
12	38076	262.6	0.198	H–2»L+1 (19%) H–1»L+2 (23%) HOMO»L+4 (17%)
13	38615	259.0	0.007	H–5»LUMO (41%)
14	39135	255.5	0.079	H–5»LUMO (10%) HOMO»L+3 (24%)
15	39164	255.3	0.002	H–3»LUMO (52%)
16	39505	253.1	0.011	H–12»LUMO (25%) H–4»LUMO (12%) H–3»LUMO (20%)
17	39591	252.6	0.016	H–4»LUMO (30%) H–3»LUMO (15%)
18	39701	251.9	0.057	H–12»LUMO (15%) H–4»LUMO (32%)
19	39944	250.4	0.005	H–5»LUMO (11%)
20	40096	249.4	0.021	
21	40432	247.3	0.075	HOMO»L+3 (25%)
22	40509	246.9	0.011	H–1»L+1 (20%) HOMO»L+2 (23%)
23	40738	245.5	0.003	HOMO»L+17 (12%)
24	40901	244.5	0.007	H–14»LUMO (11%) HOMO»L+3 (11%)
25	41135	243.1	0.005	
26	41510	240.9	0.003	
27	41651	240.1	0.005	H–6»LUMO (65%)
28	42031	237.9	0.008	H–2»L+2 (25%) H–1»L+4 (10%)
29	42159	237.2	0.036	H–13»LUMO (36%) H–1»L+3 (13%)
30	42436	235.7	0.034	H–1»L+3 (40%)
31	42786	233.7	0.021	H–3»L+6 (20%)
32	43180	231.6	0.179	H–2»L+1 (24%) H–2»L+3 (15%)
33	43212	231.4	0.203	H–2»L+1 (23%) H–2»L+3 (17%)
34	43492	229.9	0.061	H–9»LUMO (38%)
35	43560	229.6	0.108	H–19»LUMO (24%) H–18»LUMO (18%) H–11»LUMO (10%) H–2»L+3 (10%)
36	43772	228.5	0.008	H–9»LUMO (21%)
37	43941	227.6	0.017	H–20»LUMO (26%) H–16»LUMO (24%) H–11»LUMO (10%)
38	44104	226.7	0.023	H–17»LUMO (30%) H–10»LUMO (33%)
39	44335	225.6	0.005	H–17»LUMO (14%) H–13»LUMO (12%) H–10»LUMO (45%)
40	44938	222.5	0.004	H–2»L+4 (22%)
41	45185	221.3	0.014	H–1»L+2 (27%) HOMO»L+4 (41%)
42	45668	219.0	0.004	H–5»L+1 (30%) H–1»L+1 (13%) HOMO»L+5 (11%)
43	45716	218.7	0.003	H–22»LUMO (11%) H–15»L+3 (57%)
44	45784	218.4	0.080	H–19»LUMO (14%) H–14»LUMO (27%)
45	46230	216.3	0.170	H–16»L+1 (16%) H–11»L+1 (13%)
46	46456	215.3	0.152	H–7»L+3 (17%) H–4»L+3 (10%) H–2»L+2 (10%)
47	46542	214.9	0.072	H–2»L+2 (21%) H–1»L+4 (26%)
48	46668	214.3	0.046	H–16»LUMO (10%)
49	46847	213.5	0.013	H–20»LUMO (10%) H–16»LUMO (17%)
50	46979	212.9	0.018	

[a] Oscillator strength. [b] Contributions smaller than 10% are not included. H = HOMO, L = LUMO. Orbitals are numbered consecutively regardless of possible degeneracies.

Table S9. Electronic transitions calculated for **1** using the TDA/PCM(acetone)/CAM-B3LYP-GD3BJ/6-31G(d,p) level of theory.

No.	Energy (cm^{-1})	λ (nm)	f[a]	Major excitations[b]
1	31257	319.9	0.437	HOMO»LUMO (80%)
2	36320	275.3	2.490	H–1»LUMO (30%) HOMO»L+1 (40%)
3	37953	263.5	0.453	H–13»LUMO (13%) H–1»LUMO (11%) HOMO»L+3 (32%)
4	38566	259.3	0.210	H–2»LUMO (12%) H–1»L+1 (18%) HOMO»L+2 (18%) HOMO»L+6 (13%)
5	39914	250.5	0.219	H–2»LUMO (16%) H–1»L+1 (14%) HOMO»L+6 (17%)
6	40288	248.2	0.023	H–15»LUMO (15%) HOMO»L+9 (10%)
7	40447	247.2	0.002	H–2»L+4 (15%) H–1»L+7 (17%)
8	40471	247.1	0.001	H–2»L+7 (11%) H–1»L+4 (14%)
9	40839	244.9	0.001	H–16»LUMO (19%) HOMO»L+13 (19%)
10	41205	242.7	0.024	H–1»LUMO (31%) HOMO»L+1 (39%)
11	41431	241.4	0.003	H–11»L+1 (11%)
12	41446	241.3	0.003	H–12»L+1 (11%)
13	42798	233.7	0.101	H–6»LUMO (12%) H–2»L+1 (24%) H–1»L+2 (19%)
14	42991	232.6	0.016	H–3»L+4 (18%)
15	43506	229.9	0.015	
16	44179	226.4	0.005	H–2»LUMO (42%) HOMO»L+2 (27%)
17	45646	219.1	0.004	H–6»L+1 (11%) H–2»L+2 (21%)
18	45870	218.0	0.024	H–1»L+1 (41%) HOMO»LUMO (12%) HOMO»L+2 (28%)
19	46388	215.6	0.031	H–6»LUMO (20%) H–5»LUMO (16%) HOMO»L+3 (12%) HOMO»L+5 (11%)
20	47352	211.2	0.056	H–4»L+4 (24%)
21	47499	210.5	0.024	H–13»LUMO (44%) HOMO»L+3 (14%) HOMO»L+5 (14%)
22	47589	210.1	0.024	H–4»LUMO (21%) H–4»L+2 (12%) H–1»L+4 (13%)
23	47816	209.1	0.007	H–2»L+1 (39%) H–1»L+2 (24%)
24	47950	208.6	0.109	H–3»LUMO (27%) H–3»L+2 (13%)
25	48913	204.4	0.044	H–14»LUMO (17%) H–10»LUMO (18%) HOMO»L+6 (27%)
26	49029	204.0	0.134	H–6»L+2 (11%)
27	49315	202.8	0.061	H–3»LUMO (10%)
28	49492	202.1	0.068	H–3»LUMO (27%)
29	49648	201.4	0.095	H–6»LUMO (10%)
30	49693	201.2	0.152	H–14»LUMO (11%)
31	49871	200.5	0.072	H–1»L+3 (38%)
32	49907	200.4	0.013	
33	50026	199.9	0.005	H–4»LUMO (25%) H–3»L+1 (32%)
34	50067	199.7	0.020	H–6»LUMO (10%) H–5»LUMO (22%)
35	50400	198.4	0.005	H–15»LUMO (29%) HOMO»L+9 (15%)
36	50762	197.0	0.002	H–5»L+1 (10%) H–4»LUMO (18%)
37	51000	196.1	0.008	H–5»L+1 (15%) H–2»L+2 (16%) H–1»L+5 (22%)
38	51088	195.7	0.000	
39	51204	195.3	0.003	
40	51260	195.1	0.110	H–12»LUMO (10%) H–4»L+1 (12%) HOMO»L+8 (14%)
41	51321	194.9	0.001	H–6»L+1 (11%) H–5»L+1 (12%)
42	51432	194.4	0.003	
43	51523	194.1	0.022	H–4»L+1 (18%) HOMO»L+4 (15%)
44	51613	193.8	0.047	H–2»L+5 (13%) H–1»L+6 (15%)
45	51729	193.3	0.052	
46	51875	192.8	0.008	
47	51969	192.4	0.017	
48	52026	192.2	0.225	H–16»LUMO (14%) HOMO»L+13 (21%)
49	52181	191.6	0.049	H–7»LUMO (12%)
50	52336	191.1	0.047	

[a] Oscillator strength. [b] Contributions smaller than 10% are not included. H = HOMO, L = LUMO. Orbitals are numbered consecutively regardless of possible degeneracies.

Table S10. Crystal data and structure refinement for **5**·C_6H_{14}·H_2O.

Identification code	RF07A	
Empirical formula	C90 H104.40 O8.20	
Formula weight	1317.33	
Temperature	100(2) K	
Wavelength	1.54184 Ĺ	
Crystal system	Triclinic	
Space group	P-1	
Unit cell dimensions	a = 12.027(2) Å	α= 72.10(5)°.
	b = 16.806(3) Å	β= 84.41(4)°.
	c = 19.642(4) Å	γ = 85.99(4)°.
Volume	3756.7(16) Å ^{3}	
Z	2	
Density (calculated)	1.165 Mg/m^3	
Absorption coefficient	0.567 mm^{-1}	
F(000)	1420	
Crystal size	0.650 x 0.110 x 0.070 mm^3	
Theta range for data collection	2.371 to 67.997°.	
Index ranges	-13<=h<=14, -20<=k<=17, -23<=l<=23	
Reflections collected	29270	
Independent reflections	13674 [R(int) = 0.0695]	
Completeness to theta = 67.000°	99.9 %	
Absorption correction	Analytical	
Max. and min. transmission	0.968 and 0.822	
Refinement method	Full-matrix least-squares on F^2	
Data / restraints / parameters	13674 / 0 / 896	
Goodness-of-fit on F^2	1.040	
Final R indices [I>2sigma(I)]	R1 = 0.0775, wR2 = 0.2021	
R indices (all data)	R1 = 0.1039, wR2 = 0.2405	
Extinction coefficient	n/a	
Largest diff. peak and hole	0.428 and -0.460 e. Å $^{-3}$	

Table S11. Crystal data and structure refinement for **1**·3C_6H_6.

Identification code	rf05a	
Empirical formula	C98 H96 O4	
Formula weight	1337.74	
Temperature	100(2) K	
Wavelength	1.54184 Å	
Crystal system	Orthorhombic	
Space group	$Pca2_1$	
Unit cell dimensions	a = 32.979(5) Å	α= 90°.
	b = 18.110(3) Å	β= 90°.
	c = 25.513(5) Å	γ = 90°.
Volume	15238(5) $Å^3$	
Z	8	
Density (calculated)	1.166 Mg/m^3	
Absorption coefficient	0.530 mm^{-1}	
F(000)	5728	
Crystal size	0.340 x 0.150 x 0.080 mm^3	
Theta range for data collection	3.625 to 67.158°.	
Index ranges	-38<=h<=31, -17<=k<=20, -21<=l<=29	
Reflections collected	63836	
Independent reflections	20179 [R(int) = 0.0372]	
Completeness to theta = 67.000°	97.3 %	
Absorption correction	Analytical	
Max. and min. transmission	0.965 and 0.910	
Refinement method	Full-matrix least-squares on F^2	
Data / restraints / parameters	20179 / 16 / 1750	
Goodness-of-fit on F^2	1.090	
Final R indices [I>2sigma(I)]	R1 = 0.0827, wR2 = 0.2146	
R indices (all data)	R1 = 0.1053, wR2 = 0.2355	
Absolute structure parameter	-0.19(16)	
Extinction coefficient	n/a	
Largest diff. peak and hole	0.533 and -0.446 e. $Å^{-3}$	

Table S12. Crystal data and structure refinement for **1**·3.2CH_2Cl_2.

Identification code	rf07abs	
Empirical formula	C83.20 H84.40 Cl6.40 O4	
Formula weight	1375.18	
Temperature	100(2) K	
Wavelength	1.5418 Å	
Crystal system	Monoclinic	
Space group	$P2_1/n$	
Unit cell dimensions	a = 16.394(7) Å	α= 90.00(3)°.
	b = 24.705(10) Å	β= 92.58(4)°.
	c = 18.366(7) Å	γ = 90.00(3)°.
Volume	7431(5) $Å^3$	
Z	4	
Density (calculated)	1.229 Mg/m^3	
Absorption coefficient	2.621 mm^{-1}	
F(000)	2898	
Crystal size	0.550 x 0.310 x 0.170 mm^3	
Theta range for data collection	3.000 to 75.613°.	
Index ranges	-18<=h<=20, -30<=k<=26, -22<=l<=21	
Reflections collected	37405	
Independent reflections	14977 [R(int) = 0.0624]	
Completeness to theta = 67.000°	100.0 %	
Absorption correction	Analytical	
Max. and min. transmission	0.680 and 0.289	
Refinement method	Full-matrix least-squares on F^2	
Data / restraints / parameters	14977 / 16 / 936	
Goodness-of-fit on F^2	1.667	
Final R indices [I>2sigma(I)]	R1 = 0.1029, wR2 = 0.2682	
R indices (all data)	R1 = 0.1207, wR2 = 0.2891	
Extinction coefficient	n/a	
Largest diff. peak and hole	1.102 and -0.705 e. $Å^{-3}$	

Table S13. Crystal data and structure refinement for [**1**⊃DQ^{2+}][PF_6^-]$_2$·C_3H_6O.

Identification code	stepien	
Empirical formula	C95 H96 F12 N2 O5 P2	
Formula weight	1635.67	
Temperature	100(2) K	
Wavelength	0.71073 Å	
Crystal system	Monoclinic	
Space group	$P2_1/c$	
Unit cell dimensions	a = 23.011(10) Å	α= 90°.
	b = 16.617(9) Å	β= 91.04(3)°.
	c = 21.113(9) Å	γ = 90°.
Volume	8072(7) Å ^{3}	
Z	4	
Density (calculated)	1.346 Mg/m^3	
Absorption coefficient	0.138 mm^{-1}	
F(000)	3432	
Crystal size	0.380 x 0.280 x 0.120 mm^3	
Theta range for data collection	3.234 to 28.977°.	
Index ranges	-30<=h<=30, -21<=k<=13, -28<=l<=28	
Reflections collected	30480	
Independent reflections	30480 [R(int) = ?]	
Completeness to theta = 25.500°	95.8 %	
Absorption correction	None	
Refinement method	Full-matrix least-squares on F^2	
Data / restraints / parameters	30480 / 8 / 1001	
Goodness-of-fit on F^2	1.004	
Final R indices [I>2sigma(I)]	R1 = 0.0732, wR2 = 0.1862	
R indices (all data)	R1 = 0.1622, wR2 = 0.2059	
Extinction coefficient	n/a	
Largest diff. peak and hole	0.680 and -0.511 e. Å $^{-3}$	

Table S14. Crystal data and structure refinement for [**1**⊃PQ^{2+}][PF_6^-]$_2$·C_3H_6O.

Identification code	rf21a	
Empirical formula	C97 H96 F12 N2 O5 P2	
Formula weight	1659.69	
Temperature	100(2) K	
Wavelength	1.54184 Å	
Crystal system	Monoclinic	
Space group	$P2_1/c$	
Unit cell dimensions	a = 21.800(9) Å	α= 90°.
	b = 18.632(8) Å	β= 102.05(5)°.
	c = 20.532(8) Å	γ = 90°.
Volume	8156(6) Å ^{3}	
Z	4	
Density (calculated)	1.352 Mg/m^3	
Absorption coefficient	1.196 mm^{-1}	
F(000)	3480	
Crystal size	0.280 x 0.180 x 0.013 mm^3	
Theta range for data collection	3.587 to 69.093°.	
Index ranges	-26<=h<=26, -22<=k<=22, -15<=l<=24	
Reflections collected	22988	
Independent reflections	22988 [R(int) = ?]	
Completeness to theta = 67.000°	99.9 %	
Absorption correction	Analytical	
Max. and min. transmission	0.985 and 0.800	
Refinement method	Full-matrix least-squares on F^2	
Data / restraints / parameters	22988 / 1 / 966	
Goodness-of-fit on F^2	0.875	
Final R indices [I>2sigma(I)]	R1 = 0.1082, wR2 = 0.1297	
R indices (all data)	R1 = 0.3169, wR2 = 0.1680	
Extinction coefficient	n/a	
Largest diff. peak and hole	0.498 and -0.545 e. Å $^{-3}$	

Table S15. Crystal data and structure refinement for [**1**⊃AQ]·2.5CH_4O.

Identification code	rf23ra	
Empirical formula	C96.50 H96 O8.50	
Formula weight	1391.73	
Temperature	100(2) K	
Wavelength	1.54184 Å	
Crystal system	Triclinic	
Space group	P-1	
Unit cell dimensions	a = 19.335(10) Å	α= 117.13(5)°.
	b = 20.831(11) Å	β= 97.39(5)°.
	c = 21.770(12) Å	γ = 90.80(5)°.
Volume	7712(8) $Å^3$	
Z	4	
Density (calculated)	1.199 Mg/m^3	
Absorption coefficient	0.587 mm^{-1}	
F(000)	2972	
Crystal size	0.160 x 0.050 x 0.050 mm^3	
Theta range for data collection	3.462 to 67.000°.	
Index ranges	-21<=h<=23, -18<=k<=24, -25<=l<=25	
Reflections collected	60971	
Independent reflections	27037 [R(int) = 0.1548]	
Completeness to theta = 67.000°	98.4 %	
Absorption correction	Analytical	
Max. and min. transmission	0.975 and 0.936	
Refinement method	Full-matrix least-squares on F^2	
Data / restraints / parameters	27037 / 12 / 1829	
Goodness-of-fit on F^2	1.003	
Final R indices [I>2sigma(I)]	R1 = 0.1163, wR2 = 0.2483	
R indices (all data)	R1 = 0.2597, wR2 = 0.3428	
Extinction coefficient	n/a	
Largest diff. peak and hole	0.700 and -0.388 e. $Å^{-3}$	

NMR Spectra

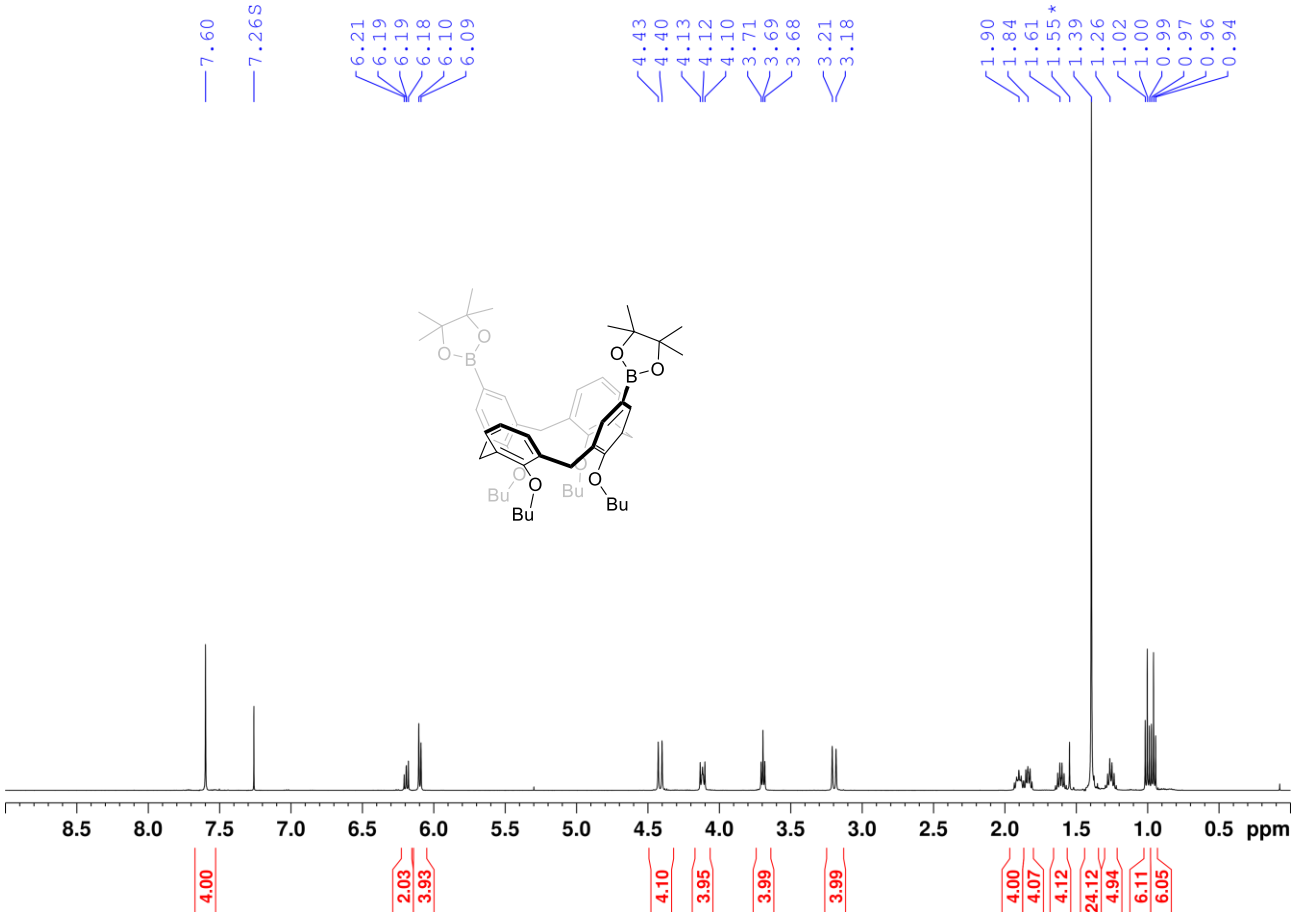

Figure S42. ^{1}H NMR spectrum of **2b** (500 MHz, chloroform-*d* , 300 K).

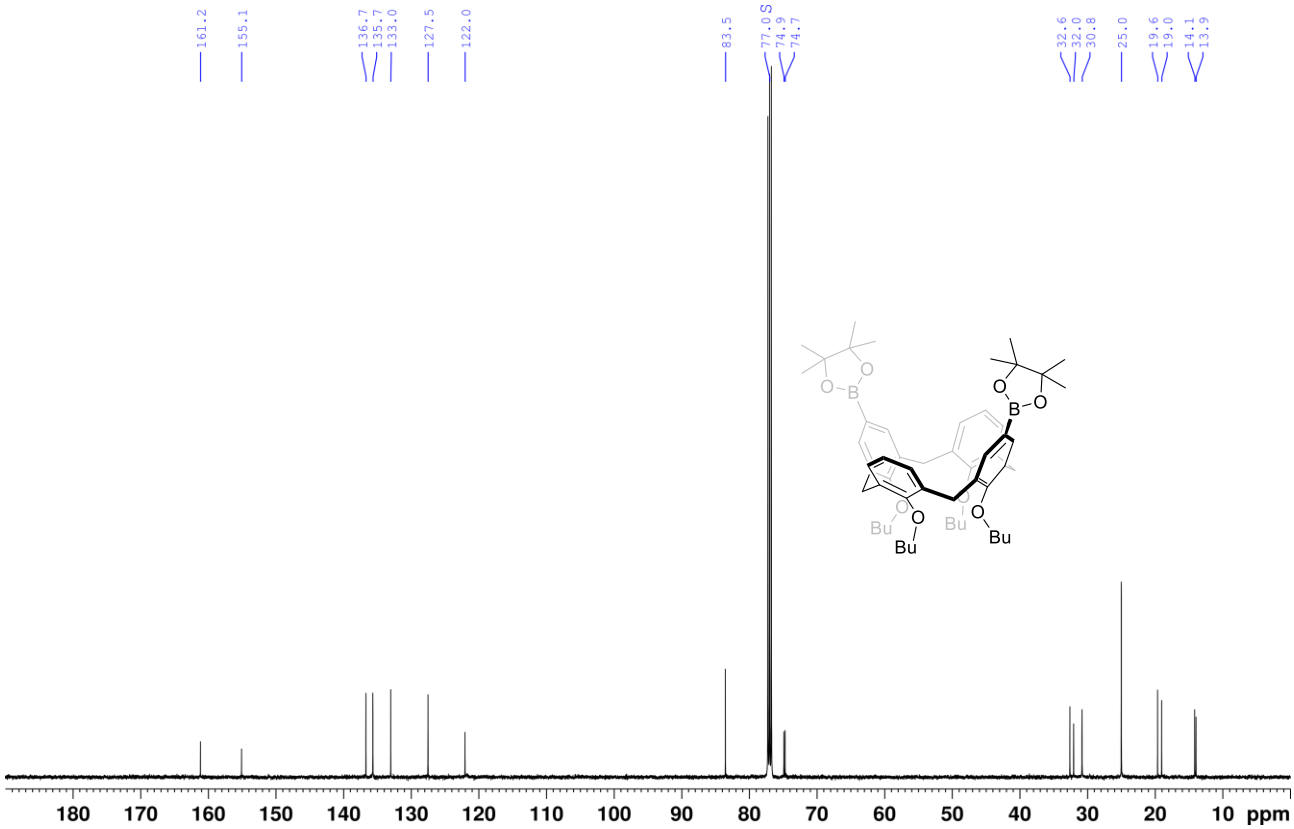

Figure S43. ^{13}C NMR spectrum of **2b** (125 MHz, chloroform-*d* , 300 K).

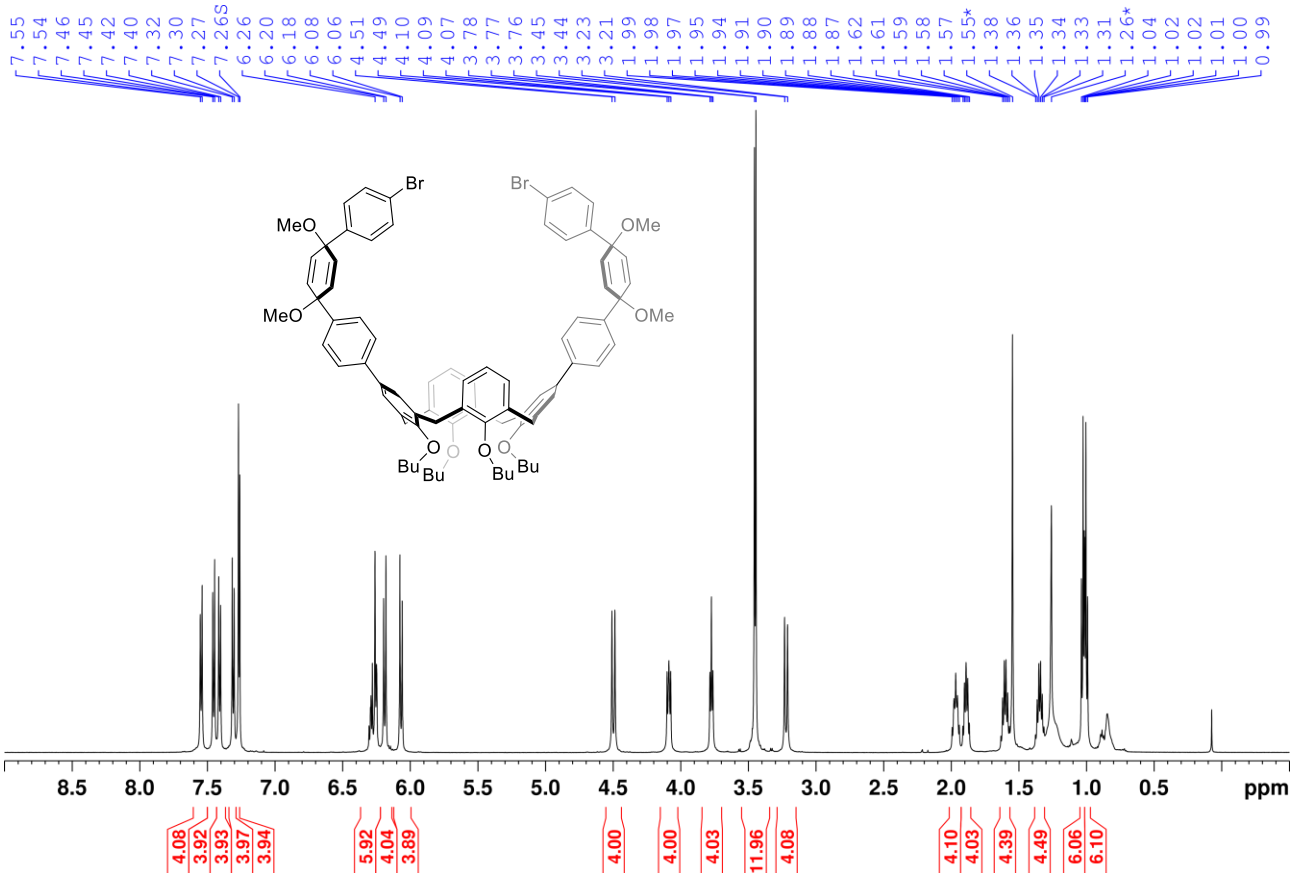

Figure S44. ^{1}H NMR spectrum of **4** (600 MHz, chloroform-*d* , 300 K).

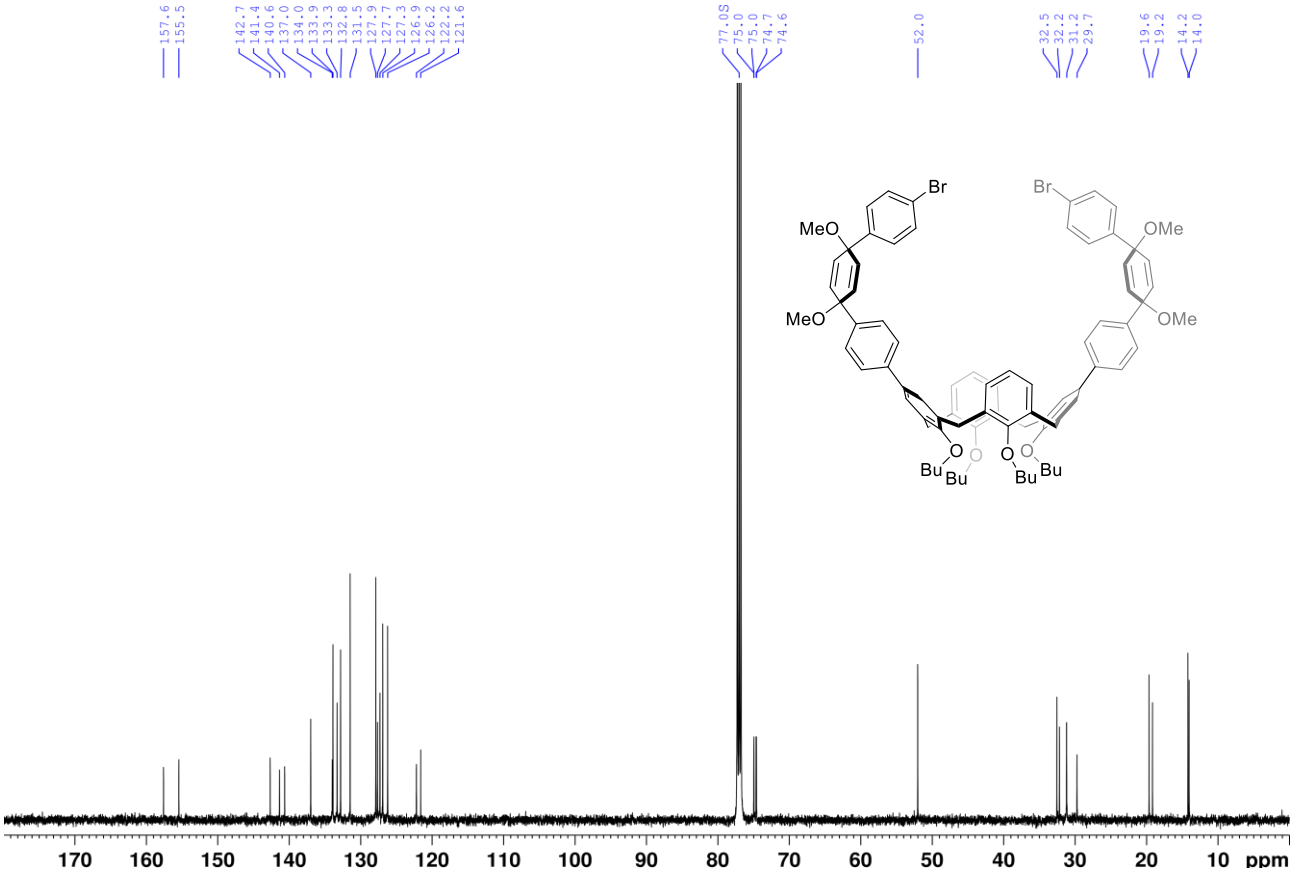

Figure S45. ^{13}C NMR spectrum of **4** (125 MHz, chloroform-*d* , 300 K).

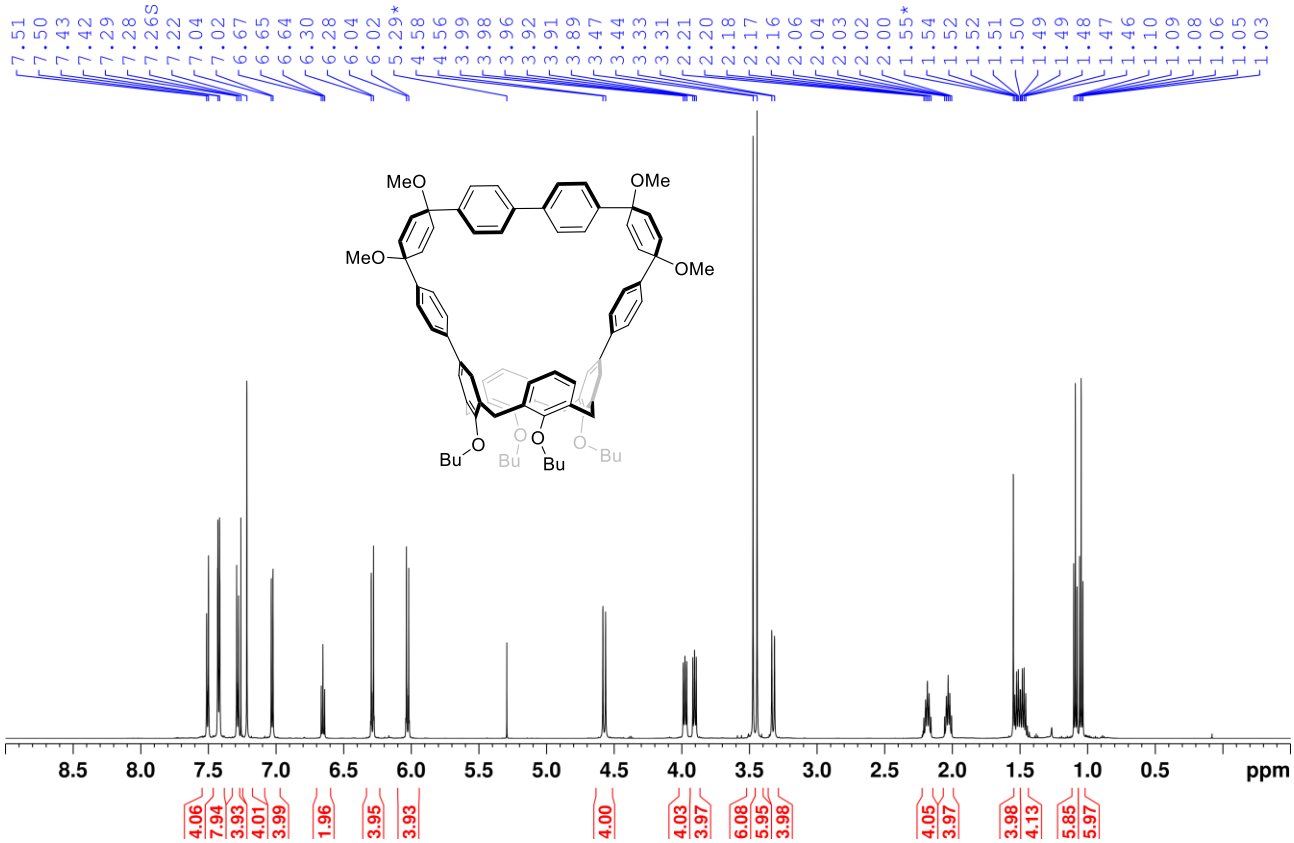

Figure S46. ^{1}H NMR spectrum of **5** (600 MHz, chloroform-*d* , 300 K).

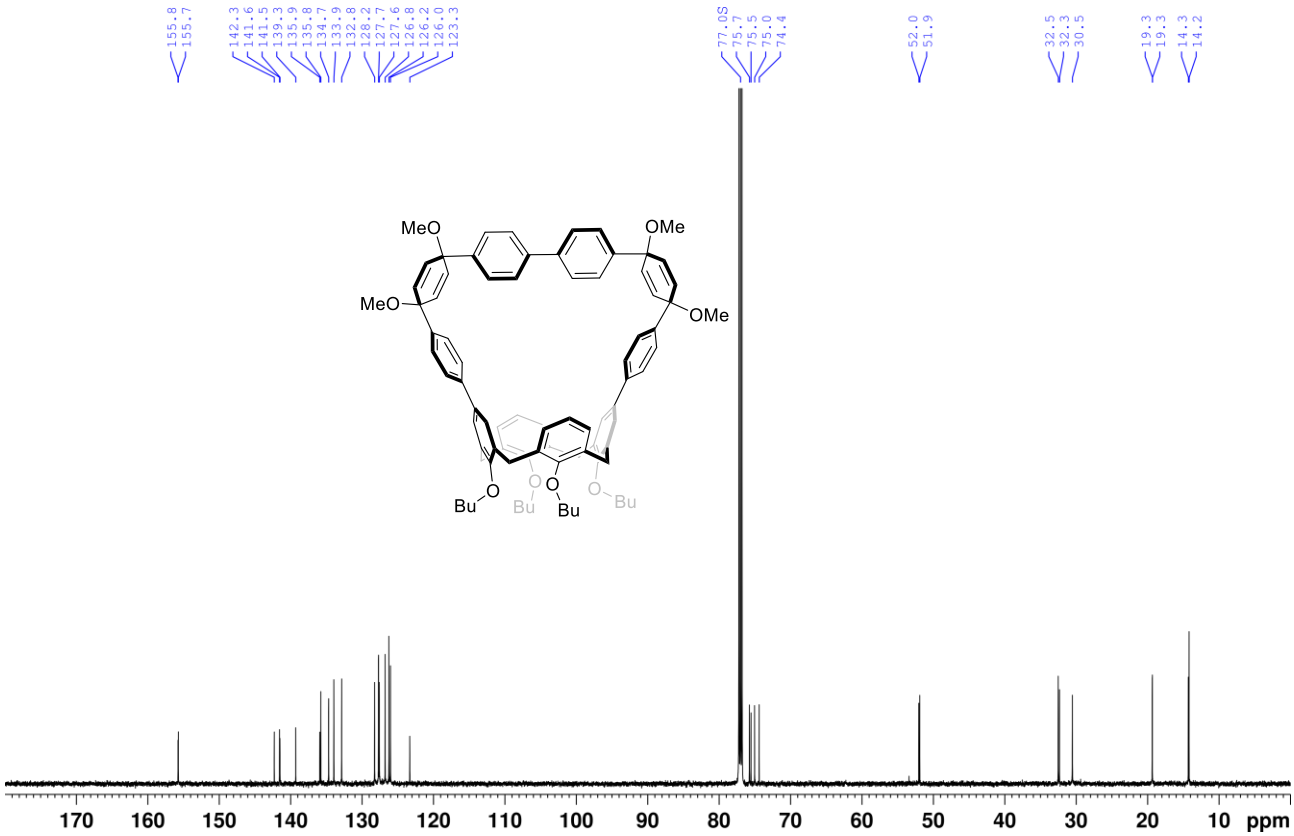

Figure S47. ^{13}C NMR spectrum of **5** (151 MHz, chloroform-*d* , 300 K).

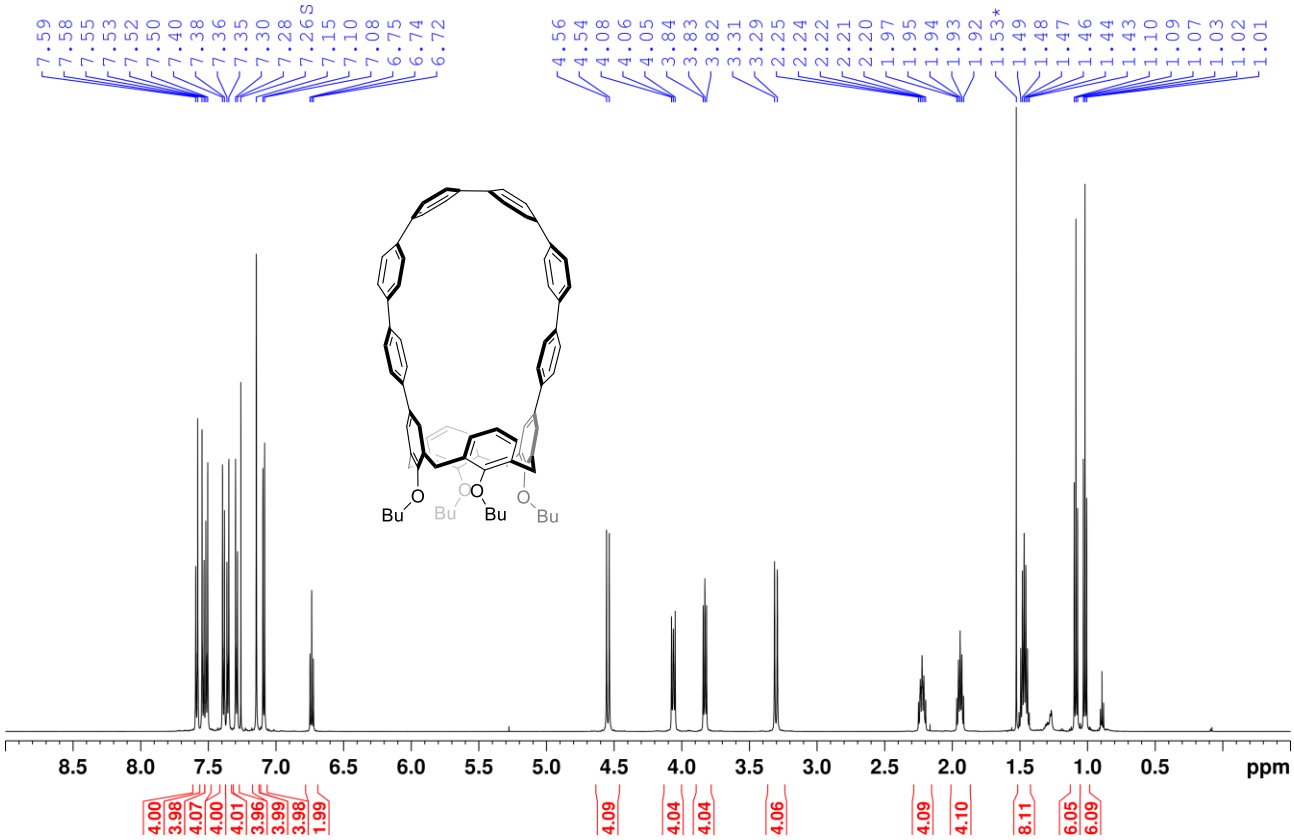

Figure S48. ^{1}H NMR spectrum of **1** (600 MHz, chloroform-*d* , 300 K).

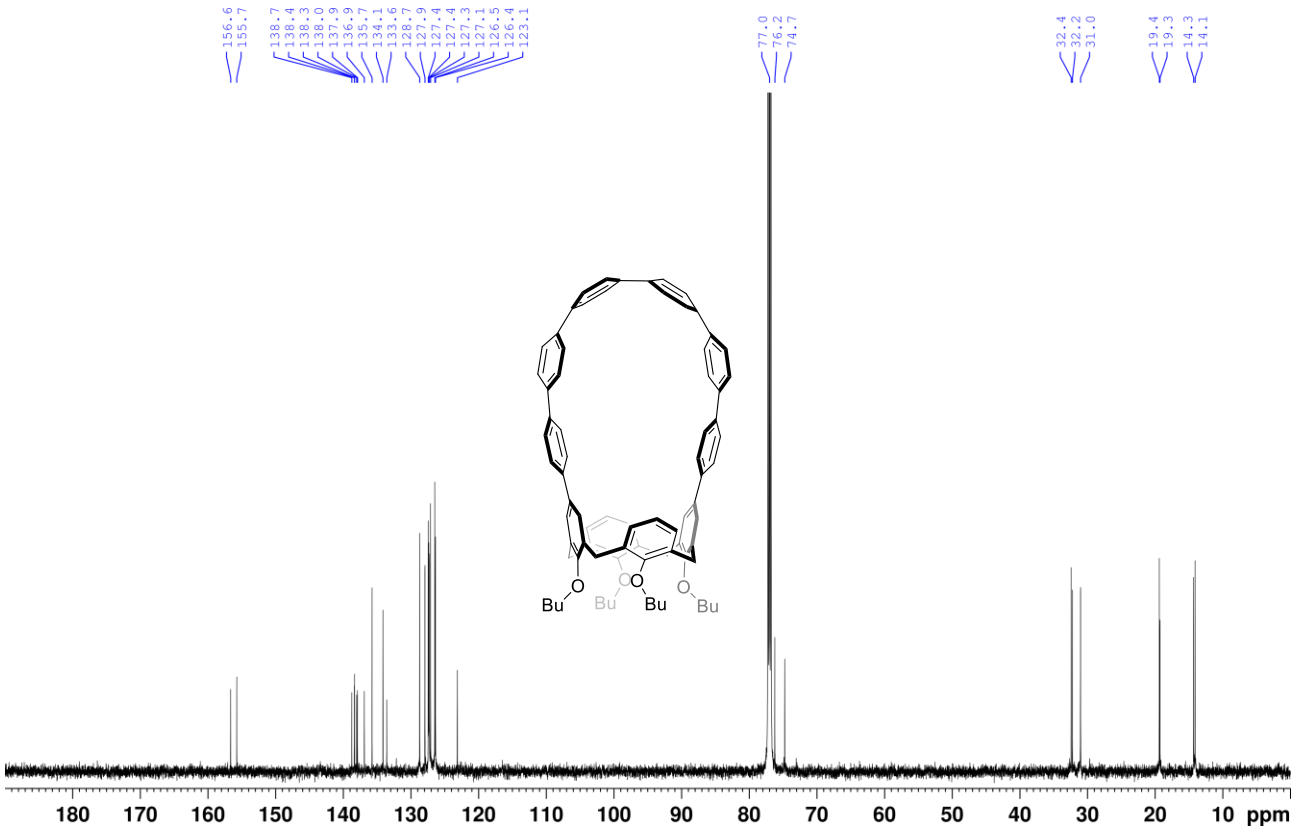

Figure S49. ^{13}C NMR spectrum of **1** (151 MHz, chloroform-*d* , 300 K).

Mass Spectra

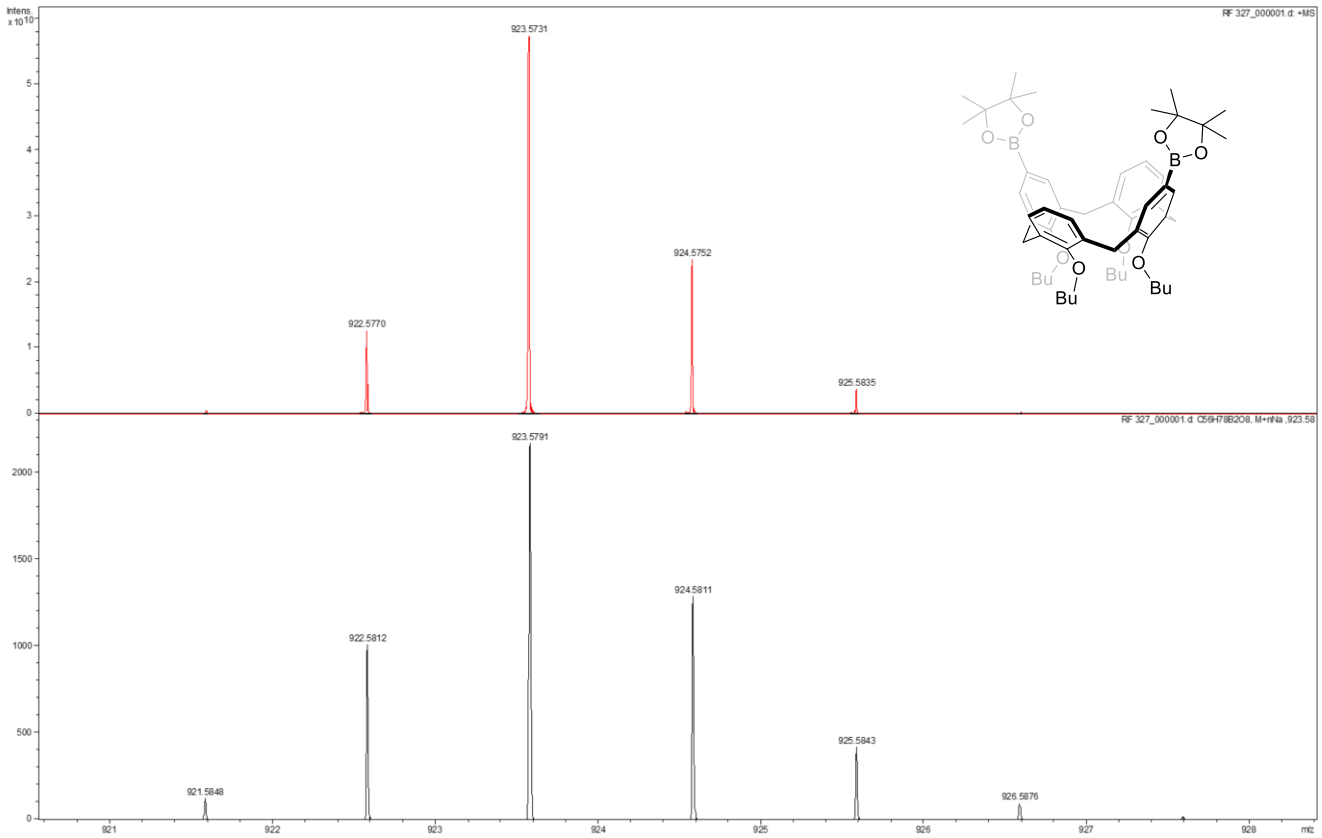

Figure S50. High resolution mass spectrum of 2b (ESI–TOF, top: experimental, bottom: simulated).

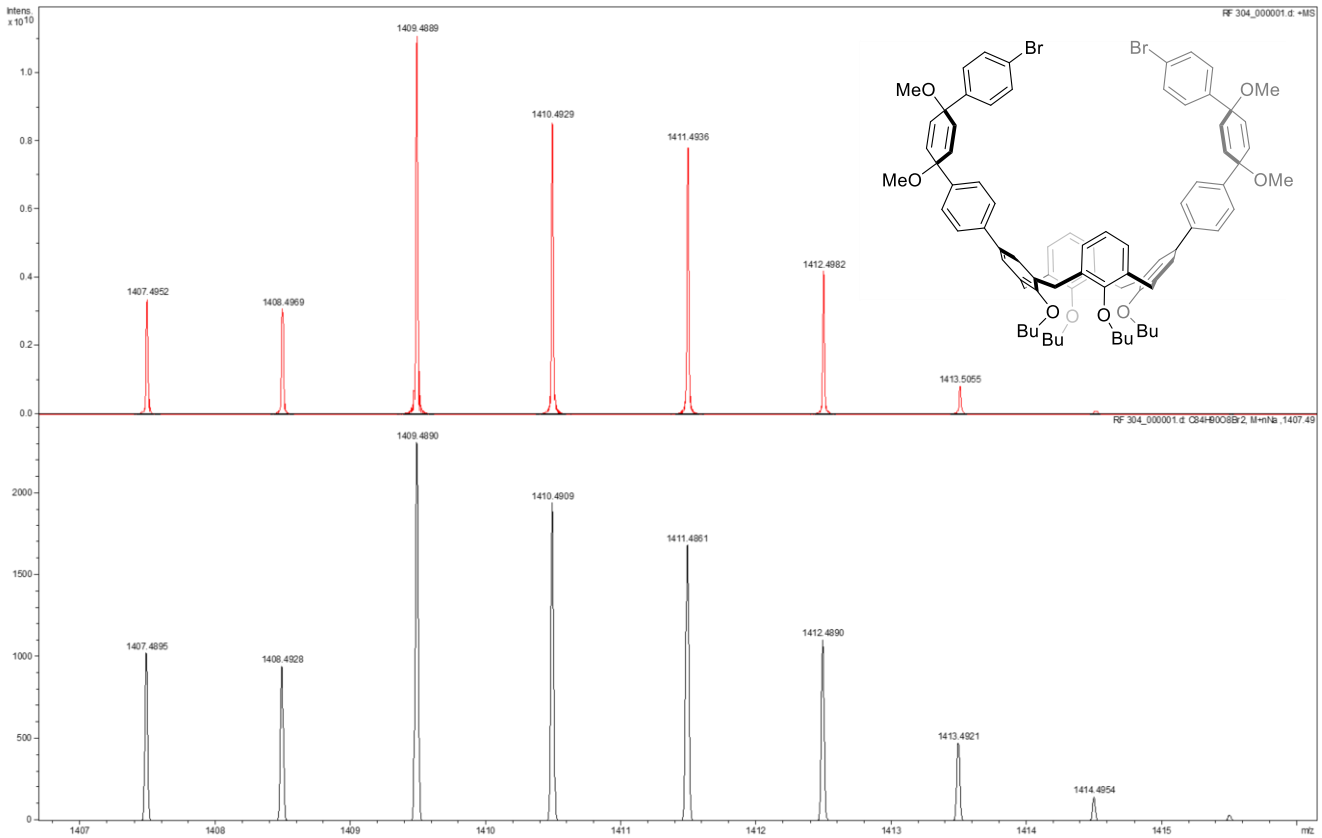

Figure S51. High resolution mass spectrum of 4 (ESI–TOF, top: experimental, bottom: simulated).

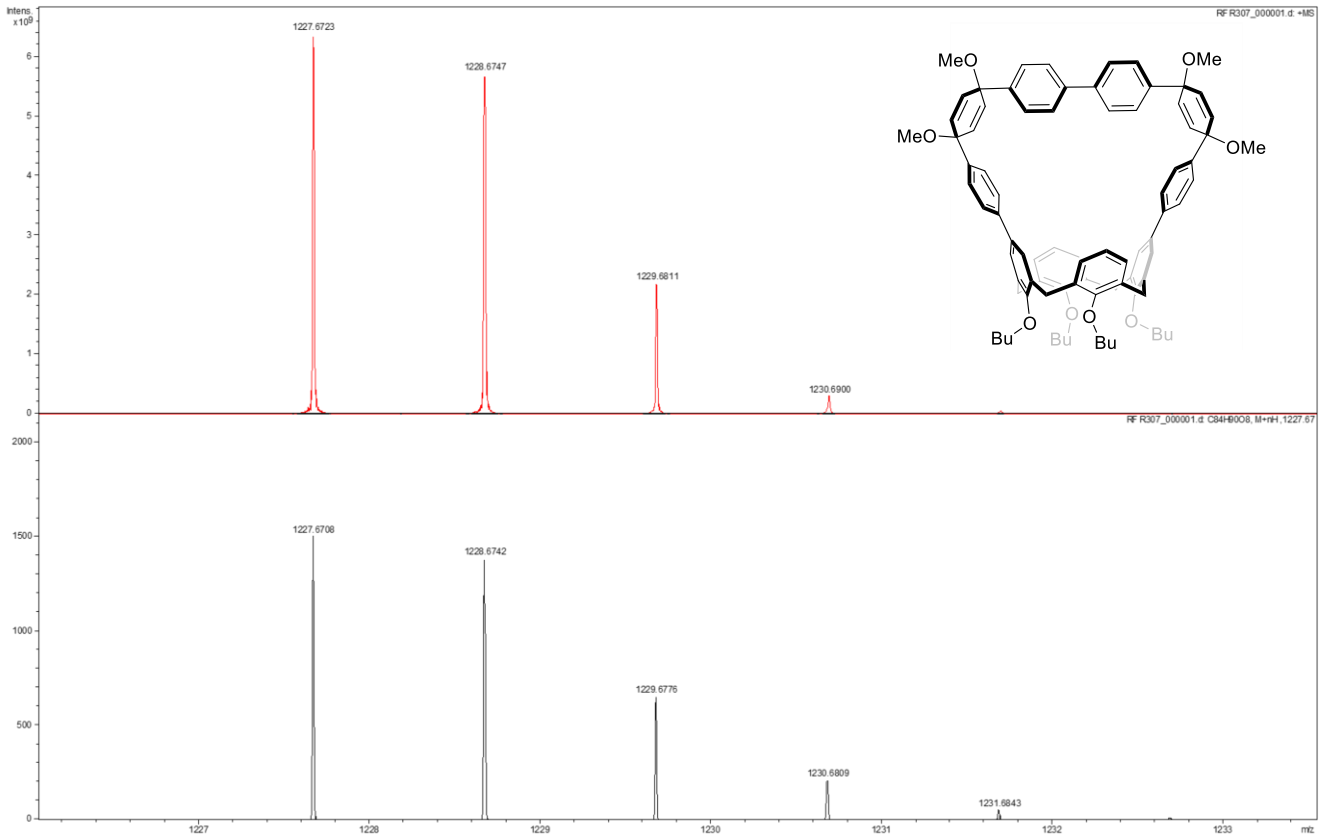

Figure S52. High resolution mass spectrum of 4 (ESI–TOF, top: experimental, bottom: simulated).

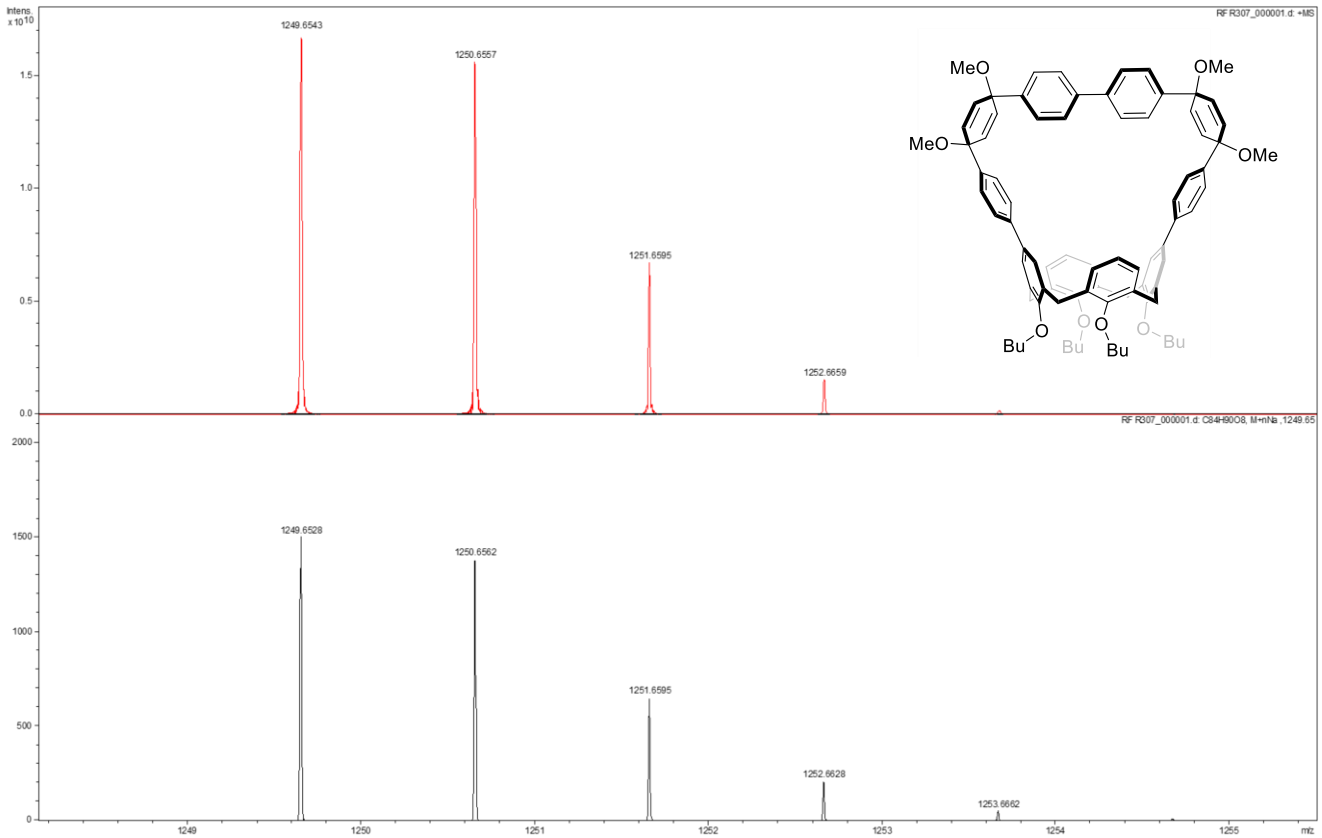

Figure S53. High resolution mass spectrum of 4 (ESI–TOF, top: experimental, bottom: simulated).

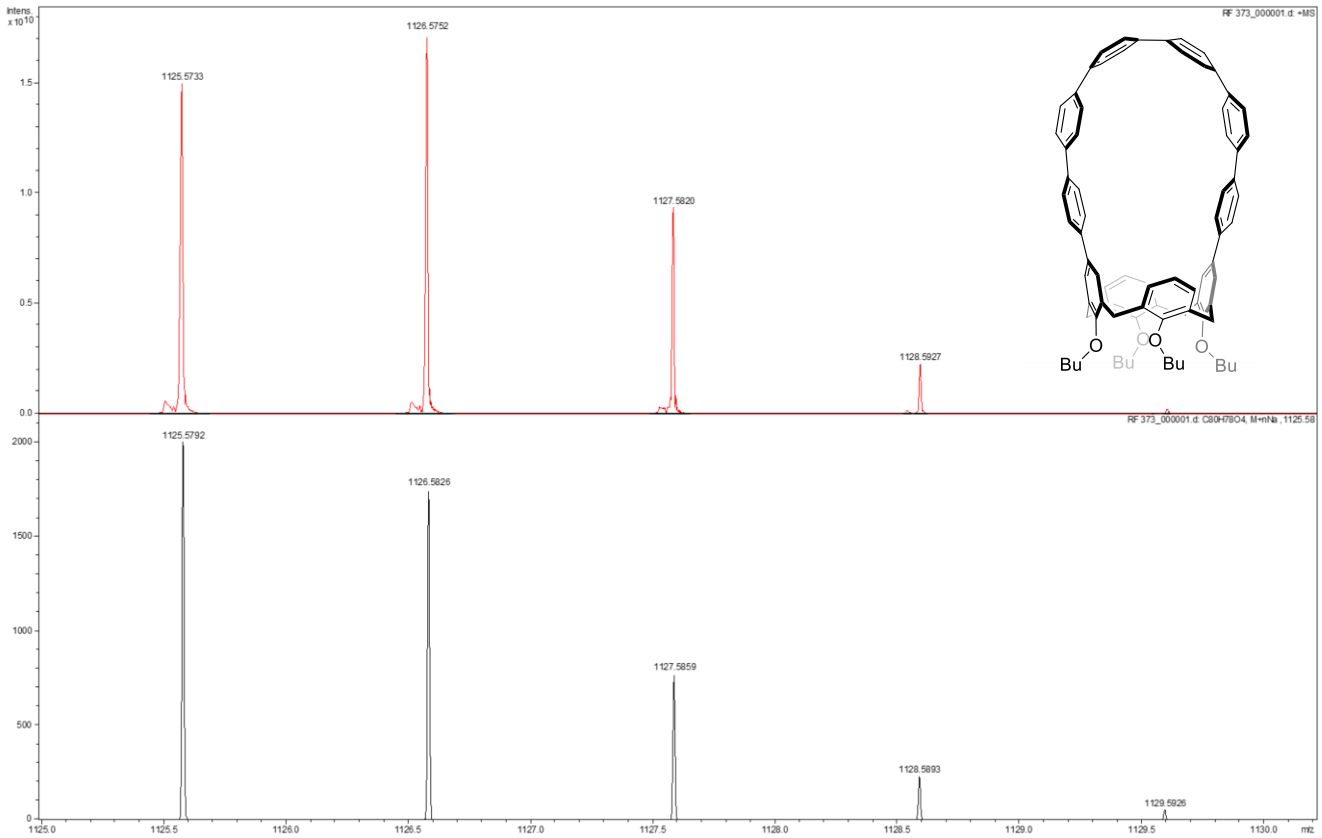

Figure S54. High resolution mass spectrum of 1 (ESI–TOF, top: experimental, bottom: simulated).

References

(1) Iqbal, M.; Gutsche, C. D. P-Tert-BUTYLCALIX[4]ARENE. *Org. Synth.* **1990**, *68*, 234. https://doi.org/10.15227/orgsyn.068.0234.
(2) Lee, J. H.; Kim, C.; Jung, J. H. Control of the Rheological Properties of Clay Nanosheet Hydrogels with a Guanidinium-Attached Calix[4]Arene Binder. *Chem. Commun.* **2015**, *51* (82), 15184–15187. https://doi.org/10.1039/C5CC06024A.
(3) Bonini, C.; Chiummiento, L.; Funicello, M.; Lopardo, M. T.; Lupattelli, P.; Laurita, A.; Cornia, A. Novel Chiral Calix[4]Arenes by Direct Asymmetric Epoxidation Reaction. *J. Org. Chem.* **2008**, *73* (11), 4233–4236. https://doi.org/10.1021/jo800301m.
(4) Guillon, J.; Leger, J.-M.; Dapremont, C.; Apollonia Denis, L.; Sonnet, P.; Massip, S.; Jarry, C. First Synthesis of 1,3-Alternate 25,27-Dialkyloxy-5,17-Diarylcalix[4]Arenes-Crown-6 as New Cesium Selective Extractants by Suzuki Cross-Coupling Reaction. *Supramolecular Chemistry* **2004**, *16* (5), 319–329. https://doi.org/10.1080/1061027042000213038.
(5) Elaieb, F.; Sameni, S.; Awada, M.; Jeunesse, C.; Matt, D.; Toupet, L.; Harrowfield, J.; Takeuchi, D.; Takano, S. Metallated Container Molecules: A Capsular Nickel Catalyst for Enhanced Butadiene Polymerisation. *Eur. J. Inorg. Chem.* **2019**, *2019* (43), 4690–4694. https://doi.org/10.1002/ejic.201901074.
(6) Thordarson, P. Determining Association Constants from Titration Experiments in Supramolecular Chemistry. *Chem. Soc. Rev.* **2011**, *40* (3), 1305–1323. https://doi.org/10.1039/C0CS00062K.
(7) Hibbert, D. B.; Thordarson, P. The Death of the Job Plot, Transparency, Open Science and Online Tools, Uncertainty Estimation Methods and Other Developments in Supramolecular Chemistry Data Analysis. *Chem. Commun.* **2016**, *52* (87), 12792–12805. https://doi.org/10.1039/C6CC03888C.
(8) Xiao, Y.; Chu, L.; Sanakis, Y.; Liu, P. Revisiting the IspH Catalytic System in the Deoxyxylulose Phosphate Pathway: Achieving High Activity. *J. Am. Chem. Soc.* **2009**, *131* (29), 9931–9933. https://doi.org/10.1021/ja903778d.
(9) Ischay, M. A.; Lu, Z.; Yoon, T. P. [2+2] Cycloadditions by Oxidative Visible Light Photocatalysis. *J. Am. Chem. Soc.* **2010**, *132* (25), 8572–8574. https://doi.org/10.1021/ja103934y.
(10) Feinberg, A. M.; Davydovich, O.; Lloyd, E. M.; Ivanoff, D. G.; Shiang, B.; Sottos, N. R.; Moore, J. S. Triggered Transience of Plastic Materials by a Single Electron Transfer Mechanism. *ACS Cent. Sci.* **2020**, *6* (2), 266–273. https://doi.org/10.1021/acscentsci.9b01237.
(11) Bindfit Http://Supramolecular.Org.
(12) Pracht, P.; Bohle, F.; Grimme, S. Automated Exploration of the Low-Energy Chemical Space with Fast Quantum Chemical Methods. *Phys. Chem. Chem. Phys.* **2020**. https://doi.org/10.1039/C9CP06869D.
(13) Grimme, S.; Bannwarth, C.; Shushkov, P. A Robust and Accurate Tight-Binding Quantum Chemical Method for Structures, Vibrational Frequencies, and Noncovalent Interactions of Large Molecular Systems Parametrized for All Spd-Block Elements (Z = 1–86). *J. Chem. Theory Comput.* **2017**, *13* (5), 1989–2009. https://doi.org/10.1021/acs.jctc.7b00118.
(14) Bannwarth, C.; Ehlert, S.; Grimme, S. GFN2-XTB—An Accurate and Broadly Parametrized Self-Consistent Tight-Binding Quantum Chemical Method with Multipole Electrostatics and Density-Dependent Dispersion Contributions. *Journal of Chemical Theory and Computation* **2019**, *15* (3), 1652–1671. https://doi.org/10.1021/acs.jctc.8b01176.
(15) Frisch, M. J.; Trucks, G. W.; Schlegel, H. B.; Scuseria, G. E.; Robb, M. A.; Cheeseman, J. R.; Scalmani, G.; Barone, V.; Petersson, G. A.; Nakatsuji, H.; Li, X.; Caricato, M.; Izmaylov, A. F.; Zheng, G.; Sonnenberg, J. L.; Hada, M.; Ehara, M.; Toyota, K.; Fukuda, R.; Hasegawa, J.; Ishida, M.; Nakajima, T.; Honda, Y.; Kitao, O.; Nakai, H.; Vreven, T.; Montgomery, Jr., J. A.; Peralta, J. E.; Ogliaro, F.; Bearpark, M.; Heyd, J. J.; Brothers, E.; Kudin, K. N.; Staroverov, V. N.; Kobayashi, R.; Normand, J.; Raghavachari, K.; Rendell, A.; Burant, J. C.; Iyengar, S. S.; Tomasi, J.; Cossi, M.; Millam, J. M.; Klene, M.; Adamo, C.; Gomperts, R.; Stratmann, R. E.; Yazyev, O.; Austin, A. J.; Cammi, R.; Pomelli, C.; Ochterski, J. W.; Martin, R. L.; Morokuma, K.; Zakrzewski, V. G.; Voth, G.

A.; Salvador, P.; Dannenberg, J. J.; Dapprich, S.; Daniels, A. D.; Farkas, O.; Foresman, J. B.; Fox, D. J. *Gaussian 16, Revision B.01*; Wallingford CT, 2016.

(16) Becke, A. D. Density-Functional Exchange-Energy Approximation with Correct Asymptotic Behavior. *Phys. Rev., A* **1988**, *38* (6), 3098–3100.

(17) Becke, A. D. Density-functional Thermochemistry. III. The Role of Exact Exchange. *J. Chem. Phys.* **1993**, *98* (7), 5648–5652. https://doi.org/10.1063/1.464913.

(18) Lee, C.; Yang, W.; Parr, R. G. Development of the Colle-Salvetti Correlation-Energy Formula into a Functional of the Electron Density. *Phys. Rev. B* **1988**, *37* (2), 785–789. https://doi.org/10.1103/PhysRevB.37.785.

(19) Grimme, S.; Ehrlich, S.; Goerigk, L. Effect of the Damping Function in Dispersion Corrected Density Functional Theory. *Journal of Computational Chemistry* **2011**, *32* (7), 1456–1465. https://doi.org/10.1002/jcc.21759.